NAVAL AIR WARFARE CENTER AIRCRAFT DIVISION
PATUXENT RIVER, MARYLAND

TECHNICAL REPORT

REPORT NO: NAWCADPAX/TR-2007/12

INITIAL EXPERIMENTAL EVALUATION OF A CIRCULATION CONTROLLED SAIL ON A SUBMERSIBLE VEHICLE FOR ENHANCED MANEUVERABILITY

by

Robin Imber
Ernest Rogers (Computer Sciences Corporation)
Jane Abramson (Computer Sciences Corporation)

14 March 2007

DEPARTMENT OF THE NAVY
NAVAL AIR WARFARE CENTER AIRCRAFT DIVISION
PATUXENT RIVER, MARYLAND

NAWCADPAX/TR-2007/12
14 March 2007

INITIAL EXPERIMENTAL EVALUATION OF A CIRCULATION CONTROLLED SAIL ON A SUBMERSIBLE VEHICLE FOR ENHANCED MANEUVERABILITY

by

Robin Imber
Ernest Rogers (Computer Sciences Corporation)
Jane Abramson (Computer Sciences Corporation)

RELEASED BY:

THOMAS G. RUDOWSKY / AIR-4.3.2 / DATE
Head, Aeromechanics Division
Naval Air Systems Command

REPORT DOCUMENTATION PAGE

Form Approved
OMB No. 0704-0188

1. REPORT DATE	2. REPORT TYPE	3. DATES COVERED
14 March 2007	Technical Report	May 2005 to September 2006

4. TITLE AND SUBTITLE

Initial Experimental Evaluation of a Circulation Controlled Sail on a Submersible Vehicle for Enhanced Maneuverability

5a. CONTRACT NUMBER

5b. GRANT NUMBER

5c. PROGRAM ELEMENT NUMBER

6. AUTHOR(S)

Robin Imber
Ernest Rogers (Computer Sciences Corporation)
Jane Abramson (Computer Sciences Corporation)

5d. PROJECT NUMBER

5e. TASK NUMBER

5f. WORK UNIT NUMBER

7. PERFORMING ORGANIZATION NAME(S) AND ADDRESS(ES)

Naval Air Warfare Center Aircraft Division
Bldg. 2187 Unit 5 Suite 1320
48110 Shaw Road
Patuxent River, Maryland 20670-1906

8. PERFORMING ORGANIZATION REPORT NUMBER

NAWCADPAX/TR-2007/12

9. SPONSORING/MONITORING AGENCY NAME(S) AND ADDRESS(ES)

Office of Naval Research
875 North Randolph Street, Suite 658
Arlington, Virginia 22203

10. SPONSOR/MONITOR'S ACRONYM(S)

11. SPONSOR/MONITOR'S REPORT NUMBER(S)

12. DISTRIBUTION/AVAILABILITY STATEMENT

Approved for public release, distribution unlimited.

13. SUPPLEMENTARY NOTES

14. ABSTRACT

The potential for the sail (bridge fairwater) of a submerged vehicle to serve as an on-demand auxiliary maneuvering control surface was experimentally investigated in a wind tunnel. The sail used circulation (lift) control in the form of mass ejection from Coanda-effect trailing edge region slots. The sail was mounted on, and tested in conjunction with, an exploratory submarine hull design. Test results show that the side force developed by circulation control equaled the side force produced by yawing the fully appended hull by 10 deg, a substantial turning diameter reduction effect. This benefit was present over the tested yaw angle range of $\pm$30 deg. Associated yaw moments are in the favorable direction of turning the hull into the turn. Roll moment increments were lower than expected due to a counter-roll effect produced by the pressure field acting on the relatively flat hull topside. For side force and yaw moment, the data indicated that the body-sail interaction effects were negligible at zero angle of hull pitch and yaw (no crossflow). For a 10-deg noseup pitch at zero drift angle, the body reacted to sail circulation by developing an in-plane side force equal to that produced by the circulation of the sail; conversely, at 10 deg nosedown, the body contribution reversed direction so that the net side force was one-half of that at zero pitch. Out-of-plane forces at angles of drift (yaw) were generally not adversely impacted by sail lift augmentation, for a given level of net vehicle side force. Slot flow rate requirements for various operational conditions, and near-term development plans, are discussed. With the successful outcome of this demonstration of a lift augmented sail, it is recommended that systematic maneuvering simulations be conducted to quantify the specific benefits of a circulation controlled sail on naval vessels of interest.

15. SUBJECT TERMS

Active Flow Control, Circulation Control, Submarine, Submersible Vehicle, Bridge Fairwater

16. SECURITY CLASSIFICATION OF:			17. LIMITATION OF ABSTRACT	18. NUMBER OF PAGES	19a. NAME OF RESPONSIBLE PERSON
a. REPORT	b. ABSTRACT	c. THIS PAGE			Robin Imber
Unclassified	Unclassified	Unclassified	SAR	94	19b. TELEPHONE NUMBER (include area code) (301)342-8533

Standard Form 298 (Rev. 8-98)
Prescribed by ANSI Std. Z39-18

SUMMARY

Circulation control (CC) is a proven technique for producing very high lift forces from a planar surface, independent of flow incidence angle, without moving parts on the surface, and is readily varied by throttling pumped flow to the Coanda-effect trailing edge slot. This technology was applied to the sail (bridge fairwater) of an investigative underwater vehicle model which, incidentally, had a noncircular, near-oval hull cross-section. Interest in the CC sail arises from an expectation of improved maneuvering capabilities in the horizontal plane, especially for turn-diameter reduction at low speed. The sting mounted configuration was evaluated in a large scale wind tunnel, quasi-statically, by recording the total vehicle load over a range of discrete pitch and yaw angles and several levels of slot flow momentum (C_μ).

The objective to demonstrate that a lift-controlled sail on a submerged vehicle could be a powerful maneuvering force generator was clearly met. The CC effect produced incremental side forces that were the equivalent to that produced by yawing the fully appended vehicle model by 10 deg. If one envisions a maneuver which calls for reversing the control force direction (by switching between the port-side and starboard-side slots), then a 20-deg equivalent yaw change is available and could be accomplished almost instantaneously or at a scheduled rate. Associated yaw moments were in a favorable direction in that they contribute to rotating the hull into the maneuver turn. Sail control effectiveness prevailed over the entire range of drift angles tested (-30 to +30 deg).

Some additional findings were:

1. The 6-component load balance readings were analyzed in detail to determine the plausible body-sail interaction effects of the novel arrangement of having a variable lift, but nonmoving, planar surface forward on a hull. At zero yaw and zero pitch angle, due to the absence of any hull crossflow, no body side force contribution was evident in response to increasing sail lift, a condition that allowed tentative examination of basic CC sail performance in comparison to the historical CC wing database.

2. Vehicle pitch angle effects, at zero yaw angle and thereby without lateral crossflow, clearly reveal the development and nature of additional force contributions arising from the hull, which were inferred to be centered about a location half-way between the sail trailing edge and the aft perpendicular of the hull. At a 10-deg pitch-up angle with its associated vertical component of crossflow, the body reacted to the sail lift increment in a manner to double the net overall side force. Conversely, a pitch-down to -10 deg generated a body force in the opposite direction, reducing the net side force by one-half, although as partial compensation, the net load center moved to a position just forward of the bow, thereby enhancing the already favorable yaw moment increment. These body effects can be explained in two equivalent ways: 1) the sail pressure field laterally unbalances the hull vertical crossflow velocities that arise with pitch angle, or 2) the result of the influence of the virtual vortex in the hull produced by the lifting sail. The presence or absence of the X-form stern appendages, which were positioned laterally, well offset from the hull centerline, generally made little difference in these effects.

3. Roll moment arising from augmented sail lift was less than expected, a favorable finding. The reduction is attributed to the sail imposing a pressure distribution on the relatively flat hull top side that resulted in a counter-roll contribution.

4. Side force increments due to CC were maintained unattenuated to $\pm$20 deg of yaw angle, with only a suggestion of a dropoff at 30 deg. Out-of-plane forces arising from angles of sideslip were generally not adversely impacted by sail lift augmentation, when viewed as a function of net vehicle side force.

5. Performance of a CC wing of unprecedented small aspect ratio was one of the technical unknowns. Although there was no separate load balance for the sail, its approximate performance was inferred from a single pair of mid-surface pressure taps and from vehicle load changes as slot flow was increased. Depending on the assessment technique used, viewed as a stand-alone CC wing, the sail response to slot flow was either 15% higher than pretest prediction or, with much less confidence, it was 20% less. However, there are now indications that inclusion of slender wing (long chord) effects in the empirically based model of CC performance would indicate that the sail performed about as expected. There was an earlier than expected onset of the single-slot lift limit, due to excessive Coanda wall jet wraparound; a proven remedy, very slight flow from the opposite-side slot, eliminated this stall. There is now reason to suspect that decreasing the planform aspect ratio increases the tendency to encounter the single-slot lift limit early. The phenomena would not necessarily impact the near-term operational viability of a CC sail, but should serve to direct continued CC technology development. One near-term objective should be to evaluate the sail as a wall mounted wing in a wind tunnel.

6. Because sail performance as a control surface appears to have exceeded pretest prediction, a re-examination was made of the numerical procedure for modeling CC characteristics at extremely low aspect ratios (less than 2) where, for conventional wings at least, additional lift (beyond linear theory) arises due to the effects of lateral edge vortex flow. This beneficial nonlinear effect was not modeled in the CC code due to lack of data indicating its applicability to the component of augmented lift. It is now concluded that lift due to CC may be similarly benefited by this phenomena. Consequently, the empirical numerical code for CC hydrofoil performance (CC3D) should be updated once sail-alone performance data are obtained to confirm and identify the suspected slender wing effect arising from lift due to CC. In the meantime, the present version of the code is adequate for use in initial exploratory maneuvering simulation models, although it is likely underpredicting CC performance if the aspect ratio is less than 2.

7. For marine applications, the pumping flow rate required for the slot has been of ongoing interest. The definitive approach to determine flow requirements is by using maneuvering simulations to identify the incremental C_L needed on the sail to meet the desired maneuvering goals, along with specifying the ship speed at the initiation of the maneuver. In lieu of such mission related specifications, test data show that the optimum C_μ for the most force benefit per unit flow is in the range of 0.06 to 0.08. For 0.08 (incremental C_L = 1.0), the rate in gallons per minute is 7 per square feet of planform area and per knot of maneuver-initiation speed. This rate can be scaled to any size surface or speed as long as the slot gap to chord ratio is the typical

0.0020. The lift coefficient for a given flow rate would be substantially greater on a larger aspect ratio surface.

In the likely event of intensified interest in the CC sail application, the following short-term developmental sequence is suggested. Experimental evaluation on a circular hull form is advisable to be confident that sail-body interaction effects are being accounted for in the numerical modeling, use of separate sail load balance for this purpose is almost essential. The existing sail model can be used in water, after design of a better interior flow distribution system, and fabrication of a shaped tip-cap and a sail-hull juncture fairing. Flow rate requirement for the model in water at 2 kt is 22 gpm at 1 psi, corresponding to less than 0.2 hp.

Contents

Page No.

ACKNOWLEDGEMENTS

The authors thank Todd Sedler and his crew at Northrop Grumman Ship Systems for outstanding support, teaming, and hard work during this first of its kind effort; David Hunt at Modern Machine for design drawings, fabrication, and model delivery; Drew Landman from Old Dominion University and the technical team at the 30x60-ft wind tunnel facility; and Ron Joslin at the Office of Naval Research for his initiative to suggest and sponsor the evaluation of a circulation control sail on the NNemo-1 model.

NOMENCLATURE AND ABBREVIATIONS

A	Axial Force (lb)
A_j	Slot exit area
AOA	Angle of attack, hull pitch angle
AR	Aspect ratio, 2s/c
c	Chord of sail (20.5 in.)
CC	Circulation Control
C_A	Axial force coefficient (A/qS_w)
C_D	Drag coefficient (D/qS_w)
C_{Dsail}	Drag coefficient of CC sail (D/qS)
C_l	Roll moment coefficient ($R/q\ S_w l$)
C_L	Lift coefficient (L/qS_w)
C_{Lsail}	Lift coefficient (L/qS)
C_m	Pitch moment coefficient ($P/q\ S_w l$)
C_n	Yaw moment coefficient ($Y/q\ S_w l$)
C_N	Normal force coefficient (N/qS_w)
ΔC_{P50}	ΔP as a coefficient
C_Y	Side force coefficient (S/qS_w)
C_μ	Slot momentum coefficient ($\dot{m}V_{jet}/qS$)
D	Drag Force (lb)
gpm	Gallons per minute
h	Slot height (gap)
hp	Horsepower for slot flow pumping
l	Length of hull model from forward perpendicular to centerline trailing edge (13.30 ft)
L	Lift Force (lb)
$\dot{m}$	Slot mass flow rate
P	Pitching Moment (in.-lb)
psi	Pounds per square inch
psf	Pounds per square foot
P_d or P_{duct}	Duct (plenum) pressure, gage units
P_{slot}	Pressure (spanwise mean) in the slot nozzle exit flow, total, gage
P_{static}	Test section static pressure, absolute
ΔP	Pressure difference port/starboard sail surfaces at mid-chord/mid-span
q	Dynamic pressure ($1/2\ \rho V_\infty^2$)
R	Roll Moment (in.-lb) and Specific Gas Constant (1716 $ft^2/s^2°R$ for air)
Rn	Reynolds number
s	Span of the sail (10.28 in.), root to tip
S	Planform area of Sail (1.46 ft^2) and also Side Force (lb)
S_w	Reference area for the hull model (130 ft^2, approximate wetted area)
t	Foil thickness
T	Temperature
V_{jet}	Slot exit velocity, calculated
V_∞, U	Freestream velocity

x	Longitudinal location, referenced to the hull forward perpendicular
Y	Yaw Moment (in.-lb)

Greek

β	Yaw angle (drift or sideslip angle)
Γ	Circulation
ρ	Density

CFD	Computational Fluid Dynamics
NGNN	Northrop Grumman Newport News
NNemo-1	Newport News Experimental Model (version-1)
ODU	Old Dominion University
ONR	Office of Naval Research

OBJECTIVE AND APPROACH

The goal is to substantially enhance the maneuvering capability of submerged vehicles in the horizontal plane, especially at very low speeds. The approach is to convert the wing-like planform of the traditional sail (bridge fairwater) into a no-moving-parts, readily controlled, side force generator to supplement the lateral forces produced by the rudder and hull. The technology applied, known as circulation control (CC), uses trailing edge mass ejection and the Coanda effect. This nonmechanical ability to vary control forces has the potential to reduce cost and complexity.

The objective of the subject experiment was to demonstrate and explore the basic attributes of a variable-lift sail mounted on a hull configuration. The test data will be used to validate maneuvering and design codes, to understand the associated hull and appendage interaction effects, and to further mature CC technology.

There are two unexplored technical areas that in part motivated this initial experimental exploration: 1) effects of an augmented lift sail on an appended body (in this case, a noncircular hull), and 2) CC wing effectiveness at the extremely low aerodynamic aspect ratio of 1.0, where the physical span is only half the chord length.

INTRODUCTION

Exploratory numerical simulations of low speed turning maneuvers on underwater vehicles have revealed substantial reductions in turn path diameter if the sail is able to be commanded to produce moderate levels of incremental side force, regardless of the flow angle at the sail. The challenge is to arrive at a mechanically viable way of controlling sail lift that has the capability of making very substantial increments in that lift.

Active lift control technology known as circulation control has been studied in detail and clearly shown to be applicable to both aerodynamic and hydrodynamic applications (references 1 and 2). This technology makes use of flow directed from slots in the trailing edge region and the Coanda effect, see figure A-1. There are now, in current production, both military and commercial flight vehicle applications of flow control based on using the Coanda effect.

When a jet sheet is emitted in a certain manner from the rounded trailing edge of a planar surface, there is a powerful influence on the fluid dynamic forces developed by that surface, independently of the incidence of the planar surface or of the local flow environment. The CC performance correlation parameter is the slot flow momentum coefficient, C_μ. For incompressible flow with a full span slot of constant gap h/c, some forms of the equations for C_μ are:

$$C\mu = \dot{m}V_{jet} / (qS), \quad (\dot{m}V_{jet}) \text{ is the slot flow momentum;} \quad (1)$$
$$= 2\,(h/c)\,(V_{jet} / V_\infty)2, \quad (V_{jet} / V_\infty) \text{ is the jet velocity ratio;}$$
$$= 2\,(h/c)\,(Pd/q), \quad (Pd/q) \text{ is the slot pressure ratio.}$$

Recently, under Office of Naval Research (ONR) sponsorship, the performance of a dual-slotted sail-like isolated CC hydrofoil-wing with an effective aspect ratio of two (figure A-2, reference 2) was verified in a large water tunnel. The data from that hydrofoil model test have been adjusted to theoretically account for the much smaller aspect ratio of a typical sail planform (one) and is represented in figure A-3. This figure shows a map of forces expected to be produced by a CC sail under the various flow conditions that may be encountered in the transient and steady state portions of a maneuvering turn. With a dual-slotted sail, large forces, either to port or starboard, can be developed by appropriate valving of the slot flows. Figure A-4 shows anticipated control capability, for an effective aspect ratio 1.0 appendage (geometric ratio of 0.5), as a function of the slot flow momentum coefficient, C_μ, while at a constant 0-deg angle of attack (AOA) and zero beta angle. Lift control range at fixed incidence exceeds that available from a non-CC surface that has a variable angle capability. The drag is predominately lift-induced and is intrinsic to high-lift from a small aspect ratio planform.

Figure A-5 illustrates the distribution of hydrodynamic pressures that result from the lifting surface circulation developed by the Coanda trailing edge slots. The surface pressures are calculated with an inviscid potential flow panel method (VSAERO, AMI) wherein, effectively, the lift coefficient is specified. Note the absence of the usual pressure loading at the leading edge. With CC, the load primarily arises from the trailing edge region, with the net load centered about the 80% chord location (not the conventional quarter-chord); this observation is useful in helping to interpret the test results. Similarly, to assist in understanding test results, figure A-6 shows how the pressure field from a lifting planar surface extends onto the surface to which it is attached.

Because of the short height (span) of a sail as compared to its length (chord), the aerodynamic aspect ratio is much smaller than that of typical wings. There are several ramifications due to that difference, the most important of which is how the lift force at a given flow angle (or slot blowing level) is attenuated for planforms with reduced aspect ratio. That effect is illustrated in figure A-7, as a reminder of the significance of sail geometry when intended to be used as a force generator.

As a first-look at the capabilities of a fairwater equipped with active lift control, a CC sail model was constructed and mounted on a large scale model of a submersible vehicle. The experimental evaluation was conducted in a wind tunnel as a 1-day extension of a primary test of various configurations of the vehicle model. All testing was with a captive model under quasi-static conditions. A balance internal to the hull measured total forces and moments. The test date was 9 December 2005.

MODEL AND TEST FACILITY

HULL

The CC sail experimental evaluation was an ONR supported extension of a Northrop Grumman Newport News (NGNN) sponsored test of their NNemo-1 underwater vehicle design. The NNemo-1 project is a NGNN initiated exploratory program examining novel hull forms and directed to future naval applications. There was a mutual interest in the CC test, because of the potential to enhance controllability of hydrodynamic vehicles.

Configuration drawings of the $1/20^{th}$ scale NNemo-1 are provided in figures A-8, A-9, and A-10. The model length is about 13.3 ft, with hull vertical dimension of 1.9 ft, width of 3.7 ft. The stern appendages (fins) could be set to specified angles of incidence, but were at a zero setting with respect to the hull centerline for the CC tests. Unappended test runs were made as well, although the bowplanes remained in place. The drawings show the two locations for a conventional sail. The CC sail was evaluated in the forward location, to better correspond to current submersible design practice and to demonstrate the control capability that the CC surface would add to the NNemo-1 at the forward location.

Particular attention is called to the hull cross-sectional profile as that of a noncircular, oval-like shape, as defined by circular arcs of two different radii. The hull shape would be expected to influence the reaction of the hull to the pressure field footprint from the sail, i.e., the wing-body interaction factors.

The hull model had been prepared with tufts for flow visualization and these were present throughout the CC test, as seen in photographs later in this report. The tuft sizes, their close spacing, and 100% coverage would be expected to have at least some impact on the measured aerodynamic characteristics of the hull. The sail itself was not tufted, however, so the current test objectives should not have been impacted by tufting of the hull.

SAIL DESIGN

Figure A-11 is the nondimensional numerical definition of the sail model cross-section, basically an elliptical profile of 20% thickness ratio, with expanded drawings of the trailing edge and slot region. The cross-section is identical to that of the dual-slotted hydrofoil model of reference 2 and closely resembles the CC airfoil reported in reference 3. This consistency in contour facilitates assessment of sail performance, wherein the only exterior parameter that is different is the lifting-surface aspect ratio. Each slot, port/starboard, is fed by a separate valve-controlled air hose to provide the ability to confirm that there is lateral symmetry of performance (model quality) and to enable exploration of simultaneous dual slot operation. Model construction drawings and photographs are provided in figures A-12 through A-15. Materials used were PVC plastic for the front half, with anodized aluminum for the aft sections.

The sail chord length is 20.50 in. with a span of 10.28 in. The span to chord ratio of 0.50 is about 10% less than that of current operational sail designs. Leading edge location is x/l = 0.21. To preserve similarity to other CC experimental evaluations, a sail-hull fairing for treatment of the junction flow was not used, nor was there a tip-cap fairing.

The sail was constructed with a static pressure probe in each plenum to provide an indication of relative slot air supply pressure. A bench test was used to identify the relationship of the interior reading to the actual total pressure head in the slot nozzle exit flow, as the model does not have a true plenum. Also, in the absence of a separate load balance for the sail, two exterior pressure taps were incorporated at mid-surface as an approximate indicator of sail loads, for diagnostic purposes. The slot air supply lines had thermocouples to identify air density.

The requirement for dual air line feeds, and the expedient of using a circular inlet, restricted the area available for the air supply inlet on the model, leading to an inlet-to-slot area ratio of about 1.7. This ratio is well below the rule-of-thumb minimum value of 3. The result is a jet-like plenum feed. The model was designed to withstand 4 psi, which is the operational value if it is eventually to be operated in water; the wind tunnel test required 2 psi. To reduce slot gap expansion due to pressurization, a mid-span support post was incorporated in a location that would minimize disturbance to the uniformity of the nozzle flow.

Construction tolerances were specified as 5 mils. Chordwise misalignment of components during manufacture or assembly can result in the nozzle lip being at the wrong location with respect to the Coanda round, potentially causing the nozzle to have a divergent geometry, with adverse CC performance impact. The critical parameters of slot position with respect to the Coanda surface, and the slot gap settings, were verified as within specifications; alignment pins are used to ensure future consistency in these settings. Surface finish smoothness was not quantified, although the Coanda surface appeared to be somewhat rougher than typical of past models, definitely not a polished appearance, perhaps due to the anodizing.

SLOT GAP DISTRIBUTION AND CALCULATED MASS FLOW

Because a flow meter was not employed to measure slot mass flow ($\dot{m}$), the following theoretical calculation for mass flow was used to obtain the value to use in the equation for C_μ (from reference 4).

$$\dot{m} = \frac{A_j\left(P_{slot} + P_{static}\right)}{\sqrt{T_{\circ R}}}\left(P_{ratio}\right)^{\frac{1}{\gamma}}\sqrt{1-\left(P_{ratio}\right)^{\frac{\gamma-1}{\gamma}}}\sqrt{\frac{2\gamma}{R(\gamma-1)}} \qquad (2)$$

where,

$$P_{ratio} = \frac{P_{static}}{\left(P_{slot} + P_{static}\right)} \quad \text{and} \quad \gamma = 1.4 \text{ (specific heat ratio for air)} \qquad (3)$$

Past experience has shown that if the slot exit area is accurately known, then the calculated mass flow comes within about 5% of the measured value, with one exception that is discussed in the next paragraph. Thus, as part of the post-test model examination, the slot gap was carefully measured with plastic feeler gages at a number of span locations. The data, presented in figure A-16, is included here as it may be relevant to future users of the sail model. The gap is within the specified tolerance, and the minor deviation that does exist corresponds to a 2 mil spanwise tilt in locating the circular cylinder that forms the Coanda surface. The mean gap, or slot height, is 0.041 in., corresponding to the design goal of h/c = 0.0020. The critical model components have locator pins, to allow reassembly with the same Coanda region alignments. No expansion of the slot gap was detected by using feeler gages at the nominal duct pressure of 1.0 psi.

Calculated mass flow is based on the assumption that the local exterior pressure is equal to freestream ambient (P_{static}), just as is always assumed when determining the V_{jet} to use in the equation for C_μ. However, depending on sail AOA, the local static pressure at the slot exit will be below freestream, even when unblown. Because of this reduced static pressure, the calculated flow rate will be lower than the actual value, as would have been measured by a flowmeter. The consequence is that the calculated C_μ will be somewhat offset from the corresponding values presented in other publications, where the flow was measured. The impact is strongest at very low C_μ (~0.005). For the current project, in the C_μ range of primary operational interest, there is no expectation of any meaningful deviation in the presented C_μ due to assuming ambient static pressure when estimating the slot flow rate.

WIND TUNNEL FACILITY

The Langley Full-Scale Tunnel, operated by Old Dominion University (ODU), was used for this test. Its large 30x60-ft open-jet test section is appropriate for a model of the NNemo-1 size, the same size as the underwater free-running test version. The tunnel was operated at a freestream dynamic pressure of 6 psf so that the velocity produced a match with the Reynolds number of the underwater data set. Sail Reynolds number based on chord was 0.80 million, which is typical of the CC airfoil database. Figures A-17 and A-18 depict the tunnel setup. The NNemo-1 model incidence was adjustable in pitch and yaw, and each angle setting had a measurement accuracy of 0.5 deg.

INTERNAL 6-COMPONENT BALANCE

Aerodynamic forces and moments were measured with a sting-mounted 6-component force balance internally located at hull center, x/l = 0.53, 7 ft from the bow, figure A-19. The stated accuracy and limits of the 6-component balance are as follows:

Component	Load Maximum	Units	Accuracy (±1% of Maximum Load)
Normal	1800	lb_f	±1.8
Axial	500	lb_f	±0.5
Pitch	7000	in.-lb	±7
Roll	4000	in.-lb	±3
Yaw	3000	in.-lb	±3
Side	1000	lb_f	±1

AIR SUPPLY AND CONTROLLER

Setting up an appropriate slot air source for a CC experiment is often a nontrivial undertaking due to the pressure available from a blower being too low and compressors generally having low flow volume. Therefore, the improvised air system for the sail is described in some detail.

At the target tunnel speed, and the required C_μ range to be tested, the sail needed about 1.5 psi plenum pressure to supply the 0.41 $in.^2$ exit area of the slot. It was determined that the facilities' utility air line might be able to meet the supply volume requirements if some flow restricting fittings were removed at the wall-outlet and a low-loss valve was used for controlling model pressure. A simple control setup was devised that did not rely on a sophisticated and expensive feedback based pressure controller, it is shown in figure A-20. A very basic adjustable pressure regulator was placed upstream of a full-bore ball-valve that served as the slot pressure adjustment device. The flow then went to a wye fitting from which each leg went to yet another ball-valve (for individual slot shutoff). For this test, mass flow is derived from a theoretical calculation based on slot flow total pressure and exit area (Equation 2). This is not the conventional practice, but can be acceptable, depending on project objectives.

Concerns with pressure loss margins led to using 2-in. diameter lines up to the model support sting and then 1-in. diameter lines into the model, see figure A-18. In retrospect, the 2-in. lines could have been 1 in. as well. Routing of the air lines from the support sting to the hull and into the sail base considered the possibility of grounding the balance and of potential hose pressure tares. The two air supply hoses were routed into the hull directly adjacent to the model support sting. The entrance area into the model had to be enlarged to give margin to preclude fouling (grounding) of the hull to the sting, which would bias the balance data. No means of automatic detection and notification of fouling events was provided; however, video camera images used for the flow visualization served as a monitor of fouling potential.

The influence of air line pressurization on balance readings was checked with the slots sealed by tape; as a precaution, a temporary air source was used that was incapable of inadvertently over pressuring a dead-headed system. The pressure tares were judged to be low enough so that tare corrections would not be needed.

TERMINOLOGY, REFERENCE AREAS, AND SIGN CONVENTION

The term “unblown” refers to the shutoff of the slot air supply line by closing a valve, in contrast to leaving the line open to draw from ambient pressure, which would result in a slot outdraft and a residual C_μ and augmented lift. When mention is made of “hydrofoil”, it refers to the precursor model to the sail, as described in reference 2. The terms yaw angle, beta angle, and drift angle are used interchangeably and mean the same as angle of sideslip. Use of “plenum” refers to the interior cavity of the sail model that receives the pressurized air, also sometimes more correctly called a “duct”, as it is not a true plenum. Unappended means the absence of the four stern planes, the bow planes were always present.

Reference area for the hull coefficients is 130 ft^2, which is the approximate wetted area of NNemo-1. The sail-based coefficients of C_{Lsail}, C_{Dsail}, and C_μ are based on the sail area of 1.46 ft^2. Reference length for all moments is 13.3 ft, with the reference point at the balance center, which was located at x/l = 0.53. Figure A-21 illustrates the wind tunnel sign convention for recorded data. Note that certain conventions differ from the practice in naval architecture. In the general discussion of the CC sail data, lateral force is sometimes presented as positive even though the actual data might have been negative due to use of the slot on the port side of the sail.

Highlighted by the fact that out-of-plane forces are often very small, the data channels sometimes showed readings when the symmetry of the aerodynamic situation would preclude a legitimate load. Occasionally, in the analysis of the test results, these data offsets were removed, which is particularly justified as appropriate because the primary analysis objective was to identify changes in balance readings in response to variation in sail slot flow rates.

TEST MATRIX, PRESSURE RANGES

The first test run was at 0 deg beta (yaw) angle, with a range of slot pressures, first the starboard slot, then the port slot, and then both equally and simultaneously. When it was proven that the two slots performed nearly the same, almost all subsequent testing used just the port-side slot. For this test setup, it took less time to step through the yaw angle range of $\pm$30 deg while at constant pressure than it did to readjust to each pressure setting at each angle.

With the port-side slot in use for all yaw angles, the negative angle range corresponded to the CC effect adding to the side force (“additive”). When at positive yaw angle, the CC developed side force was in opposite direction of that due to yaw (labeled “subtractive” on some plots as a reminder). Pitch angles of $\pm$10 deg were also examined at yaw angle of zero. One combination of yaw and pitch angle was recorded. A complete test matrix is listed in table B-1, and the test data set is provided in table B-2. Corresponding plots in dimensional units can be found in appendix C.

The number of discrete slot pressure values were limited by available test time and were selected to identify performance trends up to a C_μ of about 0.12 (1.1 psi). That C_μ value represented the anticipated beginning of the need to use a small amount of flow through the second slot (bleed flow) to maintain efficient CC action. Since the test scheduling did not permit time to identify the required level, nor to integrate simultaneous flow settings into the test matrix, dual unequal blowing was briefly explored in only one run series, run 22.

SCOPE OF TEST

To place the reported test in context, the focus was to demonstrate an operational application of the CC technology within a level of available funding. Data collection time was limited to 9 hr. There was essentially no instrumentation that could directly identify how the sail itself was performing (no separate load cell or pressure tap array). Despite the challenge of such a time compression, it will be seen that the test objectives were achieved. The efficiency of joining with a previously planned hull test, and working with experienced personnel from NGNN and ODU, made for a large payoff.

STATIC (NO FREESTREAM) CHARACTERISTICS

SLOT SPANWISE PRESSURE DISTRIBUTION

There was no detectable (by yarn tuft) wall jet disturbance produced by the duct mid-span post that was included to restrain any changes in the slot gap due to pressure. For reference, the post was circular and located 5.6 post diameters from the slot exit and, specifically, before the beginning of nozzle contraction.

The total pressure of the airflow exiting through the slot is needed to compute the slot exit velocity used in the standard computation of C_μ. The practice with CC airfoils, where the air source enters equally from both ends of the model, has been to mount a plenum pressure probe at mid-span facing the air inlets. Experience has shown that such a probe reads within about 1 or 2% of the nozzle exit total pressure, and thus can be used to compute the V_{jet} required in the conventional definition of C_μ. For the sail, due to a single-end feed at relatively high velocity and the resulting development of 3-D circulating flow patterns within the duct cavity, there was no location for a probe where one would be assured of a direct indication of the nozzle pressure. However, any reasonable location for the probe should give a reading that is linearly related to the slot exit pressure. Consequently, in post-test bench testing, the slot exit pressure was surveyed root-to-tip at several blowing levels, to identify spanwise variation and to determine the correlation between interior duct reading and the mean spanwise slot pressure. The survey probe was a handheld metal tube of diameter equal to about 75% of the slot gap setting and was aligned for maximum pressure reading. The results are shown in figure A-22. A 10% peak-to-peak variation in spanwise pressure was recorded, with the highest pressure occurring outboard (tip). This pressure gradient, although expected, is undesirable because it shifts too much of the span loading outboard, potentially intensifying the tip vortex and causing premature onset of any adverse conditions that arise from excessive local effective AOA. (A spanwise variation of slot gap setting can be used to offset the C_μ effect of such a pressure gradient.) The important finding

is that the mean slot pressure, which occurs at the 40% span, is 14% higher than that recorded from the duct pressure transducer during the wind tunnel test. Consequently, in order for the sail test results to be more directly compared to other sets of CC experimental data, the pressure used in post-test C_μ computation is based on 1.143* P_{duct}. These findings are like those initially found for the similar hydrofoil design, except that the hydrofoil model was subsequently fitted with an internal flow equalizing screen, to reduce the spanwise pressure variation. The following section describes an inherently related issue arising from spanwise pressure variations.

SKEW ANGLE OF THE WALL JET FLOW

Because the rectangular shaped duct interior is fed from one corner at a velocity equal to 60% of the Coanda jet velocity (a result of area ratios), there exists a circulatory cavity-like interior flow pattern. That pattern manifests itself as the spanwise slot pressure gradient previously shown (figure A-22) and as the production of a spanwise component of the Coanda wall jet momentum. The resulting deviation of the Coanda flow from a chordwise alignment is as high as 15 deg (figure A-23). The impact on performance of the Coanda sheet being directed inboard is not known, other than that there would be a reduction of "chordwise C_μ" by 7%. (The measured slot flow pressure used for the C_μ calculation was obtained with the slot probe aligned for maximum reading.) As mentioned, on the previous hydrofoil model, the interior geometry was kludged after construction so that the skew angle was reduced to about 6 deg. To have a proper air inlet and plenum interior layout to insure a uniform chordwise-aligned wall jet for the model would have required a significant investment in design/flow-test iterations that would have been beyond the tasking scope of this project.

DUAL SLOT FLOW CHECKOUT, PLANAR FREE JET

While not necessarily a primary part of the sail application concept, but of potential operational benefit, a check was made of dual slot operation in the absence of a freestream, with the model undergoing bench testing (not attached to the hull model). One objective was to confirm equal and consistent slot flow characteristics. As was similarly found with the hydrofoil model, sweeping a range of differential pressures for the slots correspondingly sweeps a merged-flow free-jet sheet over a range of almost 0-360 deg. Figure A-24 consists of visual evidence of the static-freestream thrust vectoring capability on the sail model.

FORCE READINGS FOR STATIC OPERATION

With the wind tunnel test section air speed at zero, load balance data were recorded for various sail slot blowing levels and combinations. One purpose was to establish that the balance performed adequately at low force levels. Figure A-25 is for single slot blowing, with the balance loads showing that the primary reaction is a backing force on the vehicle. In contrast, with both slots functioning at equal pressure, a forward thrust is produced, figure A-26, as expected. Figure A-27 shows that a nosedown pitching moment is produced from the dual slot flows with no freestream present. For single slot operation, a small side force component was also generated, figure A-28, which was not the case for the hydrofoil model under static conditions. The effective jet turning angle is 170 deg, with a thrust recovery of roughly 70%.

Figure A-29 is again for dual slot operation, this time showing with and without a freestream velocity. Observe that the amount of drag reduction from dual slot blowing is simply equal to the thrust obtained under static conditions; that is, on the scale of the plot, there does not appear to be a drag reduction "augmentation" factor. These observations are peripheral to the expected primary merit of the CC sail.

BASIC FINDINGS FOR ZERO INCIDENCE OF FLOW

Implementing lift control slots on an existing sail planform makes for a CC surface of an unprecedented low aspect ratio. Primary initial interest was whether the sail responded to slot pressurization with the expected level of force development. The predicted performance (figure A-4) is for the sail as a stand-alone wing, since it is from a theoretical projection based on tests of various CC wings and airfoils without an attached 3-D body. In the absence of a separate load cell to measure sail forces, an examination was made of vehicle side force and yaw moment trends to ascertain the extent of body-sail coupling in the integrated load readings, while at zero angles of pitch and yaw. In the circumstance of little or no indication of body-sail coupling effects, changes in vehicle side and axial loads as the slot is pressurized could be cautiously used to identify sail lift and drag coefficients.

The wind tunnel test section dynamic pressure was set to 6 psf (roughly 48 miles per hour), providing a NNemo-1 model Reynolds number 6.6×10^6. Figures A-30 and A-31 illustrate the change in vehicle side force and yaw moment as a function of slot flow momentum, while at zero yaw and pitch angles. These maneuvering forces for the entire vehicle are developed solely by the circulatory-lift action of the sail slot flow. The force levels will be placed in perspective, in the following and subsequent discussions, by comparison to what would be expected from an isolated sail (no body interference effects) and, most importantly, by comparison with the forces that arise when the vehicle is yawed in the absence of CC.

To apply a frame-work in which to judge the test results, it was assumed that there were no sail-body coupling effects. The pretest predictions of sail lift coefficient (figure A-4) and theoretical center of lift were then used to overlay expected vehicle forces and moments on the data graphs, figures A-32 and A-33. The match-up is reasonable, which might lead to the conclusion that the sail performed as expected. However, that inference depends on the actual sail-body lift carry-over benefits that may be present, as well as any other sail-originated contributors to body and appendage effects. Thus, additional data analysis was justified. (No computations of the NNemo-1/CC-sail configuration were made that would potentially identify the expected integrated effects of hull and high-lift sail.)

DETERMINATION OF SAIL CIRCULATION CONTROL LIFT RESPONSE

There are potentially two sources of force contribution that could arise simultaneously with, and thereby be indistinguishable from, the development of lift on the sail: 1) the hull, especially downstream and, 2) any other control surface appendages. Each of these two sources would have a moment arm different from that of the sail, therefore making the center of net side force likely to be displaced from the expected location on just the sail by itself. Wing theory discloses that, for the aspect ratio of the sail, the lift force due to CC-like control would arise at approximately the 80% chord location (reference 5). Experience with CC airfoils indicates that an additional 2 or 3% needs to be added to the theoretical aerodynamic center, to account for local jet effects in the trailing edge region. Comparing the location of yaw center on the complete model to the location expected on just the sail should then provide an indication of the degree of wing-body effects.

The determination of vehicle side-load center, which is yaw moment divided by side force, is shown in figure A-34. To assist in judging the position with respect to the theoretical location on the sail, the longitudinal location is shown in relation to the sail chord. It is seen that, for the nominal C_μ range (up to 0.10), the vehicle net side force does indeed arise at the approximate location expected for an isolated CC wing (approximately 83%). Also observed in figure A-34 is that, coinciding with a decline in lift, the load center eventually moves forward on the sail; this is expected at the higher single-slot blowing levels, as discussed below. Noteworthy is that the presence or absence of the stern appendages makes no significant difference in moment center location. Presumably, the off-axis lateral placement of the aft appendages on the wide body (see figure A-10) gives clearance with respect to the sail tip vortex trajectory, at least for yaw and pitch angles of zero.

The working conclusion for zero angles of pitch and yaw (no crossflow) is that changes in lateral load readings are minimally influenced by the sail tip vortex, or the corresponding hull-bound afterbody vortex, acting on other parts of the model. Therefore, it will be assumed that changes in side force arise from changes only on the sail, hence, the sail incremental lift coefficient (C_{Lsail}) will be taken simply as the incremental vehicle side force coefficient based on sail area; and similarly, sail drag properties (C_{Dsail}) will be attributed to changes in axial force. It is recognized that this assumption of essentially no lifting-sail interaction at zero hull incidence is justified only by circumstantial evidence. Also, be reminded that prior experience with circular hulls may be less applicable compared to the broad flattened topside profile of the present hull. Furthermore, there likely has never been previous data wherein sail lift could be generated and varied at zero hull flow incidence. The relatively flat hull deck should also permit sail performance to be closer to that of a wall-mounted semispan wing.

With the sail performance as a wing tentatively quantifiable, albeit somewhat insecurely due to absence of direct measurement of sail loads, an examination of CC performance characteristics can be conducted.

CIRCULATION CONTROL PERFORMANCE AND THE SINGLE-SLOT LIFT LIMIT

For the configuration at zero incidence and using the port slot, figure A-35 shows the variation of C_{Lsail} and C_{Dsail} with increasing coefficient of blowing, both with and without stern appendages. Since the appended configuration did not change the inferred sail performance, some of the subsequent figures will combine data from both configurations in order to portray a broader parametric range. Figure A-36 superimposes the data from when the slot flow was switched to the starboard slot (sign of C_{Lsail} reversed for plotting); both slots separately performed identically, and all further test data were acquired using the port slot.

The initial rate of lift response to blowing is as expected with a lift gain rate of about 23 times the slot flow momentum (figure A-37). This near linear gain then takes on more of a square-root relationship with C_μ, again as expected, and reaches C_L levels beyond 1.0, a notable achievement for the planform of the sail. Full performance potential is not reached, however, because of a somewhat earlier than expected onset of lift rollover, due to what has been described as excessive jet-wraparound, also called trailing edge drawdown. The phenomena results in the adverse development of suction pressure on what is normally the high pressure region of the trailing edge, due to excessive turning of the jet onto the side of the foil opposite the blowing slot. This lift stall beyond a C_μ of 0.08 was attributed to onset of jet wraparound primarily by noting the movement of the chordwise center of lift on the sail toward the leading edge, as plotted in figure A-34. (There is a detailed discussion of the phenomena in reference 2.) Another identifying characteristic is that the drag continues to increase despite the reduction in lift-induced drag that would occur following lift dropoff. This lift limitation was expected (but at a higher C_μ of 0.11), and an operational remedy has been previously established that involves producing a small flow from the second jet, to limit the primary-jet turning angle. A short data run was conducted with this “second-slot bleed” concept and the results show elimination of the early stall and continued lift gain (figure A-37). The flow from the second slot was metered at a momentum rate equal to 7% of that of the primary slot; this was the only rate tested and, for expediency, was selected as representing double the minimum value expected to be required for jet turning control.

DATA RANGES TO BE DISREGARDED IN ASSESSMENT OF SAIL TEST RESULTS

Due to the general absence in this test of using second-slot flow to delay single-slot lift stall, all data taken for P_{duct} pressures of greater than 0.9 psi (C_μ of about 0.09) are to be disregarded, and that applies to any images made of the tuft flow pattern. There is the one exception, when dual flow was briefly used as explained above. This data range exclusion is just outside the primary range of interest; therefore, there is no impact on achieving test objectives. The high C_μ condition was tested and the data are listed in appendix B only for CC research purposes.

PRESSURE DIFFERENTIAL AT MID-SURFACE

As described previously, the sail model was equipped with a single pair of surface pressure taps to measure the port-starboard pressure differential at mid-span/mid-chord, referred to here as ΔP. Theory and experience for larger aspect ratio CC wings has shown that such a centered pressure differential is uniquely and linearly related to the total wing lift, as long as the surface flow patterns are largely unseparated and "well behaved" (reference 2). The anticipated usefulness of such a load related signal is to provide supplemental insight into performance in a test environment and, in full scale application, to provide a feedback signal to maneuvering control equipment. Accordingly, the ΔP readings were examined for conformity to expected behavior and also to see how the ΔP derived C_{Lsail} compared to the C_{Lsail} based on the vehicle side force data.

For a wing of aspect ratio 2, the ΔP coefficient needs to be multiplied by 1.42 to derive the C_L. There was only one available potential flow calculation case for the aspect ratio of the sail upon which to judge a factor to use for the NNemo-1 CC sail test, that value is 1.72. As a check, figure A-38 presents the results for unblown data points covering a beta angle range of -20 to +20 deg. If it is assumed that the sail is thereby exposed to a corresponding change in flow incidence angle, then the derived lift curve slope should be consistent with the historical data base for conventional wings. (The unblown lift curve slope for a CC foil is generally the same as that for conventional designs.) Although the nonlinear nature of the data in figure A-38 makes slope assessment problematical, it can be interpreted as being fairly close to the expected value of 0.031 C_L per deg (compare with figure A-7 for AR=1), thus tending to roughly confirm the reasonableness of the conversion factor for ΔP to C_{Lsail}. However, there is some quite obvious deviant behavior in the ΔP response at low angles, including basically a step offset occurring at 5 deg. The irregularity may be a result of the pressure taps being located right at the seam of the model components, where sealing tape may have directly influenced local readings, or possibly caused an abnormal tripping of the flow at the somewhat low Reynolds number of the sail (Rn = 800,000). With that cautionary observation, plus recognizing that the ΔP unblown "calibration check" was with a yawed hull that would cause a higher velocity field at the sail, the ΔP readings will now be examined under slot flow conditions.

Figure A-39 shows the C_{Lsail} estimate based on the empirically expected relationship of C_L to ΔP for the sail planform. The prominent feature in the curve is the radical change coinciding with the side force (C_Y) derived lift peaking and then sharply falling, thus confirming that a drastic change in sail flow pattern (as in onset of excessive jet wraparound) is involved with single-slot lift stall. Prestall, the characteristic of concern is that the ΔP based lift estimate is about 70% of both the indicated and predicted sail C_L. If true, then there was a short-fall in sail response to slot flow, or the ΔP parameter and its conversion to C_L is somehow invalid for the sail model. One factor that questions the ΔP based C_L credibility is that the assumed lift-induced drag data do not correspond (figure A-37). To rectify the drag data with the ΔP based C_L would require that the Oswald span efficiency factor be 0.3, an implausibility low value (should be about 0.8, which does agree with the pretest expected C_L). In any case, it would appear that, relative to theory, the flow patterns on the sail are somehow different from those on the similar CC hydrofoil that had

double the aspect ratio. This possibility of a substantial flow pattern variation between aspect ratios of 1 and 2 has not been checked with a computational code. There are differences between the hydrofoil and the sail model other than the relative span length: chord distribution (taper), slot flow skew angle, and C_μ spanwise gradient. The question raised by the discrepancy in ΔP based C_L estimate and the expected C_L is in need of a basic flow visualization experiment in a wind tunnel (just the sail), to make sure that nothing presently unrecognized happens to CC on extremely low aspect ratio surfaces, where the tip chord is twice the length of the spanwise blowing slot. The concern is that the sail flow may be less 2D-like than on the earlier hydrofoil test, thereby impacting CC design criteria for optimum implementation.

In the analysis of effects of beta and pitch angles, the ΔP parameter in the form of a pressure coefficient ΔC_{P50} will continue to be observed as a relative indicator of consistency of sail generated forces, to help identify force changes that really arise elsewhere on the body.

OVERVIEW OF SAIL PERFORMANCE AS A WING

Figure A-40 summarizes the two approaches used to estimate the incremental lift coefficients produced on the sail, while at a fixed vehicle incidence of 0 deg in pitch and yaw. Attributing the incremental lateral loads as arising exclusively on the sail produces a performance curve that is about 15% higher than pretest prediction of sail C_L, but that assessment hinges on there not being any beneficial body-wing coupling effects on the hull-form of NNemo-1, in the absence of any crossflow. In contrast, relying on the mid-surface pressure differential to identify the C_L would say that the sail CC lift fell short of the prediction by about 20%, which would imply that favorable body lift carryover made up the (20 + 15%) difference.

If there is the possibility that the sail was delivering less than the expected lift due to CC, it would mean there was a favorable wing-body lift carryover that caused the net side forces to be as high as they were. If the body in the immediate vicinity of the sail was contributing to side force, then it might be evident from the location of the roll moment center.

CENTER OF ROLL FORCE, A COUNTER-ROLL CONTRIBUTION

Just as the yaw moment was used to identify the longitudinal location of where the net side force due to CC was acting, the roll moment was examined. The roll center location as a function of sail blowing level is presented in figure A-41, with the position on the vehicle depicted on the photograph in figure A-42. Strikingly, it is seen that the roll moment produced by sail lift does not correspond to the lift acting at a location on the sail, but rather well below the sail base, half-way to the hull centerline. (This is a virtue in that yaw-roll coupling of sail forces arising from CC is minimal.) The reduced roll is conjectured to be primarily a result of a noncircular hull acted upon by the pressure field imposed by the suction and pressure sides of the sail. Because the NNemo-1 hull is noncircular, a pressure distribution on the hull can produce roll, which makes for a hull contribution to roll in a direction opposite to that of the direct contribution from the sail, as sketched in figure A-43. (Refer to figure A-6 which is a potential flow computation of the pressure distribution on a flat plate produced by a high lift wing.) The counter-roll reaction to a loaded sail would seem to be limited to noncircular hulls, because pressure forces on a circular

cylinder do not have a moment arm about the center of the hull and thus cannot cause a roll moment about the longitudinal axis; however, the sail lift carryover on a circular hull may lower the roll center somewhat, for a given net sail side force. Because of the hull shape, it is not possible to readily deduce the level of sail-to-body lift carryover, based on location of the center of roll moment.

In the interest of completeness, there is the possibility that the always-present bow planes were producing a roll moment contribution as the sail was loaded, due to sail-induced distortion of the oncoming flow field; this possibility was not explored.

EFFECT OF STERN APPENDAGES AT ZERO ANGLES OF PITCH AND YAW

Figure A-35 compares the basic data for with and without stern appendages in place, under conditions of no body crossflow. There is little or no difference in the response to slot flow because, as speculated earlier, the sail tip vortex, even at high lift, passes between the widely separated aft appendages.

OUT-OF-PLANE FORCES WHILE AT ZERO DRIFT ANGLE

Cross-coupling of augmented sail lift with out-of-plane moments and forces while at the unique condition of zero pitch and zero drift angle will be covered in the later section on yaw angle effects.

This concludes the analysis of the basic aerodynamic attributes of the CC sail, as were best identified with the hull model aligned with the oncoming flow field (zero yaw and pitch angles). The next section will show that the incremental maneuvering forces and moments produced by the actively controlled sail are maintained over a wide range of yaw angles.

PERFORMANCE AT YAW AND PITCH ANGLES

PITCH ANGLE EFFECTS AT ZERO DRIFT ANGLE

Hull pitch angles of $\pm$10 deg were investigated at beta=0, both with and without stern appendages. This experiment is likely unprecedented because the sail will be developing lift up to the equivalent of a beta of 25 deg while in the absence of any lateral crossflow on the hull. As the circulation strength of the nonmoving sail is incremented, the only crossflow will be the purely vertical component of freestream velocity. The data set is of wing-body research interest, as well as providing insight into the practical application of a controlled-lift sail.

There is a strong influence of pitch angle on side force, as shown in figure A-44. Roughly, relative to zero pitch angle, the side force is doubled for +10 deg and halved for -10 deg. The initial question is whether the differences result from changes in the ability of the sail to respond to CC in the flow field produced by an inclined body. To verify the consistency of CC response, figure A-45 examines the mid-surface pressure differential for the three angles; there is no change with pitch angle. An examination of yaw moment trends shows a strong dependence on

pitch angle, but in a direction opposite to the side force trends (figure A-46). The indication is that the effective center of side force location is changing very substantially with pitch, even though the lift output of the sail does not vary. Figure A-47 reveals that +10 deg causes the net load center to move back one sail-chord length, while for -10 deg it moves forward by almost 3-chord lengths, in relationship to the location at zero pitch. The conclusion is that body generated lateral loads are becoming dominant at these pitch angles and are a function of sail circulation.

Similar identification of the equivalent roll moment center for horizontal force permits locating the net side force point of action as function of pitch angle, as portrayed in figure A-48. The relative strength of the side force is indicated by the length of the arrows, which, while drawn vertically, are to be taken as applying to the horizontal (lateral) plane.

Sail circulation causes the hull to develop a longitudinal distribution of bound vorticity whose strength corresponds to the intensity of sail circulation, see figure A-49. This hull bound vorticity is the counterpart of the sail tip vortex. From the Kutta-Joukowski theorem, any flow component perpendicular to the line of bound vorticity will produce a hull force at 90 deg to the crossflow. For a given direction of sail lift when at pitch angle, the resulting body net side force would either add to the sail force or subtract, depending on the direction of the crossflow: from above the hull (nosedown) or from the underside (noseup), hence the results seen in figures A-44 and diagrammed in A-48. Observe that the location of the body contribution, obtained by subtracting the sail force and its moment from the balance readings, has its center at a point halfway between the trailing edge of the sail and the stern of the hull. The implication is that the hull force contribution is uniform along the downstream hull, a topic of recent and historical research in relation to horizontal crossflow due to drift angle (references 6 and 7). It may be a coincidence, but also note in figure A-48 that the line connecting the centers through which the lateral forces act is parallel to a line that connects the sail trailing edge mid-point to the aft-most point on the hull centerline.

Due to the mathematical complication of the hull being neither circular nor elliptical, no attempt was made in this report to identify or develop an analytically (non-numerical) based expectation of sail-body coupling magnitude.

As for the effect of stern appendages on/off, the previous several figures reveal little difference, except for the -10-deg angle. In figures A-44 and A-46, a sudden shift in the moment and forces can be seen at a C_μ of 0.07 and, when the load center location is examined (figure A-47), a very large excursion is revealed (goes offscale). It is probable that with the nosedown attitude, the lift-deflected trajectory of the sail tip vortex eventually comes in close proximity to one of the laterally located stern appendages. For a hull with a centerline rudder, the effect of appendages could be higher (or at least more frequent) than seen in this test.

YAW ANGLE EFFECTS

Yaw angle settings of up to ±30 deg were tested at several levels of sail duct pressure, with and without appendages. Effective operation of a low aspect ratio CC wing at angles of up to and beyond 25 deg has been demonstrated; nevertheless, the planform of the sail and a location on a 3-D body are new experiences and, therefore, direct sail performance is examined. In figure A-50, the response of the mid-surface pressure differential to C_μ is consistent from -20 to +20 deg beta. As expected from the indicated consistency of sail force augmentation, figure A-51 shows that the incremental side force benefit of the CC prevails over the full beta range. The data with the symbols and solid line were obtained with the port-side slot active. By data transformation that is permitted by symmetry, the dashed lines in figure A-51 represent the probable data trend if the starboard slot were active and thereby provides a complete performance map. The reversal of C_μ generated force enabled by simply valving pumped flow to the other slot, while at a drift angle, potentially corresponds to a near instantaneous change in side force equivalent to a drift angle change of 20 deg.

Figure A-51 calls attention to the equivalence of sail control to a corresponding change in vehicle beta angle, with the reminder that the data are for the stern appendage controls fixed at 0 deg with respect to hull centerline. A modest C_μ of 0.05 at zero beta produces the same lateral force on the submersible as a change in beta angle of 8 deg. By taking the mean slope of ΔC_Y /Δbeta and dividing that into the C_Y versus C_μ curve of figure A-32, a side force equivalence between C_μ and incremental drift angle can be obtained, as illustrated in figure A-52. These results would have been even more favorable to CC if the stern controls had been set to counter the yaw moment; for the unappended configuration, the 8 deg mentioned above was nearly 10 deg. Above a C_μ of 0.1, little additional maneuvering control is gained.

As a more direct portrayal of the CC sail as an alternative control effector, figure A-53 depicts the buildup from a bare hull (with appendages), to plain sail, to CC sail, and finally to reversal of slots, with moderate C_μ and all at 10 deg beta angle. It is seen that the force increment produced by the circulation augmentation is dominant.

One observation from figure A-51 that might be of tactical operational value is that slot flow can hold the side force at zero even with the hull yawed to 8 deg, in effect, allowing a vessel to proceed in a straight path with the bow pointed off-course. An equivalent observation is that the same side force is available with various combinations of beta and slot flow rates. Figure A-54, the yaw moment counterpart of figure A-51, confirms the essentially uniform offset of yaw moment over the tested drift angle range, a complementary turn-assist contribution due to the forward location of the sail.

OUT-OF-PLANE FORCES AT ANGLES OF SIDESLIP

For yaw angles other than zero, there will be a lateral crossflow, with subsequent forces and moments in the vertical plane due to reaction with the virtual vortex in the hull created by the side-force producing sail. Of importance is how this undesired cross-coupling of horizontal and vertical response to a directional input compares for CC originated, versus conventional body-sail originated, steerage forces.

Figures A-55, A-56, and A-57 consist of plots of the out-of-plane components C_m and C_N, as well as the roll moment, all as a function of drift angle. For clarity, only two curves are shown, for unblown and for $C_\mu = 0.053$; it is recognized that a 50% increase in CC lift is available at higher values of C_μ. Because the port slot is active in the displayed C_μ data set, the negative beta side of the graphs corresponds to CC adding to the magnitude of the C_Y, and means that the sail is at a positive AOA, in CC airfoil convention. Conversely, the positive beta range represents CC subtracting from C_Y, and with a negative sail AOA because the active slot is then on the windward face.

Activation of CC makes little difference in the pitching moment C_m, especially when viewed in relation to the moment that would arise with pitch angle (+10 deg depicted on the plots to provide scale), figure A-55. Change in normal force, C_N, is higher at conditions shown on the right side of the plot (figure A-56) where CC is subtracting from side force. The difference is roughly equivalent to 2 deg of pitch. (No specific reason has been identified for the nonsymmetric behavior of the test data about zero beta, when unblown.)

Effect of CC on roll moment, when viewed as a function of beta angle in figure A-57, is to produce a nearly constant increment in the unblown curve. The appearance of an increased roll moment, due to CC, over a good part of the operational envelope is misleading. Since the operational objective is to produce a required level of steerage force (C_Y), and that force can be generated by various combinations of slot flow and drift angle, the most relevant plot is one that shows roll directly as a function of C_Y, rather than of beta angle. If the roll moment is now viewed with respect to C_Y (figure A-58), it is apparent that over this ±30-deg beta range that there is only one rather narrow region in which augmented lift results in a higher roll moment (corresponds to the region beyond conventional capability). In fact, over most of the C_Y range, maneuvering using forces developed with CC would have less roll impact, as compared to non-CC.

Another graph based on C_Y, figure A-59, makes the point that the yaw moment is independent of the source of the side force, except for a deviation that occurs in the slot-flow data centered around zero beta. The deviation may be because of the unique situation at zero beta wherein CC side force is generated in the absence of crossflow and, therefore, the moment arm for the force is about the sail pressure centroid; the center of net side force then changes with beta as body crossflow effects arise.

Because lift-induced drag goes as the square of the lift coefficient, the production of high lift on a low aspect ratio surface carries with it a large associated induced drag. This is readily seen in

figure A-60. Under conditions calling for very high C_Y, there is less difference in drag between CC on and off, for the same C_Y.

The drag coefficient of the sail when unblown is expected to be twice that of a conventional sail, a result of the necessary rounding of the trailing edge. The increase in sail drag due to the CC trailing edge may not be that important, because when viewed in relation to the total vehicle, the increment is estimated as roughly 1% of overall drag, on the NNemo-1 model. If desired, providing a light flow through both slots simultaneously will reduce the unblown drag down to conventional values.

SUMMARY ASSESSMENT OF OUT-OF-PLANE EFFECTS

It is concluded that there are no particular out-of-plane force issues unique to the production of augmented lift on a sail, at least on the NNemo-1 hull form. There will be a greater roll moment under some conditions, but only to the extent that is proportional to the greater side force control magnitude now possible with CC. The reaction to sail lift augmentation for a hull employing a body-of-revolution would be expected to have some properties different from those identified for the NNemo-1 hull-form.

COMBINED DRIFT ANGLE AND PITCH ANGLE

Only one configuration of combined pitch angle (8 deg) and beta (12 deg) was tested. The notable feature of that data set (not shown) is the strong presence of the additional side force arising from the pitched body in response to CC, as seen when the model was pitched at zero beta. The oddity is that the unblown side force, part of which would have come from the sail, did not change with pitch angle. If that single data point is representative, it would mean that somehow the sail-body interaction responds differently for augmented circulation versus for the conventional AOA component of circulation. That is an improbable conjecture; it is left to future experiments to definitively identify pitch angle effects at angle of drift, with CC present.

ASSESSMENT OF CIRCULATION CONTROL TECHNOLOGY EFFECTIVENESS ON THE SAIL

The following discussion addresses the question: Did circulation control technology perform as expected on the planform of the sail? The question is important as it relates to the maturity of CC and/or the adequacy of the computational design tools to be applied to future applications. As a reminder, there is the caveat on any assessment that instrumentation limitations prevented identification of the precise force increment produced solely by the sail.

Several figures have shown a predicted performance curve, where the sail was taken to be a semispan wing mounted on a reflection plane. The prediction technique, as coded in CC3D, was to use a combination of linearized lifting-line and lifting-surface wing theory to adjust the database of the AR=2 hydrofoil test (reference 2) to correspond to AR=1; the concept can be described as a transformation of a finite-wing data set. This procedure in CC3D has been validated for applicability to higher aspect ratios, but no CC data have been available to check

validity for AR below 2, which represents the expected beginning of certain effects unique to slender (long chord in comparison to span) wings.

Test results show that the sail performance was underpredicted, that is, the apparent sail lift was higher than had been predicted (figure A-40). Initially, the discrepancy was attributed to the possibility of favorable body effects (which is still a possibility). However, the more likely explanation is an inadequacy in the CC3D modeling for ARs of less than 2. The basis for this hypothesis is illustrated by a close examination of figure A-7, Prandtl's classic data set that illustrates the effect of aspect ratio on conventional wings. In figure A-7, if a straight edge is placed on the curve for AR=1, it will be seen that the curve is not linear like the other ARs, but rather, has an upward curvature, representing higher performance as AOA (C_L) increases. CC3D presently models only a linearized curve, which would be tangent to the nonlinear curve at C_L =0, thus underpredicting performance. This nonlinear response to AOA at AR=1, observed in most data for small aspect ratio wings, was not incorporated into CC3D because at the time there was no relevant data to confirm that the effect seen with AOA would arise with augmented lift from CC. The sail test results suggest that this beneficial effect is present for lift due to CC. Because the lift due to CC arises at a different chordwise location than for lift due to pitch angle, it is not known if there is an exact equivalence between AOA effects (figure A-7) and C_μ effects, for phenomena arising from slender wings. A dedicated sail-alone test on a load cell is needed to adequately identify the nature of the augmented lift response for AR=1, thereby permitting a refinement to the empirically-based CC performance prediction code. It is fortunate that the definitive CC wing database is for AR=2, because it is the demarcation between linear and nonlinear finite wing effects: simple linear techniques allow the transformation of existing data to a higher aspect ratio, while for lower ARs, the nonlinear effects can be added to the basic transformation (as a future code upgrade). Finally, the predicted sail drag matched test results, based on changes in vehicle axial force as a function of sail lift augmentation.

In summary, sail response to CC was within expectations, however, the prediction code CC3D needs improvement to better cover the unique behavior of extremely low aspect ratio surfaces. The only unexpected performance was the early onset of the single slot lift limit, much earlier than on the AR=2, but otherwise identical, hydrofoil model. Without laboratory identification of the geometric parameters that influence this presumed jet-wraparound lift limit, no means of prediction of the single-slot lift limit on a new planform is available. Of course, second-slot bleed has been shown to successfully extend the lift limit, however, a mass-flow saving passive means of preventing excessive turning of the Coanda wall jet is preferred.

APPLICATION IMPLEMENTATION DETAILS

SLOT FLOW VOLUME RATES

Determination of slot flow rates (gallons per minute, gpm) is straightforward once there has been identification of both the desired incremental lift coefficient (C_L) on the sail and the vessel speed at which the C_L is to be produced. Figure A-61 is a graphical depiction of flow volume and slot pressure requirements, based on the required C_μ, which is known only after the sail lift requirement has been established. Figure A-62 is a companion graph that indicates the pumping power. Both figures give results that are per square foot of sail area for the purpose of scaling and are valid for any CC planform having the nominal slot gap ratio of 0.0020. Reduction in the slot gap ratio will lower the flow volume, but will increase required pumping pressure for the same C_μ. Based on data from previous circulation control investigations, it is believed that the gap can be varied $\pm$50% without performance impact; such a change can be used to better match available pump and piping loss characteristics.

In the absence of a stated maneuvering improvement requirement from which the required C_L could be derived, one rationale for arriving at a plausible working design point is to examine efficiency in terms of lift gain per unit flow volume. Figure A-63 shows C_L as a function of flow rate, based on the predicted sail performance in figure A-4. The largest sail force per unit of flow rate occurs for a C_L of 1.0, corresponding to a C_μ of 0.08. This value of 0.08 can then be the provisional design point as it represents optimum flow volume efficiency and is in contrast to a previous, now less justifiable, design philosophy that was based simply on maximizing CC forces ($C_\mu \sim 0.25$). The required flow rate can be read from figure A-63, with linear adjustment to any speed and planform area. The corresponding sail generated force would exceed the capability of a hypothetical conventional sail that could be rotated like a rudder to an angle of 30 deg. For a pump sized to produce that value at design speed, the available C_μ would rapidly (and beneficially) increase as vehicle speed declined, due to the speed loss in a turn, for instance.

There remains the other factor governing slot pumping requirements: speed at turn initiation. Again, this requirement arises from operational specification. Pumping power requirements, for a given C_L, increase as the cube of vessel speed; as such, CC is not as practical at higher speeds. Fortunately, control force augmentation is usually needed only at very low speed, in fact, on conventional control systems, it is not uncommon to intentionally inhibit control surface authority at the higher speeds.

Returning to figure A-63 that identifies a tentative design condition for sizing a slot flow system, a mnemonic for the essence of figure A-63 is a “7/70” rule-of-thumb: at a given vehicle speed, 7 gpm of slot flow per square foot of planform projected area per knot of speed will produce 70% of the maximum practical force from a CC surface. This rule should (not verified) be applicable to any wing-like planform geometry that has the nominal slot gap ratio of 0.0020. The actual incremental force developed at the 7/70 condition would be in accordance with aspect ratio effects, as illustrated in figure A-7.

With the present CC dual-slotted foil design, at C_μ 's above about 0.10, there needs to be a small bleed flow from the second slot to restrict excessive turning of the Coanda wall-jet flow from the primary slot. As for the impact of dual slot operation on flow rates, bleed flow from the second slot is not needed at a design C_μ of 0.08. As vessel speed decays in a turn, and if the pumped flow volume remains constant, the C_μ inherently goes up to where flow from the second slot is needed to maintain efficient behavior of the Coanda wall jet. The slot flow momentum then needs to be split about 95/5% between the two slots, or it could always be split, without known adverse performance impact (reference 2). This division of flow between the two slots above C_μ = 0.10 does not necessarily raise the maximum flow rate requirements in a maneuver scenario.

A more insightful view of gpm requirements that simultaneously highlights the significance of C_L and speed is presented in figure A-64 for a full scale sail. The anticipated envelope of primary operational application is indicated. To provide a pump sizing reality reference, the flow rate of the sea water cooling system on a Military Sealift Command fleet oiler transport is 9,200 gpm; it is higher on combatant ships, reaching 170,000 on an aircraft carrier, according to public domain sources (see pages 13-16 of reference 8 for a listing of ships). In the 1990's, there was a multiyear program to develop advanced technology pumps for underwater applications, with emphasis on acoustics and compactness. These pumps were electric rim driven types and should be investigated for applicability to CC installations. If there will be a pump system dedicated to the CC sail, the intake could be on the hull near the leading edge of the sail, to assist in suppressing the horseshoe (necklace) vortex (reference 9), or in controlling leeward flow separation on the hull-sail fairing at yaw angle.

Slot nozzle gap at full scale would be about ¾ in., with a nozzle lip thickness of ¼ in. CC has been found to function satisfactorily with a wide range of lip thickness ratios, the limit at which performance is impacted is not known.

MANEUVERING SIMULATIONS

The lift requirement specification needs to come from maneuvering simulations that address operational mission needs in terms of turn diameter reduction. These simulations should, ideally, be based on a representation of incremental C_L as a function of C_μ, because vessel speed usually decays in a turn, thereby making C_μ (and, consequently, the C_L) vary in the course of the maneuver. For this situation, there exists an empirically based numerical model (CC3D) of CC performance as a function of slot pressure. That model has been incorporated into one version of a maneuvering code, for which there has been at least one demonstration run. One finding: using the sail to shorten a turn diameter does not necessarily mean that it is wise to apply the slot flow immediately at the initiation of the maneuver, because the hull may need time to first establish the center of pressure location associated with a beta or drift angle in order to better react to the additional yaw moment that can be commanded from the CC sail. A proper simulation model will be sensitive to, and thereby reveal, these implementation strategies.

Turn diameter for a conventional vessel is largely independent of speed, the steady-state diameter depends purely on control surface angular positions, since the forces from all vessel components follow the same force versus speed relationship. The force from a CC surface does not follow the conventional speed relationship, but rather follows in a manner such that, for a given slot flow rate, the turn diameter reduction benefit increases as the vessel speed slows. This relationship with speed is a desirable property, however, it does necessitate that a design speed be specified, in the form of a maneuver initiation speed, in order to determine required flow rate.

In lieu of an all-up representation of a C_L - C_μ relationship within a code, an acceptable first-look simulation could be conducted by incrementing the sail C_L by a constant amount, independent of vessel speed change. Note that this means the sail C_L will still vary in response to changes in the flow field incidence, as it should. One benefit of simulation is that the effects of the curvilinear flow field would be included. As turn diameter is reduced, the longitudinal variation in hull local flow incidence increases. The angles arising at the rudder and sail need to be monitored. A useful plot arising from any of these simulations would be percent reduction in turn diameter versus incremental C_L on the sail.

DISCUSSION AND RECOMMENDATIONS

This project has served to call attention to the benefits of an augmented-lift sail that can be used as an auxiliary maneuvering control surface. However, as intended, this was only an initial step in the gathering of information that would lead to consideration of fleet applications. There are limitations to having only a single day of data collection, such as no time to study test results to recognize subtle oddities in the data trends that would ordinarily call for test matrix refocus, or data channel verifications, or even for reaudit of the potential of the model grounding to the support sting/hoses. Hence, especially when combined with limited model instrumentation, this report is entitled "Initial Experimental Evaluation of a Circulation Controlled Sail on a Submersible Vehicle for Enhanced Maneuverability".

Two concurrent next steps are recommended, 1) use maneuvering simulations to quantify operational merit, and 2) explore existing questions about the fluid dynamics of the CC sail planform as a stand-alone model in a wind tunnel:

1) The maneuvering simulations would eventually need a full modeling of CC wherein the input specification is a control-law schedule of slot pressure variation. This can be accomplished by providing an interface for the CC performance module, known as CC3D, plus a confirmation of the handling of body-wing interference effects; the current NNemo-1 data would be useful for validation purposes.

2) An important goal of the recommended sail-as-a-wing test would be to obtain the precise C_L versus C_μ data necessary to rectify what now appears to be an inadequacy in the empirical modeling of CC performance for aspect ratios less than 2. The nature of the current underprediction of CC sail performance suggests that CC lift incurs a beneficial nonlinear response to slot flow similar to that noted in the C_L-AOA response of conventional-lift wings of extremely low aspect ratio. (The issue is illustrated in figure A-7 by placing a straight edge to the

AR=2 and AR=1 response curves; envision the x-axis as being C_μ, rather than AOA.) Additionally, of paramount importance, is to have an experimental setup that allows a hands-on determination of exactly what predisposes CC wings to encounter single-slot lift stall. Until the causative geometric factors are identified, future CC applications, especially those requiring a dual-slotted symmetrical geometry to provide bidirectional lift, will remain vulnerable to unexpected early lift rollover. Finally, performance sensitivity to variations in the internal flow feed to the slot nozzle is in need of examination, duct inlet and interior flow conditioning design is long overdue for study. Other objectives of the sail-alone experiments would be directed toward gaining insight into possible design refinements, in support for later use of the same model components on a hull in water, either on a carriage or free running. Use of small tip end-plates in the trailing edge region is one example of an exploratory refinement to reduce flow rate requirements.

There are secondary modes of slot operation that can have additional maneuvering benefits. If a slot is segmented and valved such that a portion of the slot span can be shut off, then there is a vehicle deceleration mode wherein lift-induced drag can be developed without net production of sail side force. This is accomplished by alternating to port/starboard along the span which slot segment is active (reference 10, for the CC Duct). In addition, at zero or very low forward vehicle speed, applying simultaneous differential pressures to the port/starboard slots will produce a controllable thrust-vectoring effect over nearly 0-360 deg (reference 2).

Experiments will eventually be necessary with a body-of-revolution hull shape, because it is expected that some of the body/appendage/sail interactions will be different from those found on the NNemo-1 hull form. One use of future data is to confirm that the interaction effects modeled in current maneuver codes can correctly deal with a high lift sail on a circular hull wherein the rudder is in alignment with the sail. Ultimately, free-running tests will be required to encompass the effects of a curvilinear flow field and provide data for control-law development.

CONCLUSION

The technical conclusions of the project are located in the SUMMARY section on page ii.

REFERENCES

1. Joslin, R. D. and Jones, G. S., editors, (2006), *Applications of Circulation Control Technology*, Volume 214, Progress in Astronautics and Aeronautics, 623 pages, Lu, F. K., editor-in-chief, American Institute of Aeronautics and Astronautics, Inc. Reston, VA. ISBN 1563477890.

2. Rogers, E. O. and Donnelly, M. J., "Characteristics of a Dual-Slotted Circulation Control Wing of Low Aspect Ratio Intended for Naval Hydrodynamic Applications," AIAA 2004-1244, 42nd Aerospace Sciences Meeting, Reno, NV, Jan 2004. DTIC ADA436473.

3. Abramson, J., "Two-Dimensional Subsonic Wind Tunnel Evaluation of a 20-Percent-Thick Circulation Control Airfoil," DTNSRDC, ASED 311, Jun 1975.

4. Englar, R. J. and Williams, R. M., "Test Techniques for High Lift Airfoils with Boundary Layer and Circulation Control for Application to Rotary Wing Aircraft," Canadian Aeronautics and Space Journal, Vol. 19, No. 3, pp. 93-108, Mar 1973.

5. Campbell, I. J., et al., "Aerodynamic Characteristics of Rectangular Wings of Small Aspect Ratio," ARC, RM No. 3142, Dec 1956.

6. Bridges, D. H., et al., "Experimental Investigation of the Flow Past a Submarine at Angle of Drift," AIAA Journal, Vol. 41, No. 1, Jan 2003.

7. Mackay, M., "A Review of Submarine Out-of-Plane Normal Force and Pitching Moment," DRDC Atlantic, Technical Memorandum TM 2004-135, Aug 2004.

8. "Seawater Cooling Overboard Discharge," "Uniform National Discharge Standards," DOD/EPA, unds.bah.com/Nod/sew_cool.pdf.

9. Philips, D. B., Cimbala, J. M., Treaster, A. L., "Suppression of the Wing-Body Junction Vortex by Body Surface Suction," Vol. 29, No. 1, Jan-Feb 1992.

10. Imber, R. I., "Exploratory Investigations of Circulation Control Technology: Overview for Period 1987-2003 at NSWCCD," NASA/CP-2005-213509 PT2, Proceedings of the 2004 NASA/ONR Circulation Control Workshop, Compiled by G.S. Jones and R.D. Joslin, Mar 2005. NTRS Document 20050196645 (Part of 20050196628).

APPENDIX A
FIGURES

Page No.

Page No.

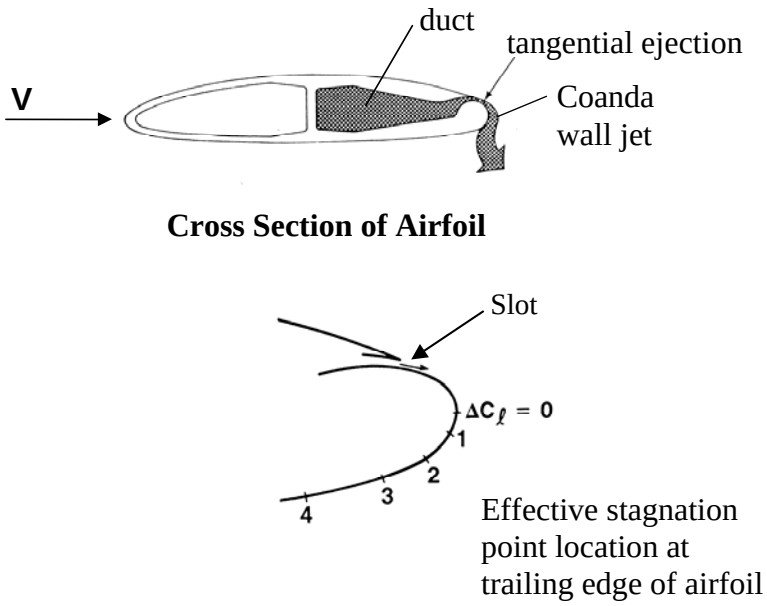

Figure A-1: Circulation control airfoil configuration: rounded trailing edge with tangential mass ejection from a slot; single-slot implementation shown. A change in effective stagnation point location increments lift as indicated.

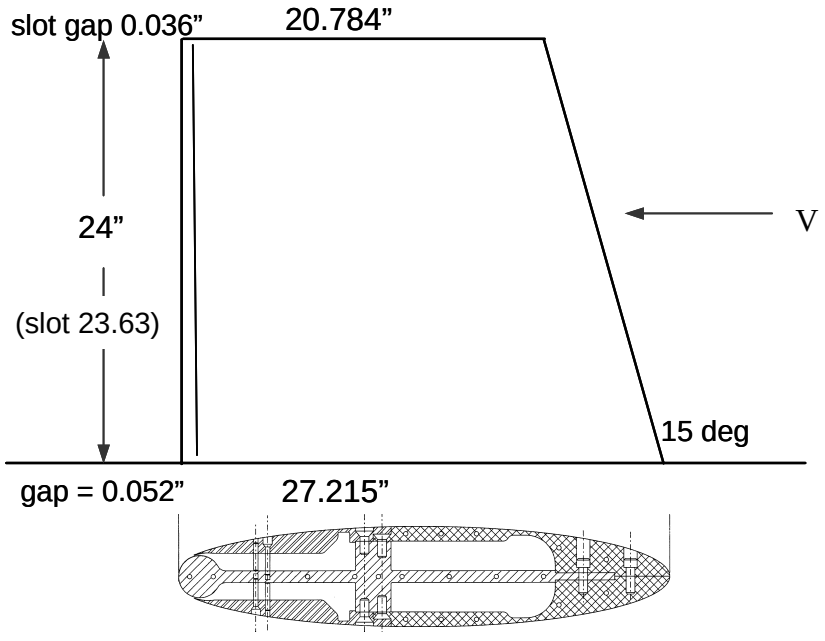

Figure A-2: Planform geometry and cross-section of a dual-slotted hydrofoil wing evaluated in 2002 (reference 2). Dual slots allow bidirectional force control.

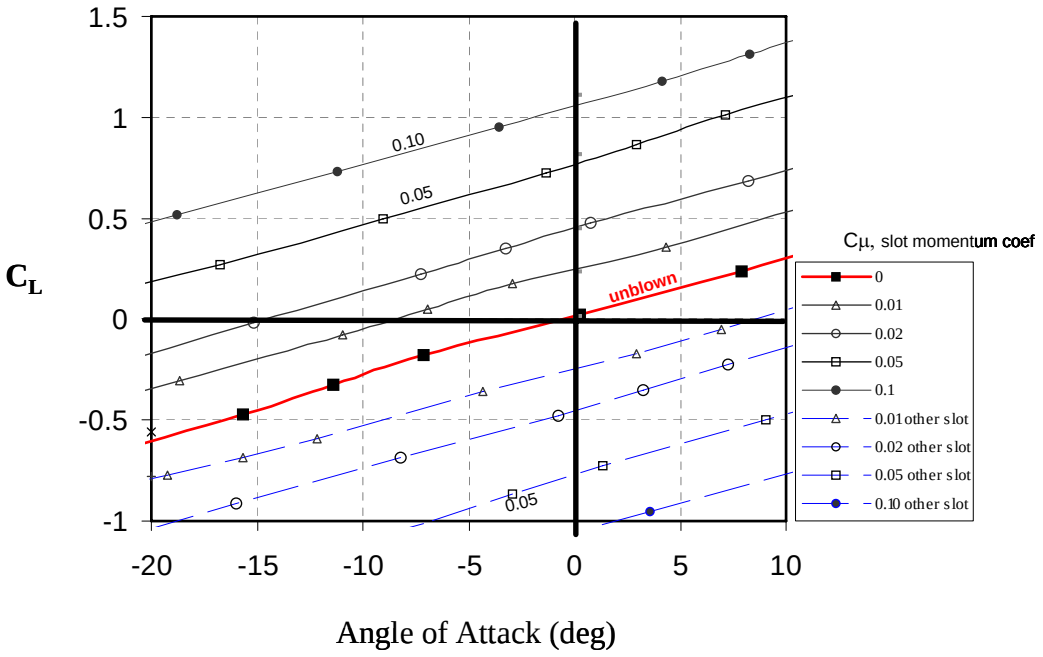

Figure A-3: Predicted performance map of a CC control surface of effective reflected aspect ratio of 1 (rectangular sail).

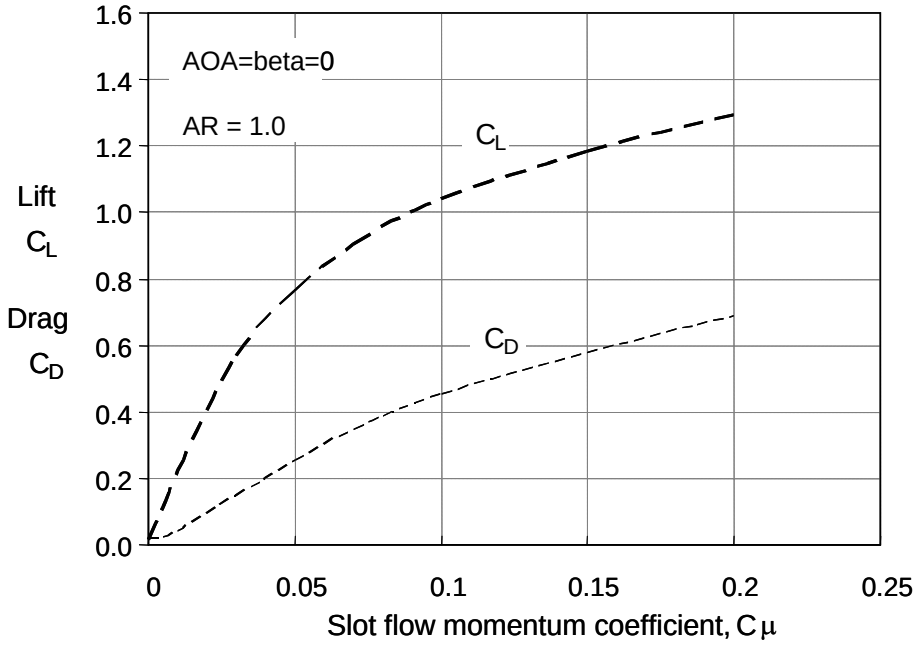

Figure A-4: Expected incremental lift on a CC sail at zero angle of attack. Slot flow momentum coefficient, C_μ, is linearly proportional to slot nozzle pressure.

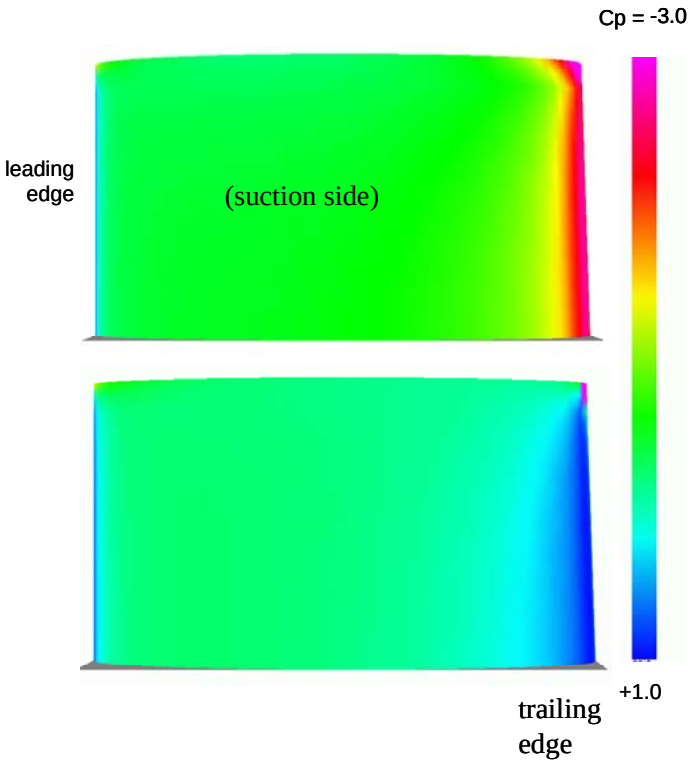

Figure A-5: Calculated pressure distribution for a sail planform while developing lift from CC (at zero pitch angle). The pressure loading develops primarily in the trailing edge region, due to low aspect ratio effects. Code: VSAERO.

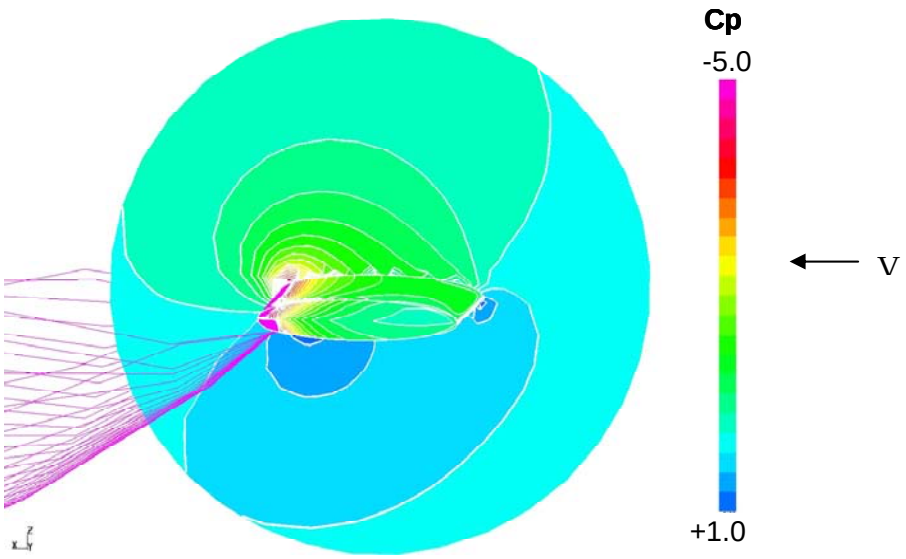

Figure A-6: Wall-imposed pressure field from a high-lift wing mounted on a wall. VSAERO computation. Planform shown in figure A-2.

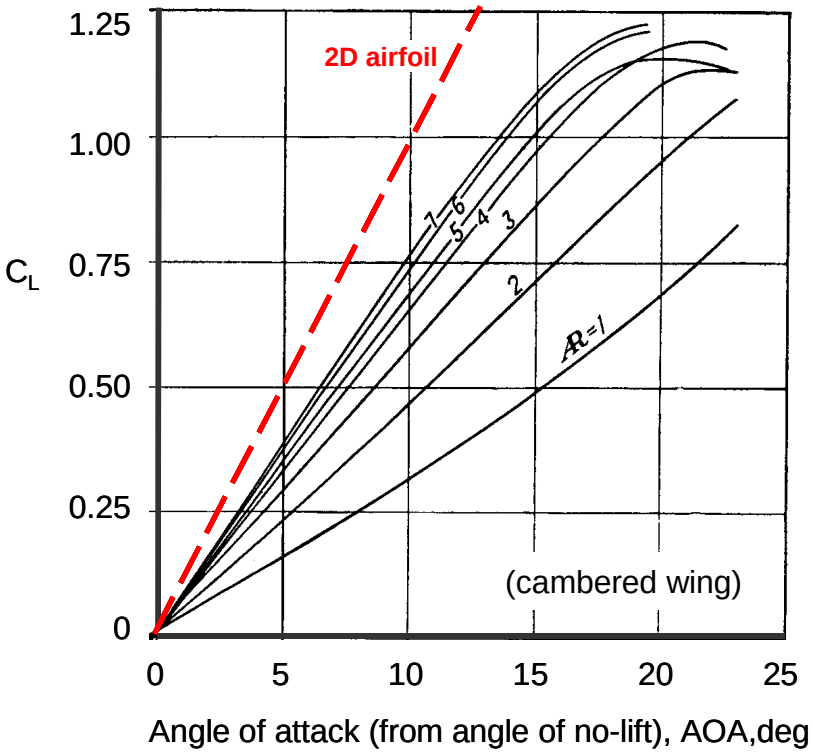

Figure A-7: Aspect ratio effects for conventional wings: a reduction in C_L-AOA slope. Similar reduction would occur for C_L versus C_μ. (Source: Prandtl's data for a cambered wing with a no-lift AOA of -5 deg).

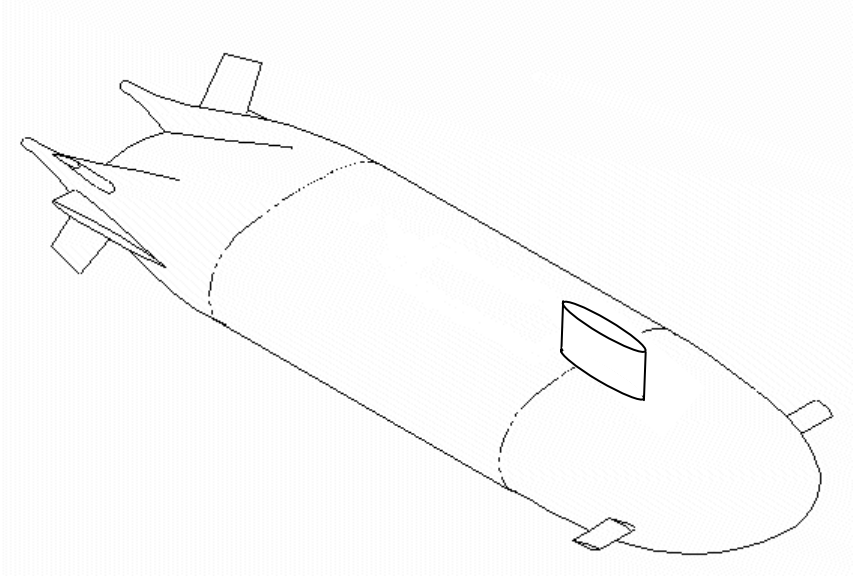

Figure A-8: Sketch of NNemo-1 configuration with CC sail.

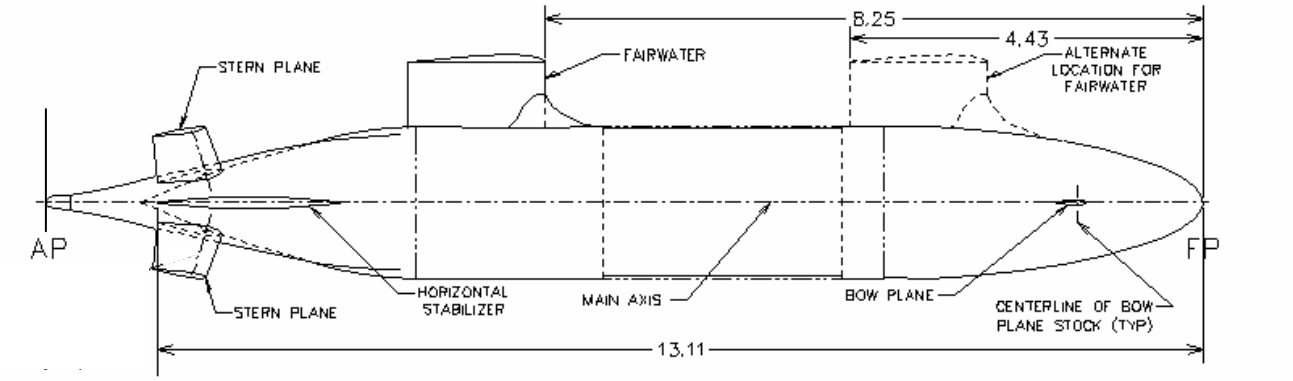

Figure A-9: NNemo-1 configuration, showing two options for sail location. CC sail was forward and without the hull juncture fairing. (Dimensions in feet, AP to FP is 14.50.)

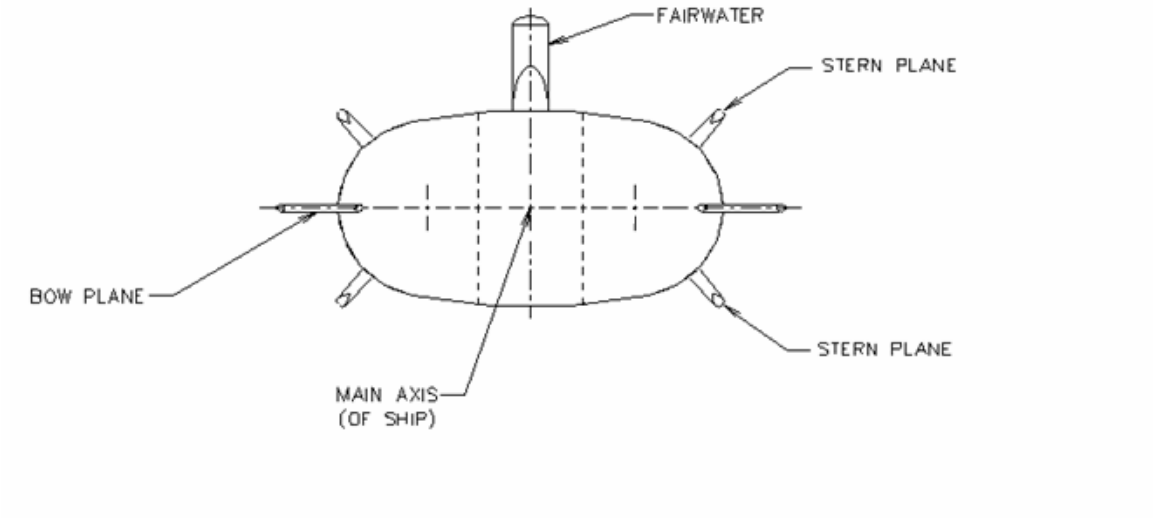

Figure A-10: Front view of NNemo-1.

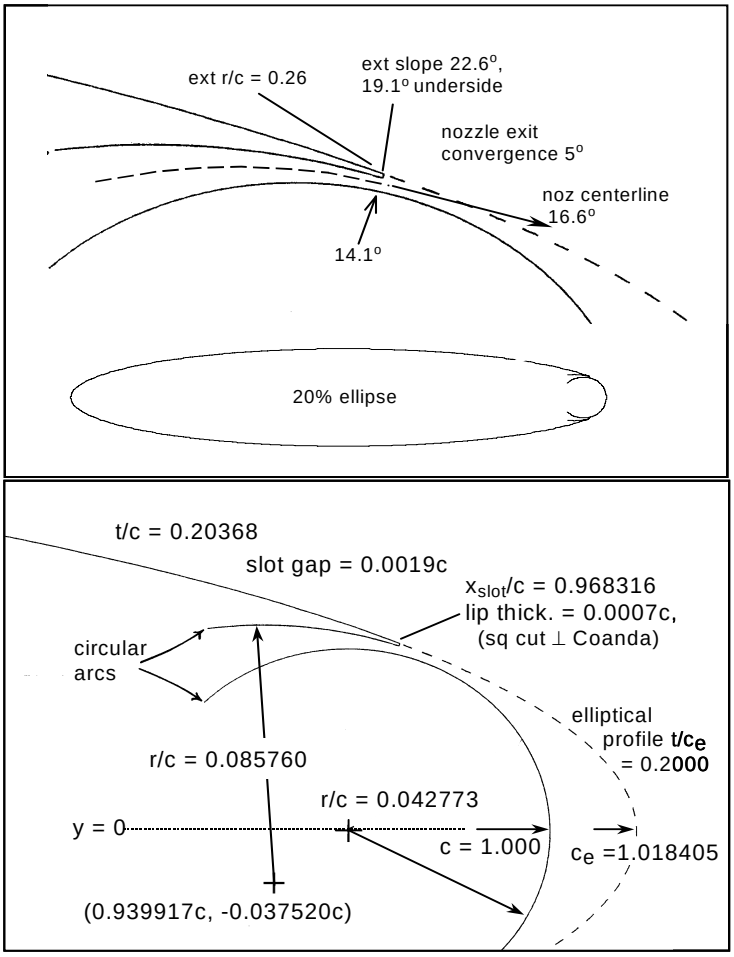

Figure A-11: Definition (nondimensional) of the CC sail cross-section. Derived from an elliptical profile of 20% thickness.

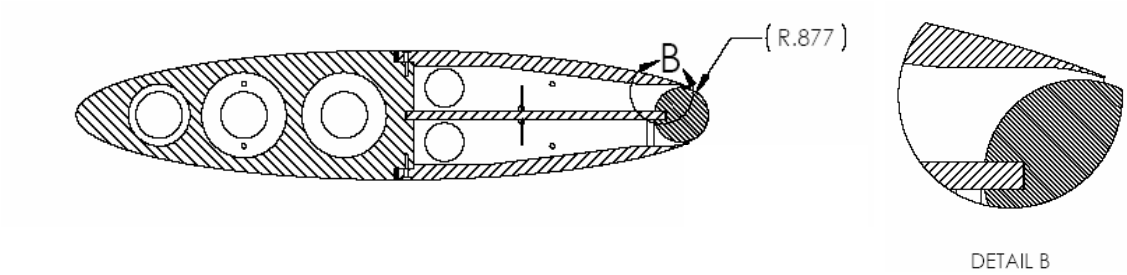

Figure A-12a: Model construction details, cross-section cut.

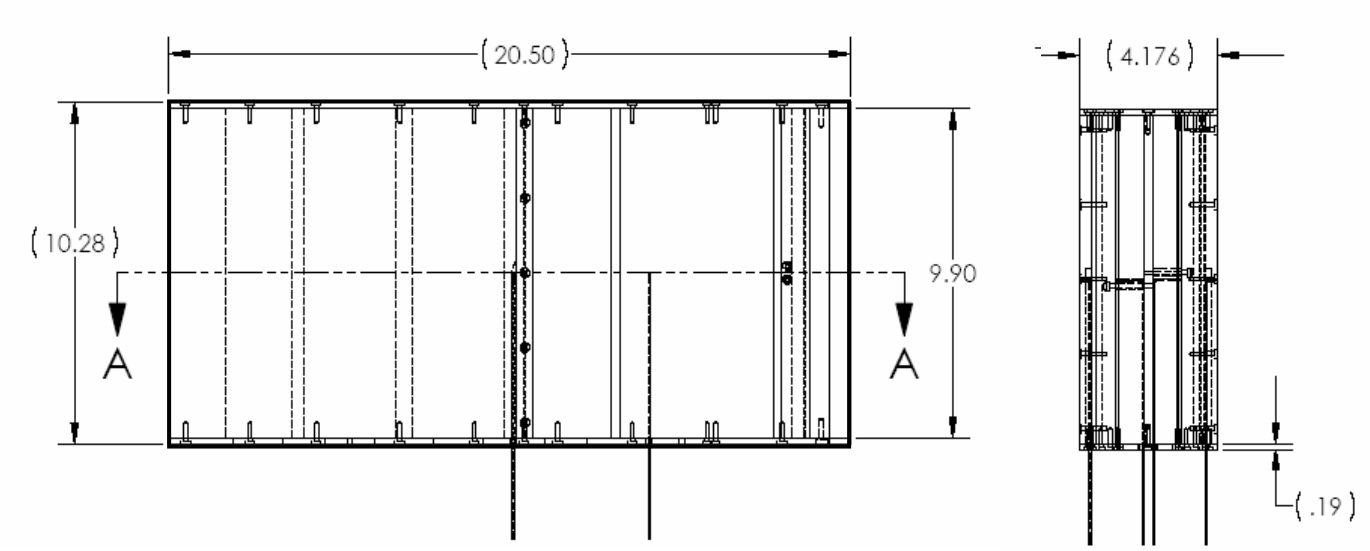

Figure A-12b: Model construction details, side and front. (Dimensions in inches.)

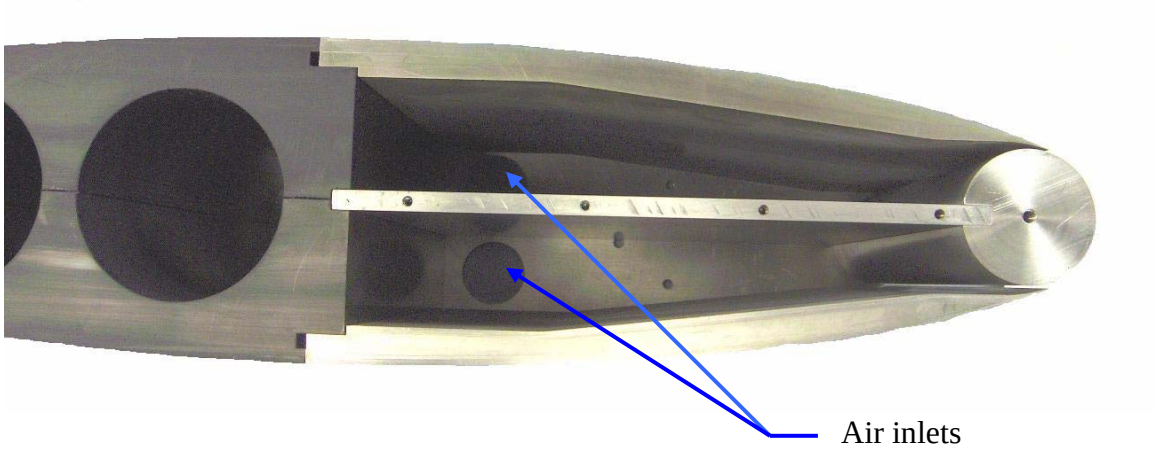

Figure A-13: Photograph of initial assembly check shows air inlet at far end; large openings to the left are for weight reduction. Forward half of the sail is PVC plastic, aft half is anodized aluminum.

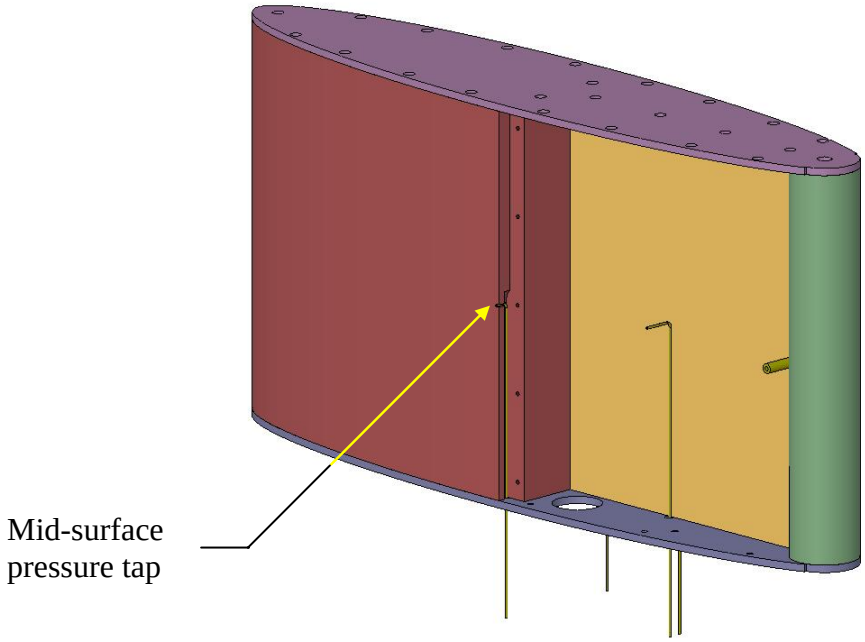

Figure A-14: Sail graphic with slot nozzle plate removed. Mid-model surface pressure tap and interior probe shown.

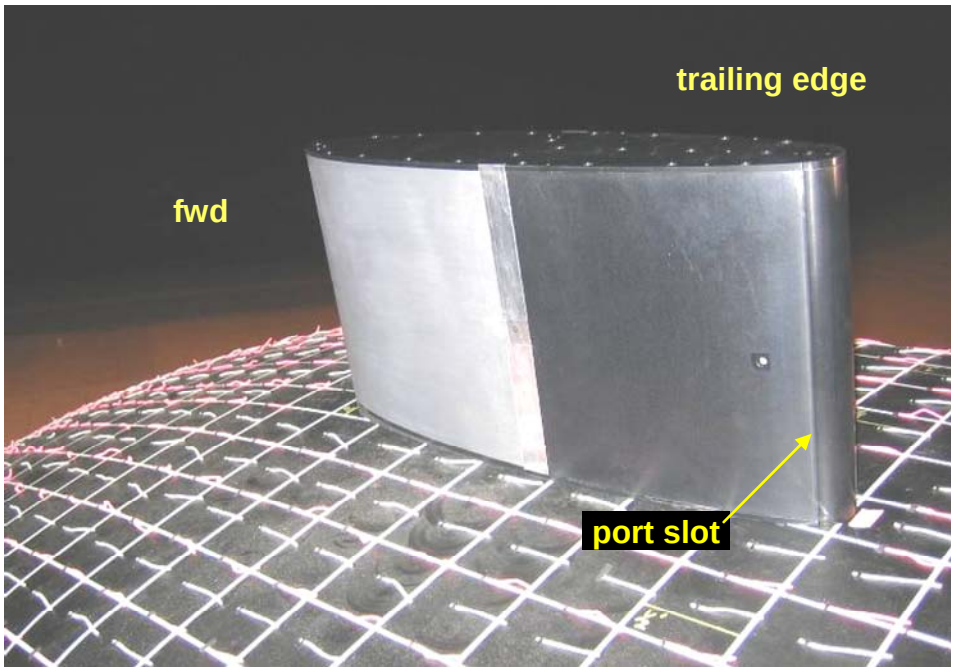

Figure A-15: Placement of the CC sail on the NNemo-1 hull.

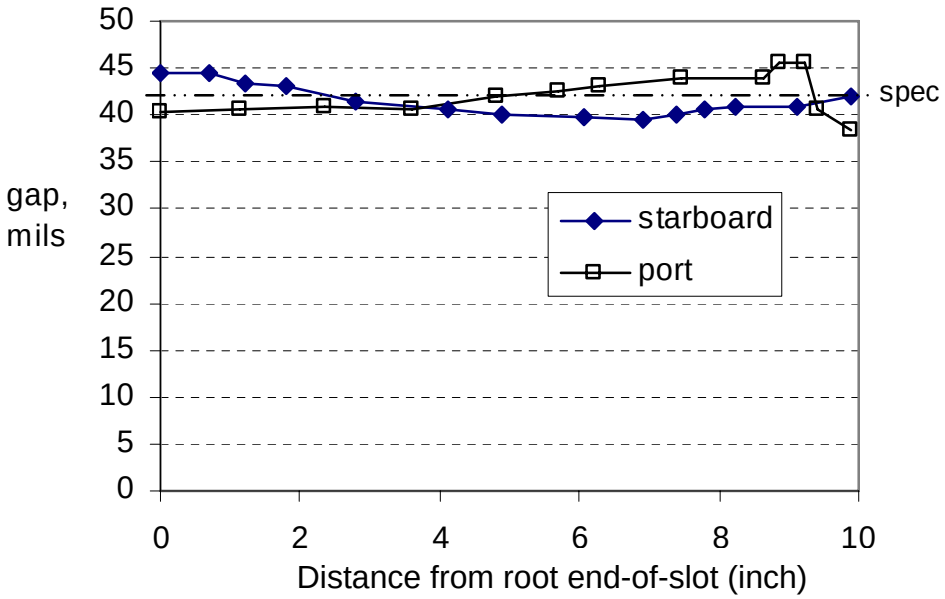

Figure A-16: Slot gap spanwise variation.

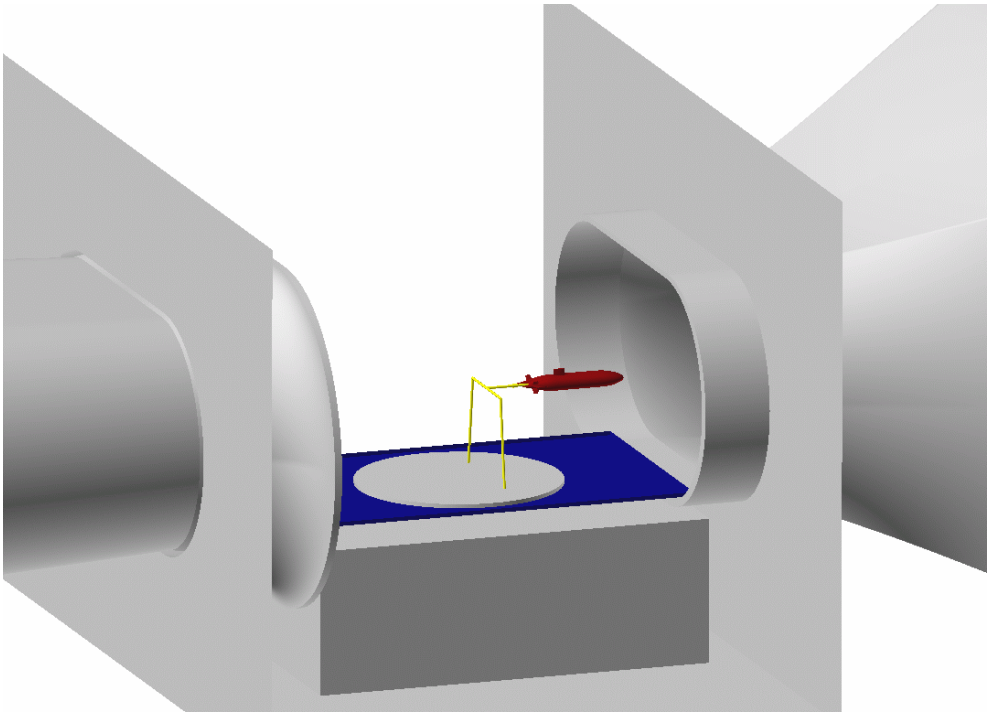

Figure A-17: Schematic of test section emplacement.

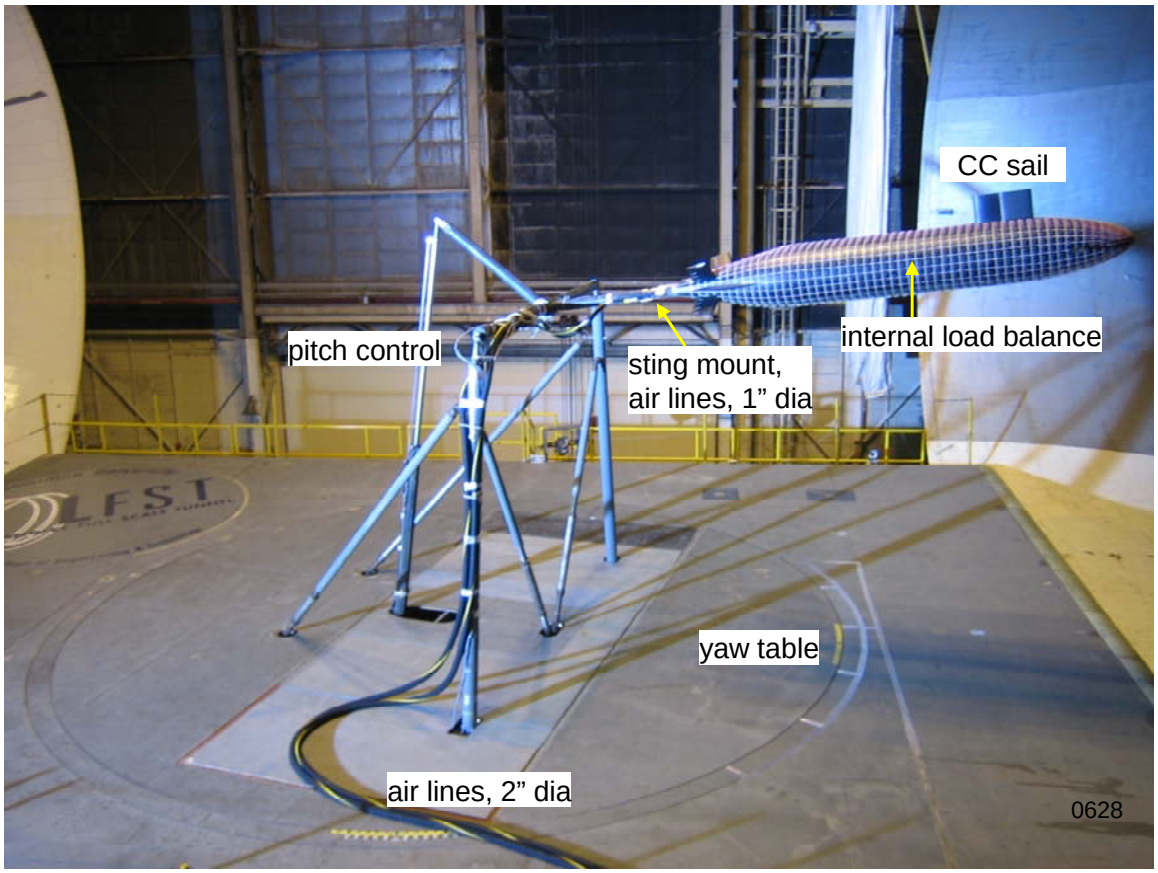

Figure A-18: NNemo-1 model mounting and test setup details.

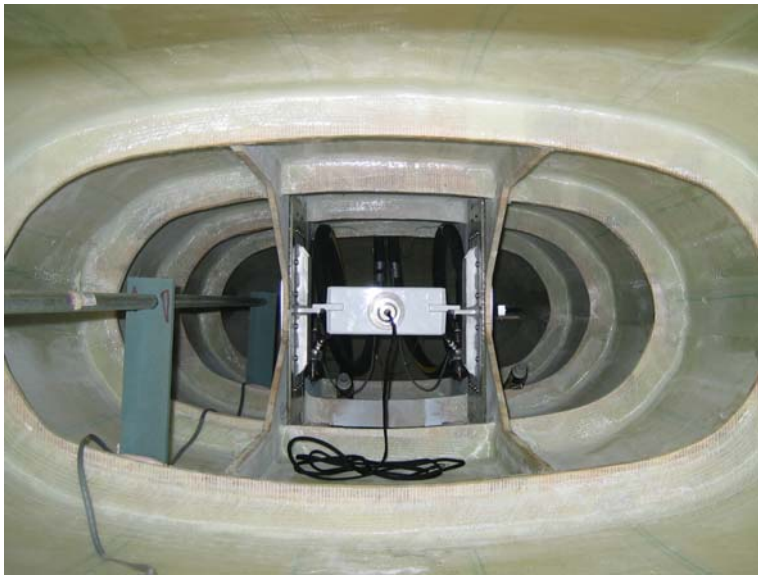

Figure A-19: Photograph of 6-component internal balance on hull centerline.

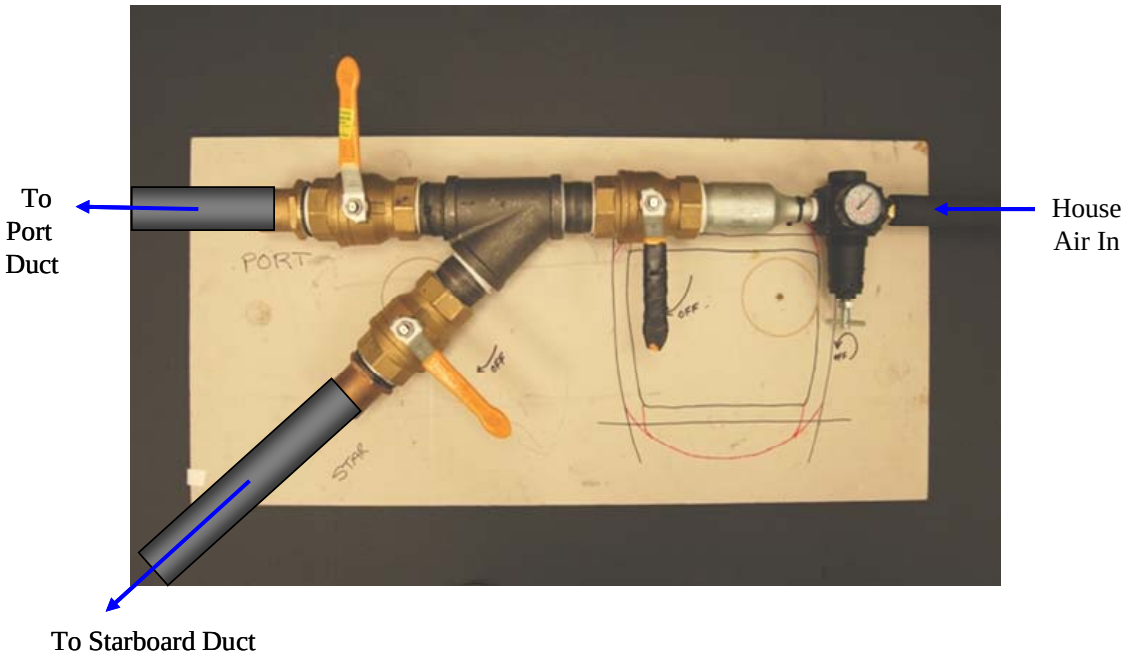

Figure A-20: Supply air plumbing and control arrangement.

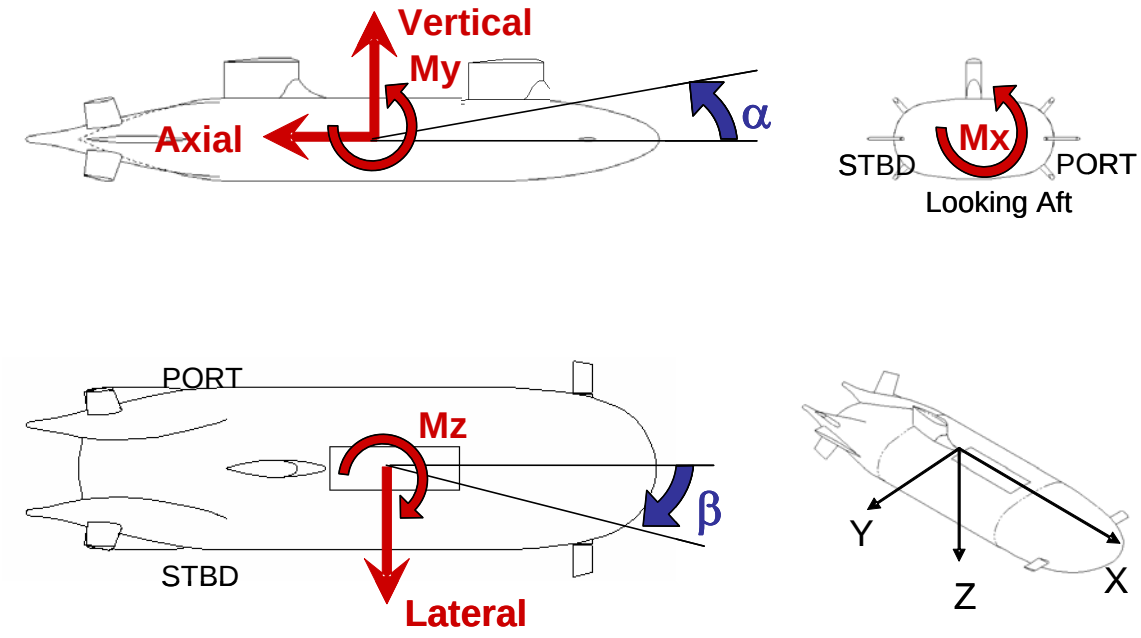

Figure A-21: Wind tunnel axis system, heavy red arrows denote positive sense for recorded data. For reference only, the XYZ Cartesian system commonly used in hydrodynamics is also shown.

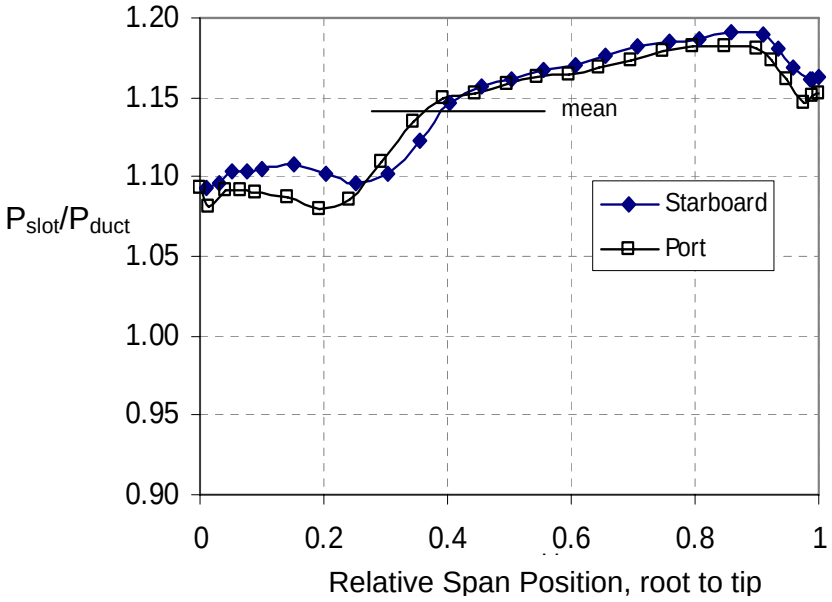

Figure A-22: Slot exit pressure survey, in ratio to pressure sensed by the internal pressure probe.

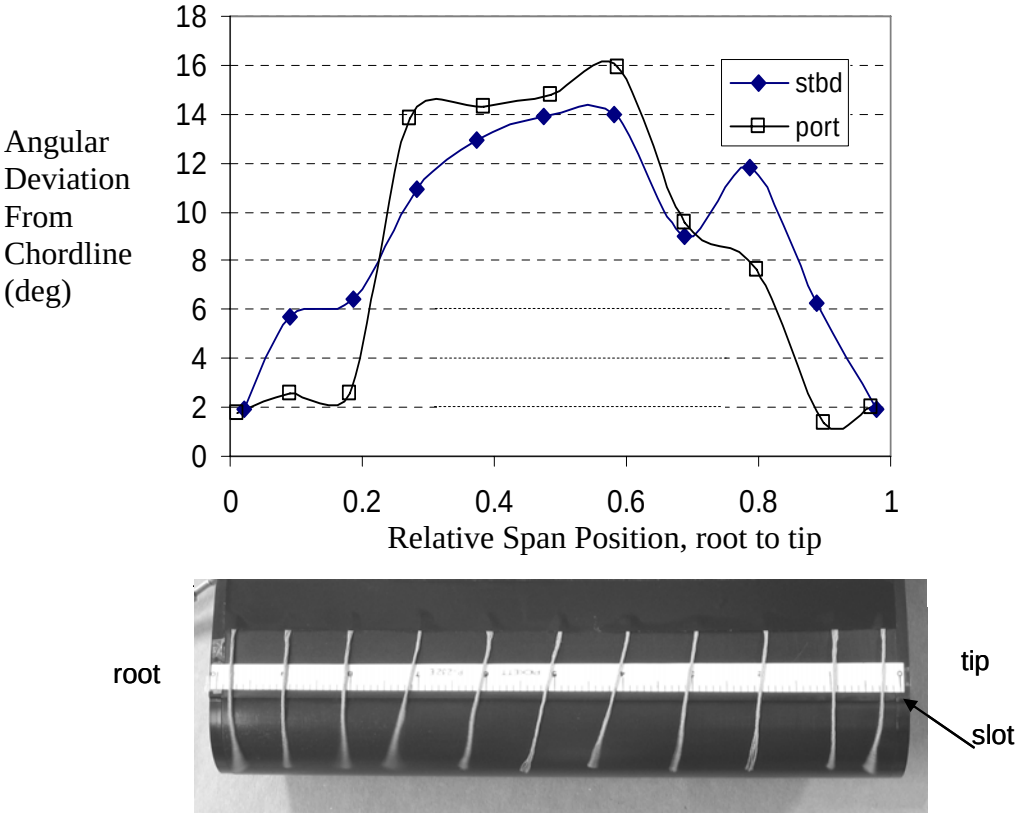

Figure A-23: Survey of wall jet skew angle, arising from spanwise component of flow (toward the root) within the model duct cavity.

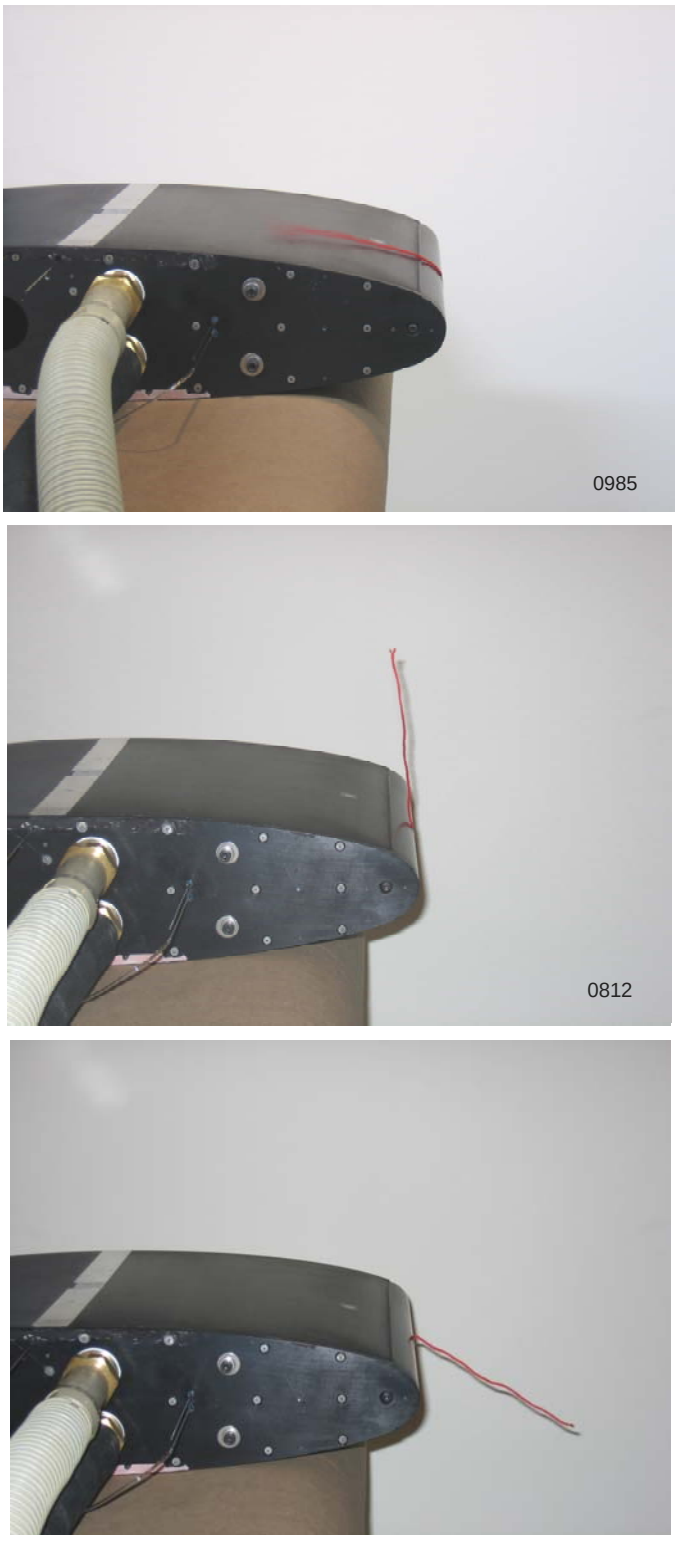

Flow out lower slot only

Flow out lower slot with slight flow introduced from upper slot

Slightly more flow out of upper slot

Figure A-24: Bench evaluation of dual slot operation in absence of an external flow. Red yarn tuft illustrates ability to control the angle of (thrust-vector) the free-jet sheet that results from the merger of the two wall jets.

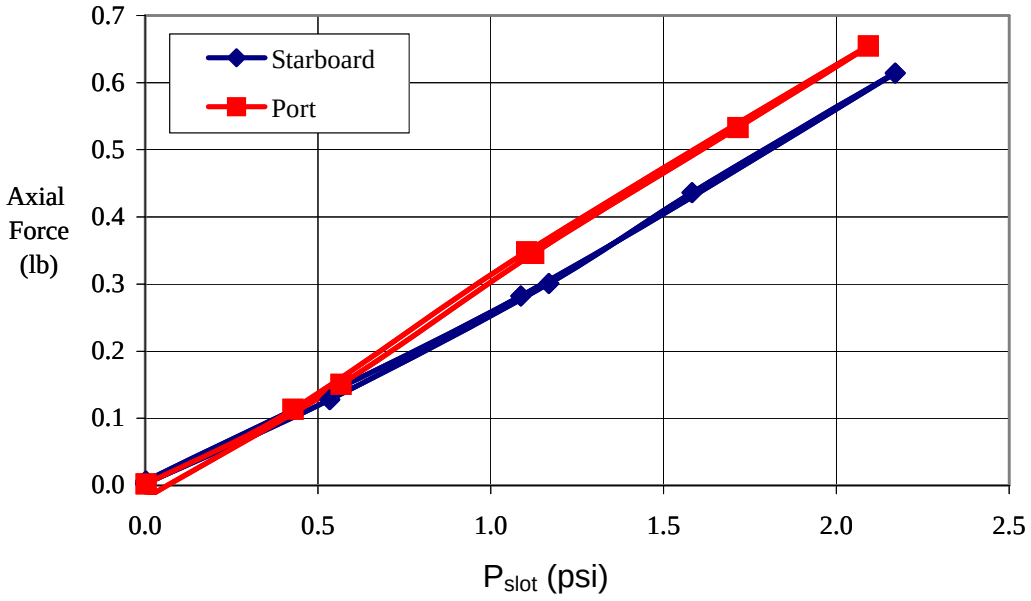

Figure A-25: Static freestream (wind off) evaluation of single slot operation. A backward thrust (positive axial force) is demonstrated due to the jet turning around the Coanda trailing edge.

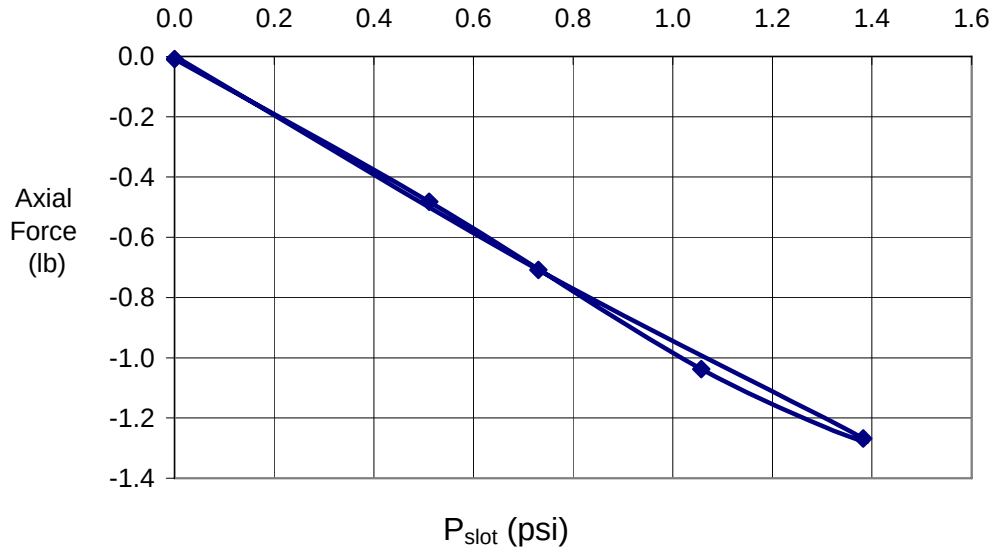

Figure A-26: Static freestream (wind off) balance readings with both slots operating at equal pressure. A forward thrust is produced.

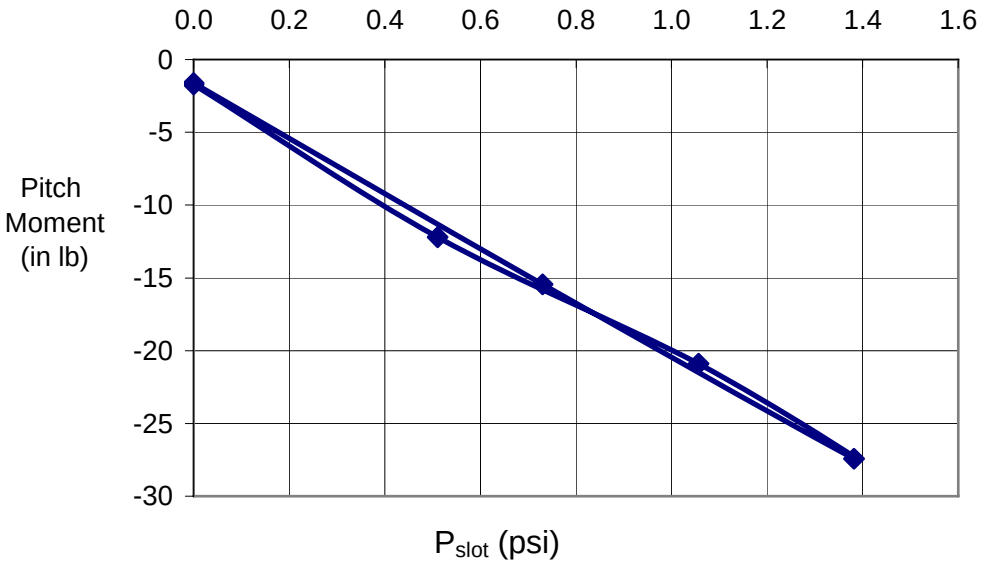

Figure A-27: Static freestream (wind off) balance readings with both slots operating at equal pressure. A nosedown pitch moment is produced.

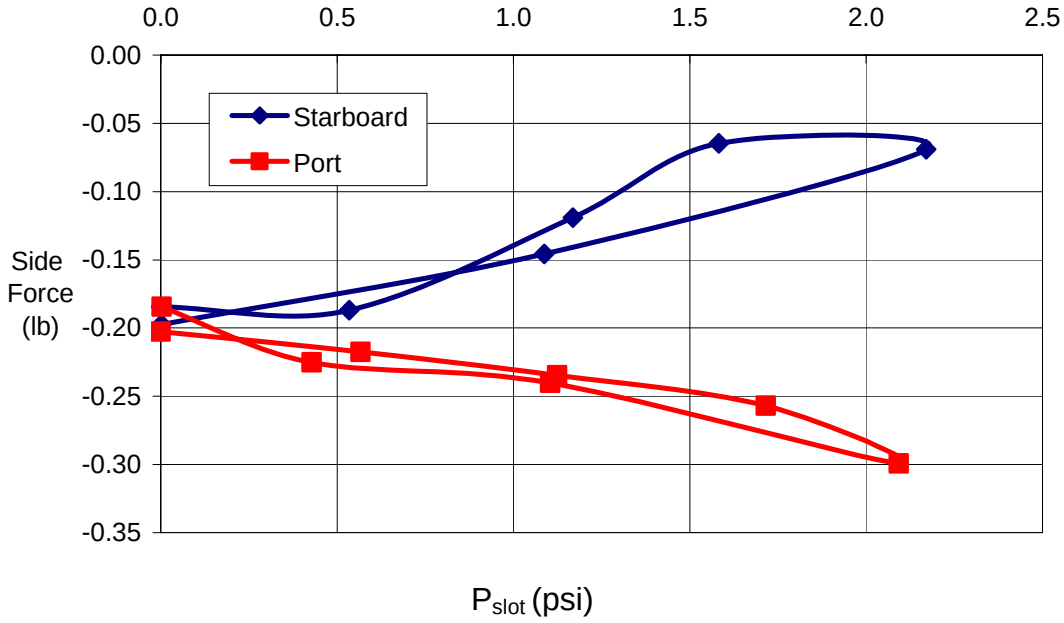

Figure A-28: Static freestream (wind off) evaluation of single slot operation. The small component of side force indicates a 170-deg wall jet deflection. (Data zero offset was not corrected for this plot).

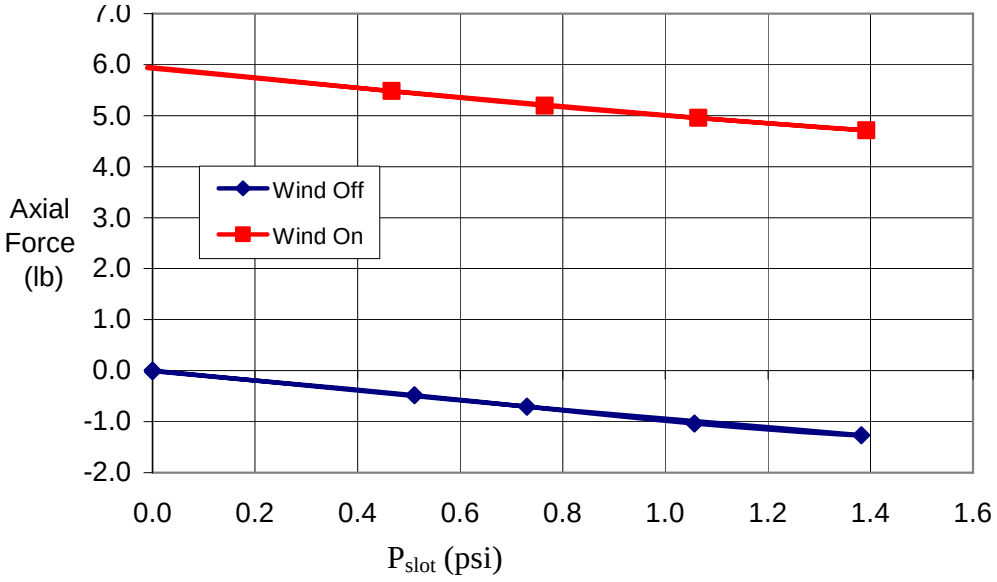

Figure A-29: Influence of wind-on for dual slot operation. Static thrusting level is preserved and equates to a corresponding reduction in drag.

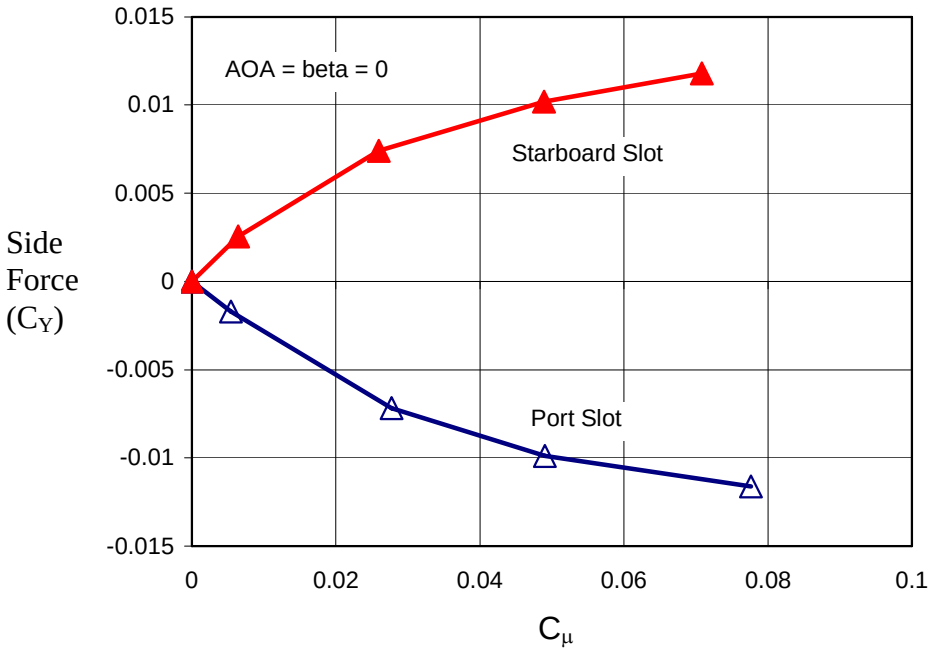

Figure A-30: Maneuvering side force developed by the CC sail at zero angles of pitch and yaw.

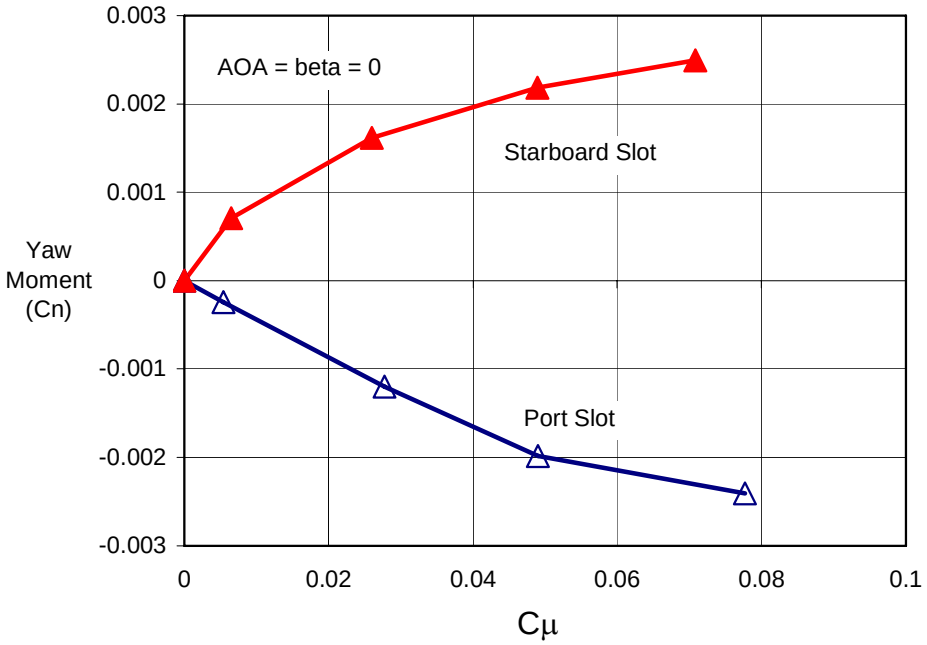

Figure A-31: Yaw moment corresponding to figure A-30.

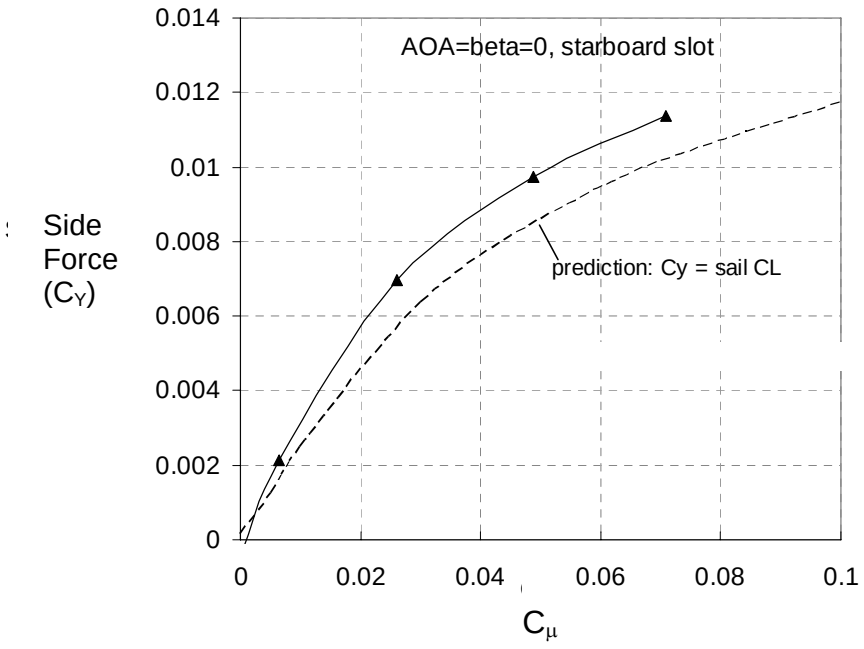

Figure A-32: Test data from figure A-30 with superposition of pretest expected results, under the assumption of no contributions from the body.

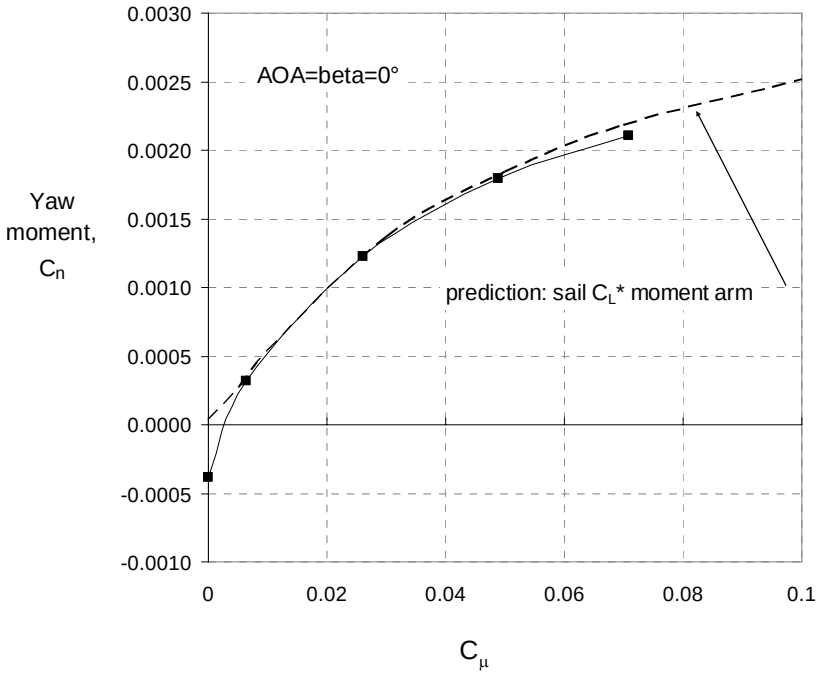

Figure A-33: Test data from figure A-31 (yaw moment) with superposition of pretest expected results if there were no body effects.

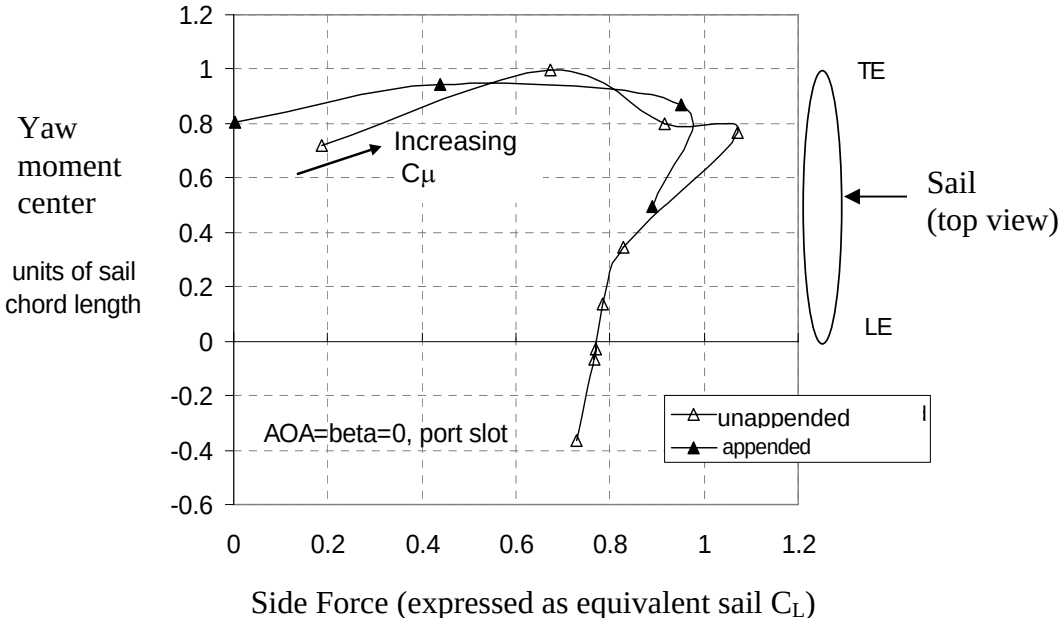

Figure A-34: Longitudinal center of side force in relation to sail chord. The location of the yaw moment center is as expected for an isolated CC wing. Location is in reference to the sail leading edge, positive aft.

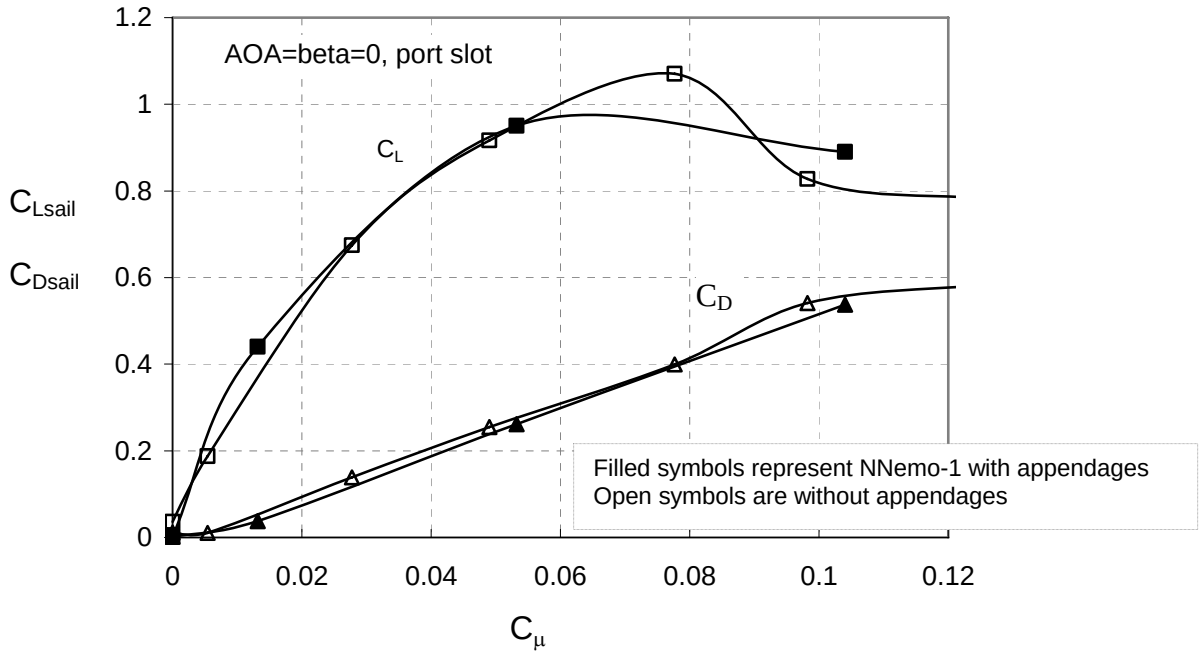

Figure A-35: Derived sail performance (C_L and C_D) is independent of the presence of the aft appendages.

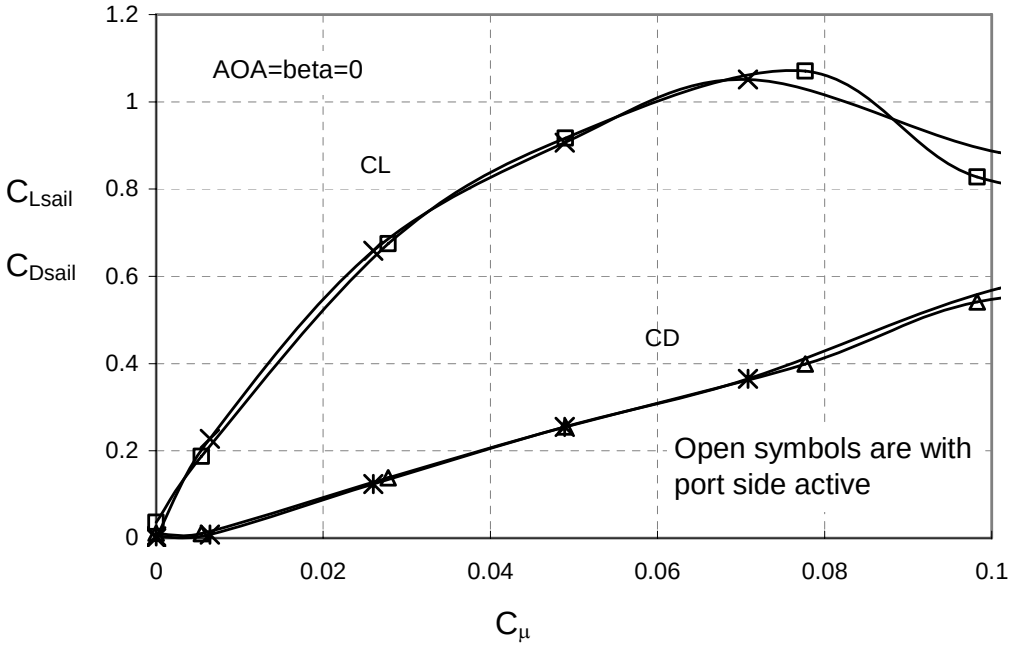

Figure A-36: Confirmation of identical performance for the port and starboard slots.

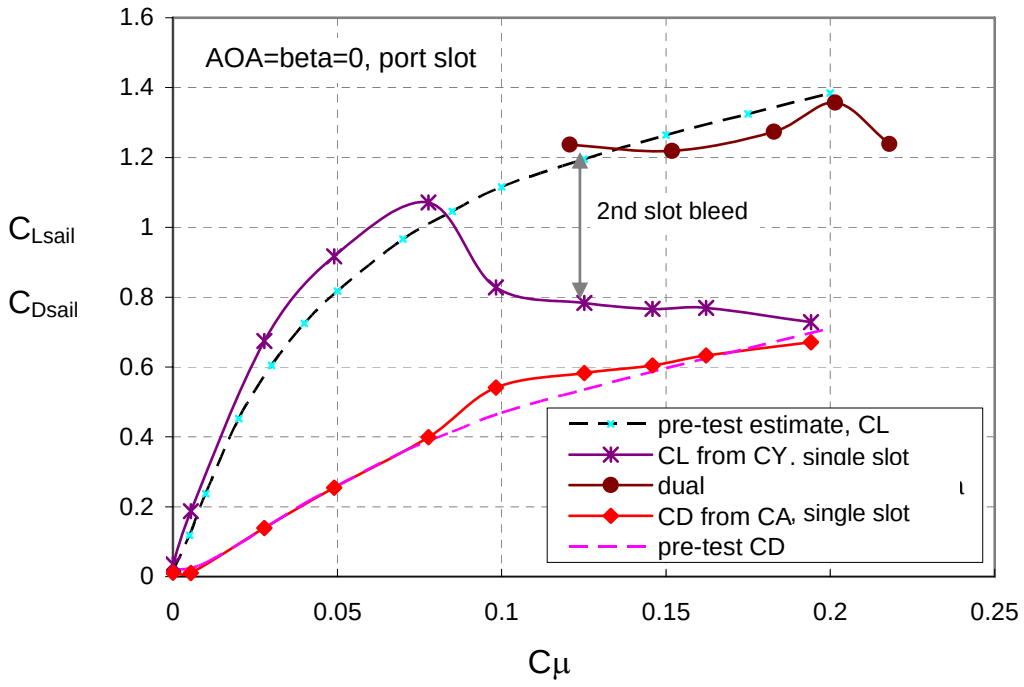

Figure A-37: Influence of enabling second-slot bleed flow on single-slot lift stall. Post-stall lift is restored to expected level.

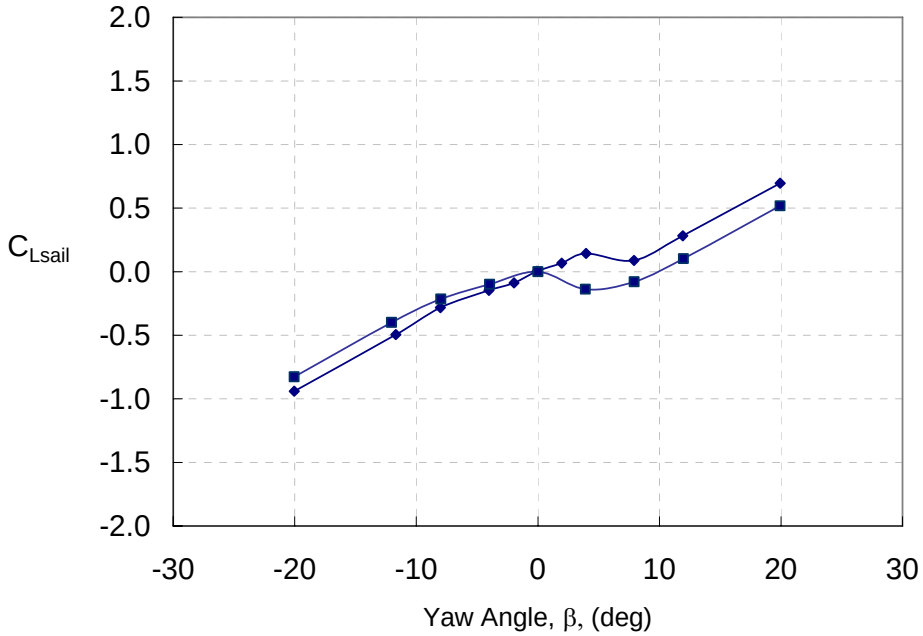

Figure A-38: Unblown lift coefficient estimate based on mid-surface pressure differential. Data are from two separate beta angle sweeps.

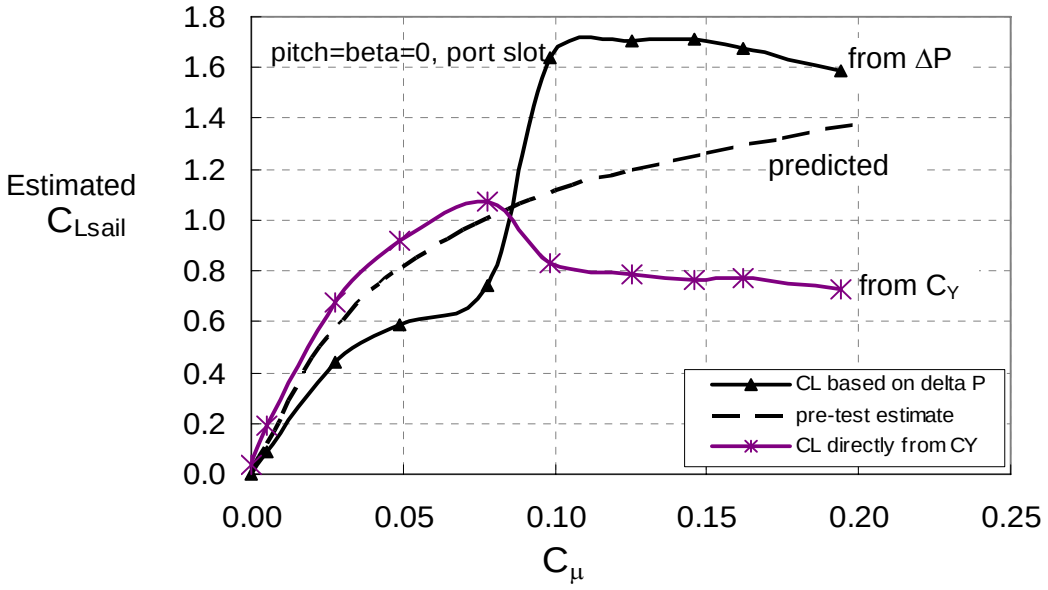

Figure A-39: Lift coefficient estimate based on mid-surface pressure differential. Obvious deviations are present.

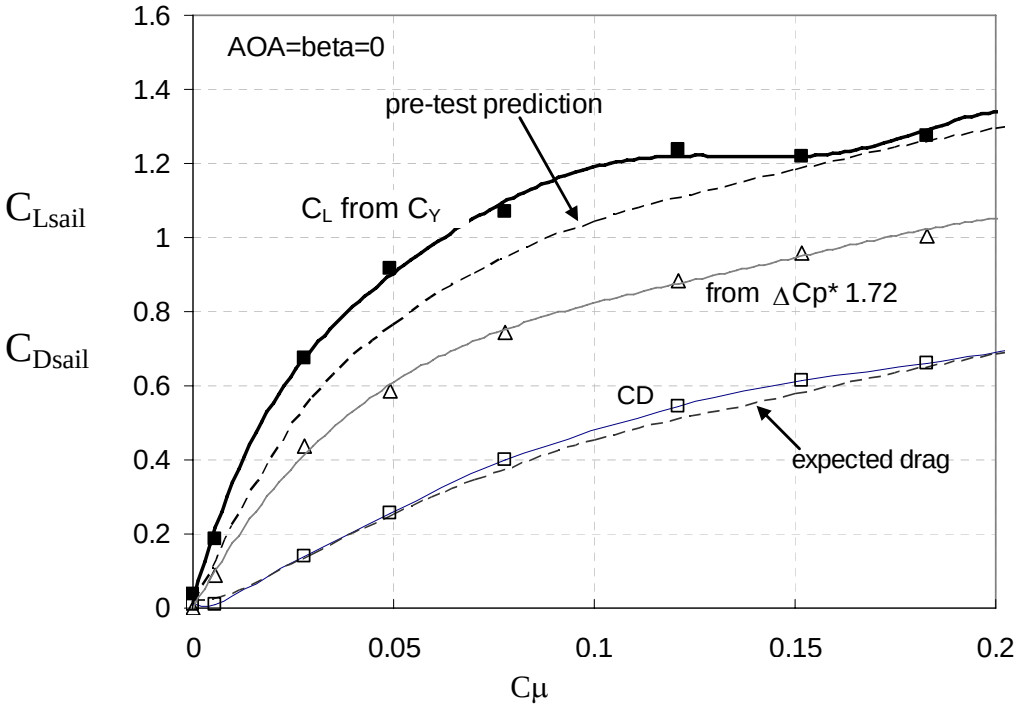

Figure A-40: Perspective on the assessments of sail response to slot flow. Data sets have been concatenated so that the jet wraparound stall data are replaced by dual slot flow data.

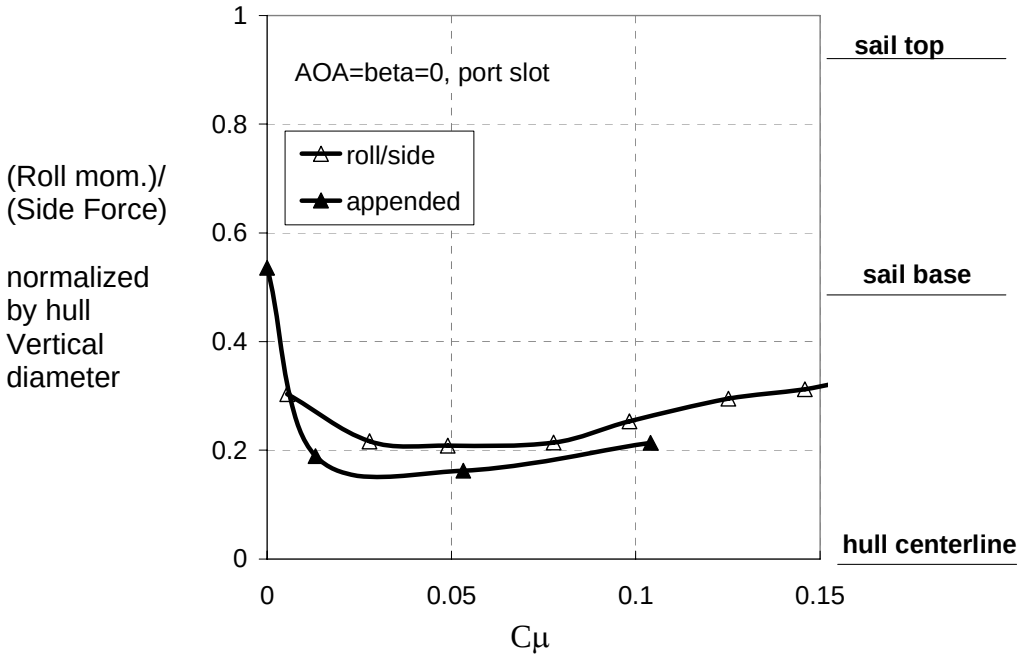

Figure A-41: Roll moment center in relation to hull diameter.

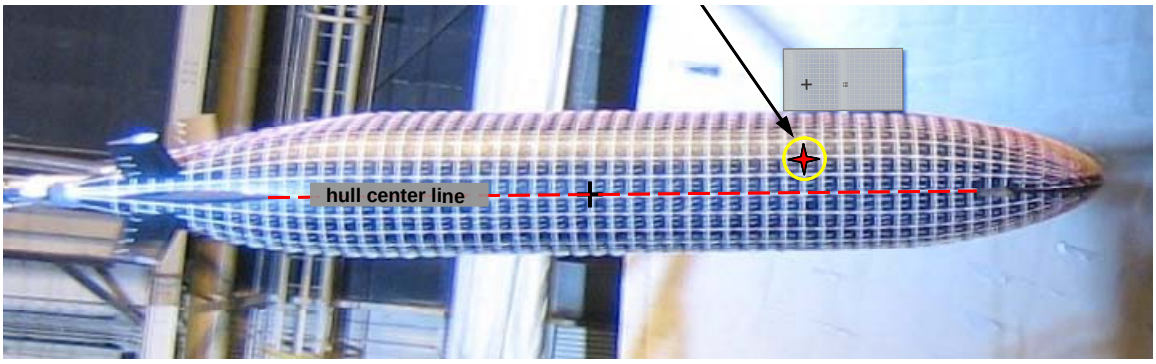

Figure A-42: Location of side force center of action at zero pitch and zero drift angle with active flow control present.

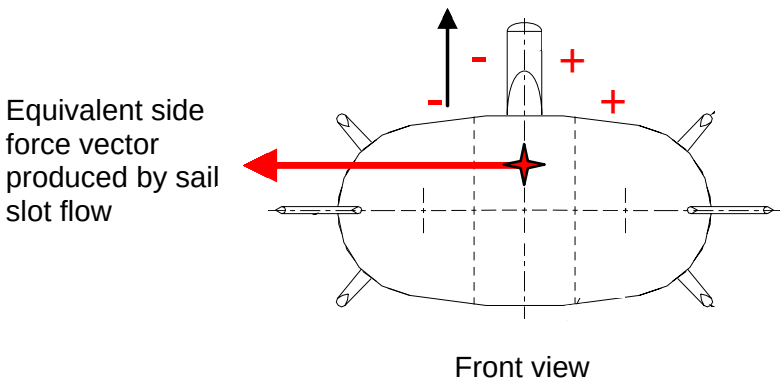

Figure A-43: Illustration of how the pressure imposed by the sail onto the hull will cause a counter-roll contribution by the non-axisymmetric hull of the NNemo-1 model.

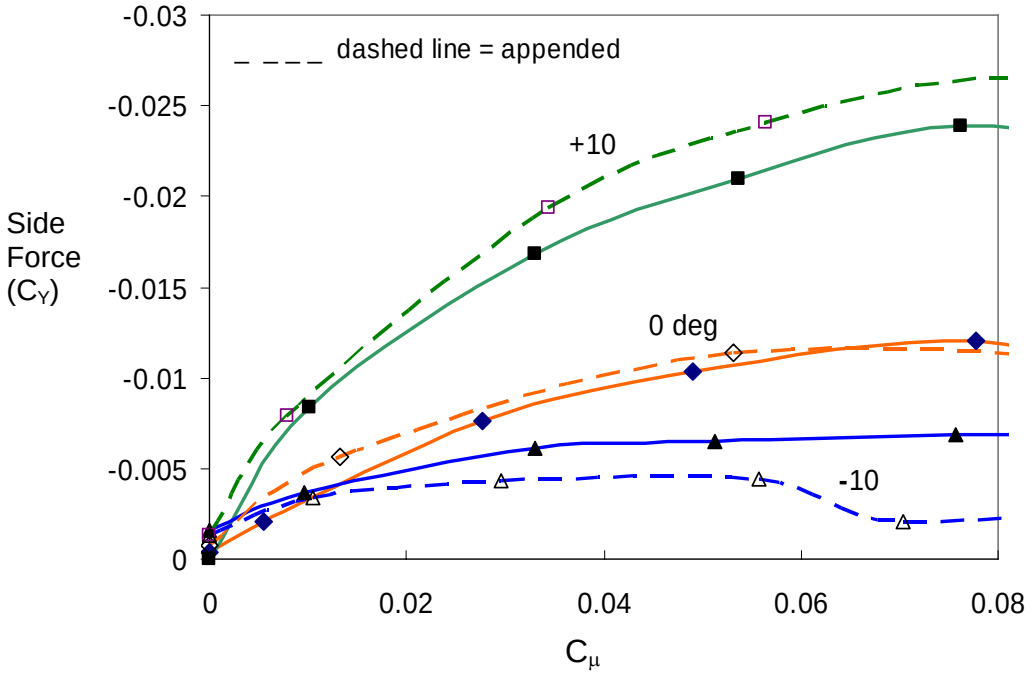

Figure A-44: Side force for three pitch angles, with and without stern appendages. Zero drift angle.

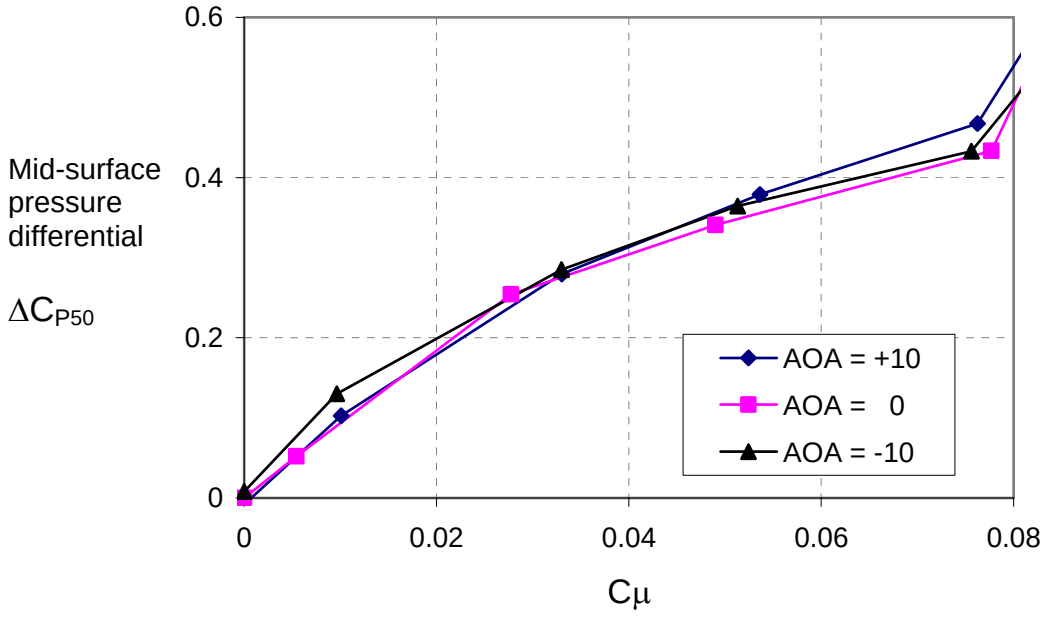

Figure A-45: Sail pressure loading consistency with respect to hull pitch angle.

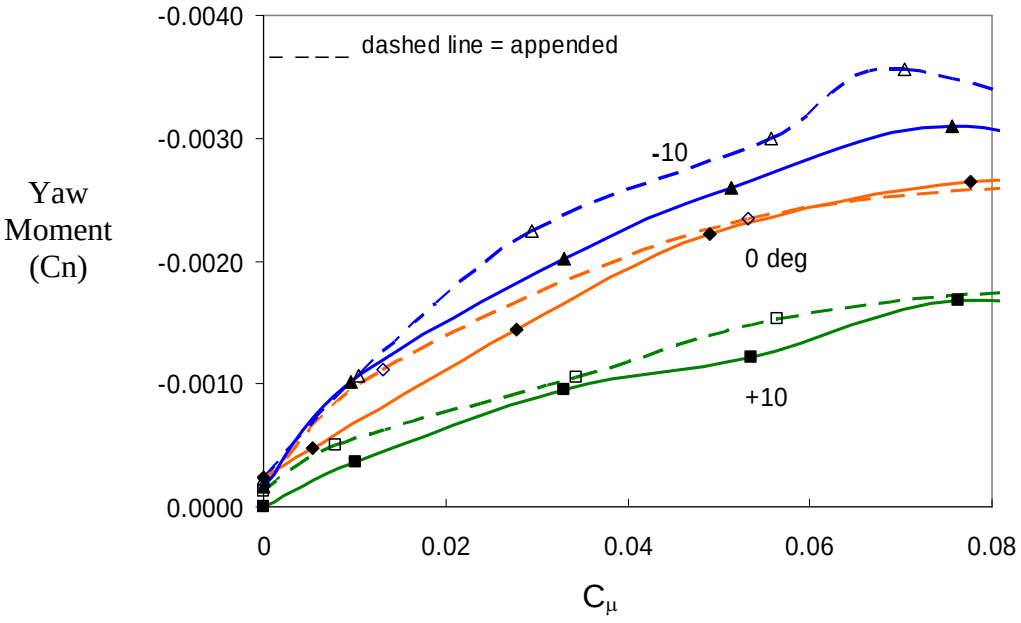

Figure A-46: Yaw moment for three pitch angles, with and without stern appendages. Zero drift angle.

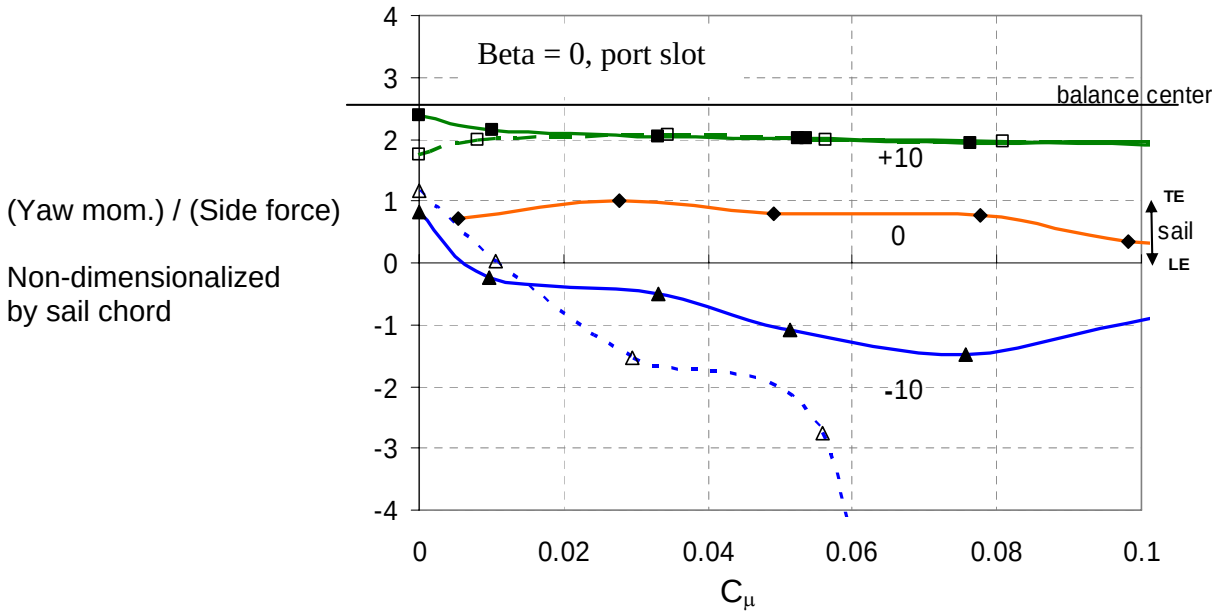

Figure A-47: Changes in location of the center of the net side force indicates the role of the sail-body interaction at nonzero pitch angles.

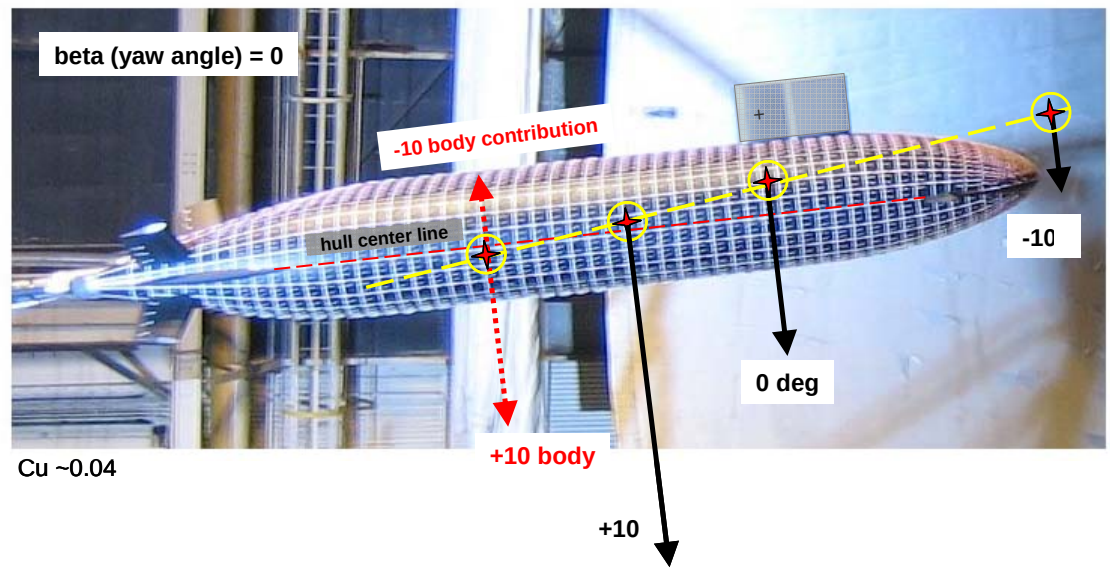

Figure A-48: Net side force vectors resulting from sail CC as a function of pitch angle, in the horizontal (y-axis) plane, scaled to magnitude. Dashed vectors are the inferred contributions from the hull. Zero drift angle.

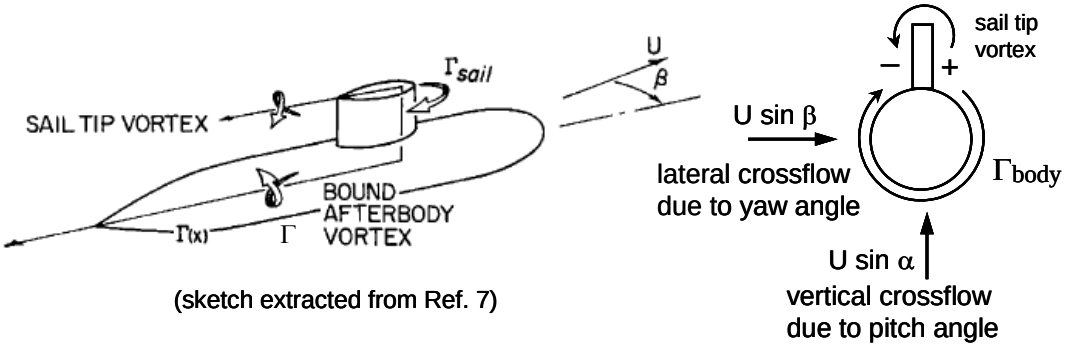

Figure A-49: Origin of body forces: the sail-induced afterbody circulation reacts to lateral or vertical crossflow, a body force arises perpendicular to the crossflow component: = ρ Γ V.

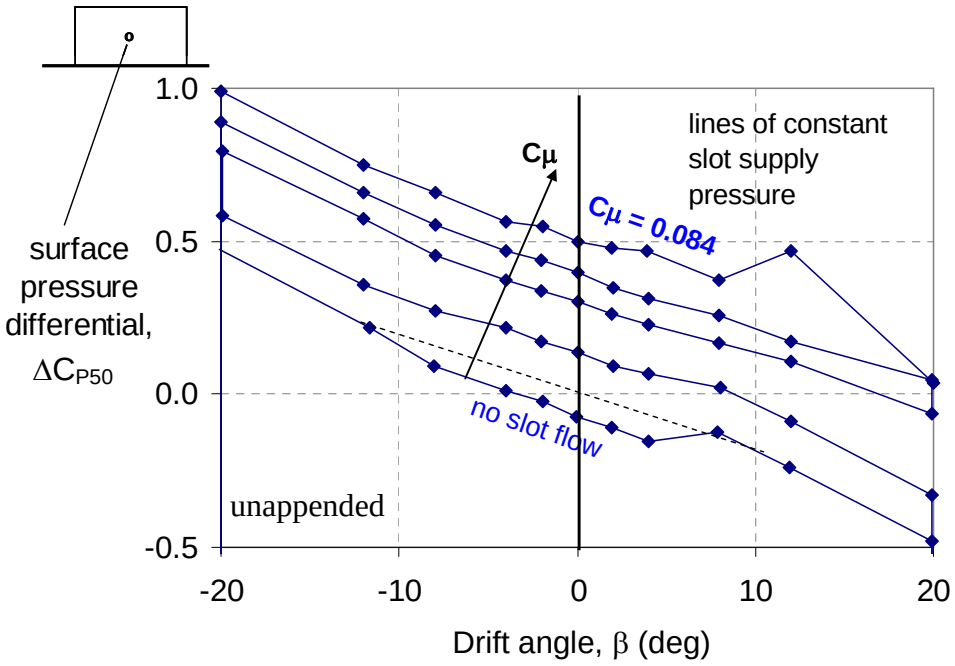

Figure A-50: Consistency of sail circulation performance over the full beta range, based on mid-surface pressure differential.

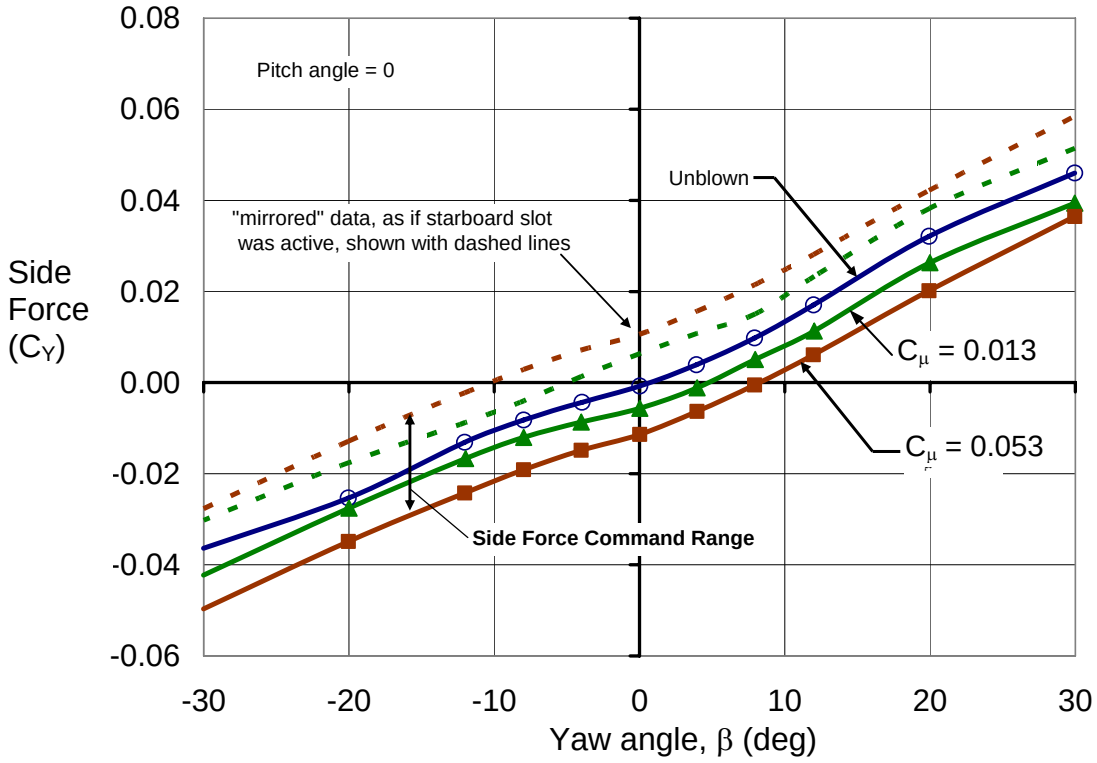

Figure A-51: Side force coefficient with drift angle (beta).

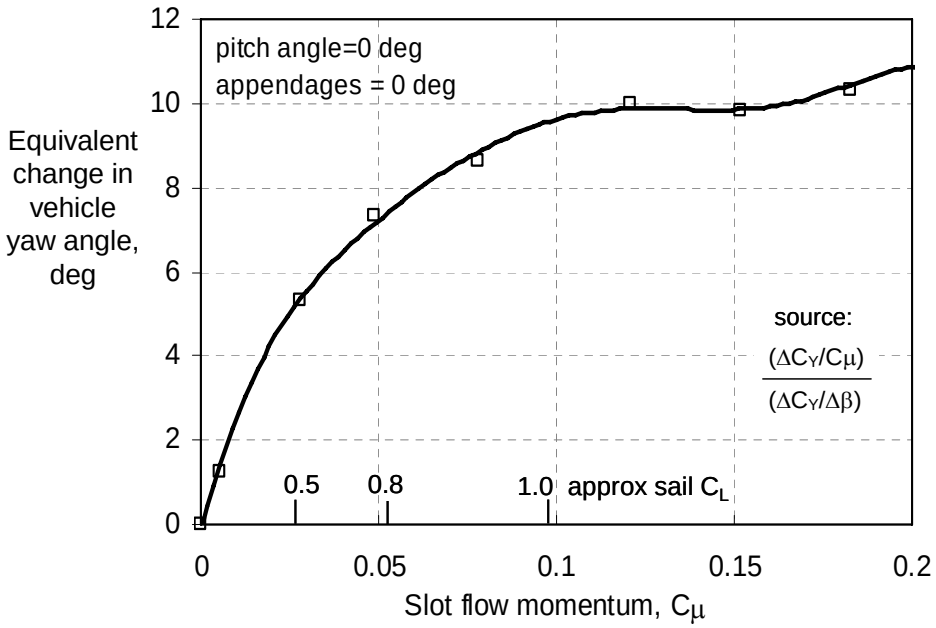

Figure A-52: CC sail maneuvering force effectiveness viewed as an equivalence to yawing the fully appended vehicle to a sideslip angle. Estimated incremental sail lift coefficient due to slot flow is noted.

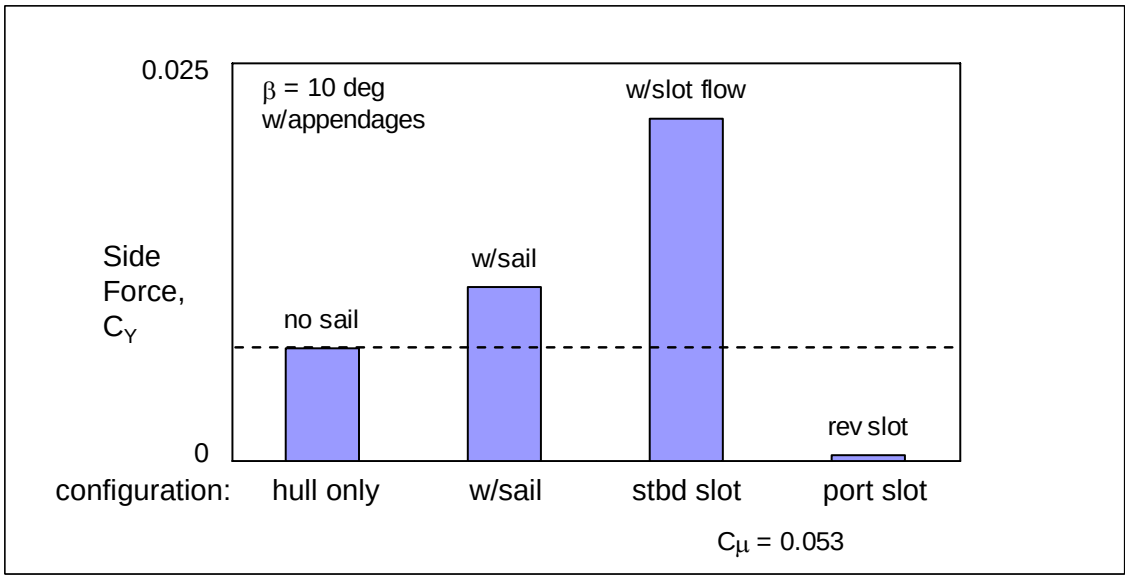

Figure A-53: Relative contributions to lateral control force at yaw angle of 10 deg. Buildup from hull alone to inclusion of a CC sail with moderate slot flow rate and then with slot valving switched for turn-force reversal.

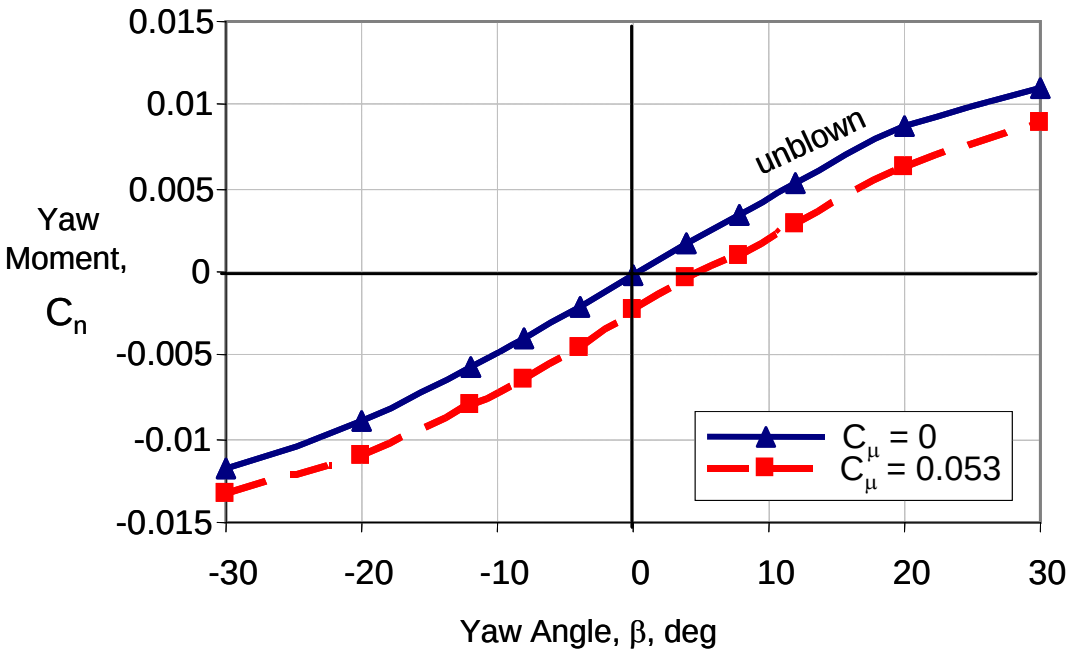

Figure A-54: Yaw moment response to slot flow, port-side slot active.

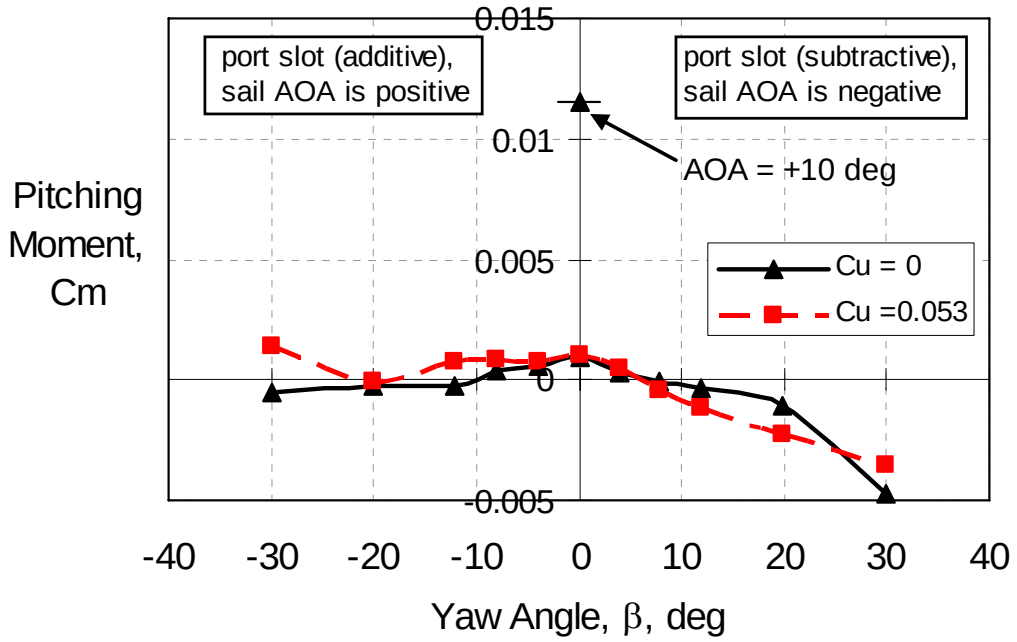

Figure A-55: Drift angle effects on pitch moment, with and without augmented lift, for AOA = 0. The value for a pitch angle of +10 deg is noted, to provide a C_m scale reference.

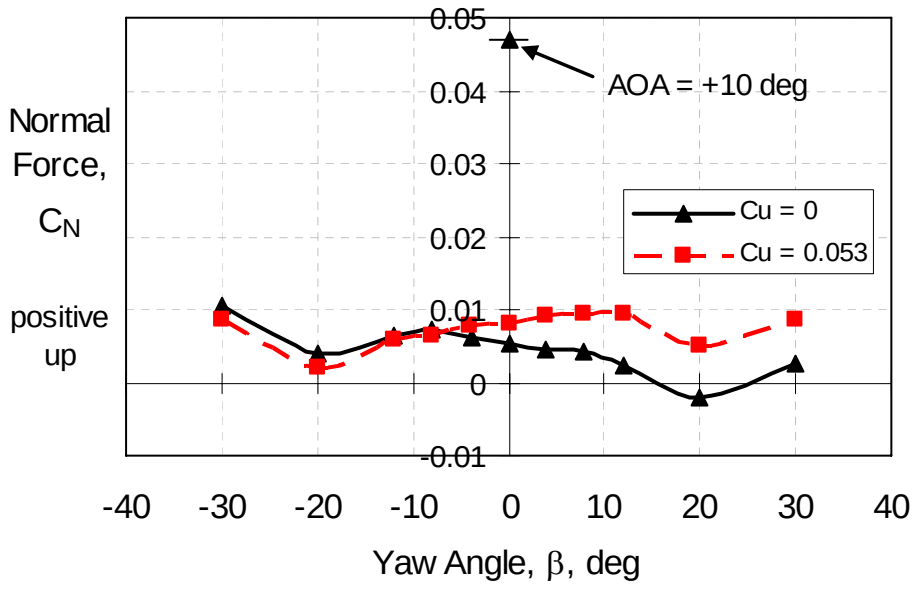

Figure A-56: Drift angle effects on normal force. Pitch angle = 0, except as noted.

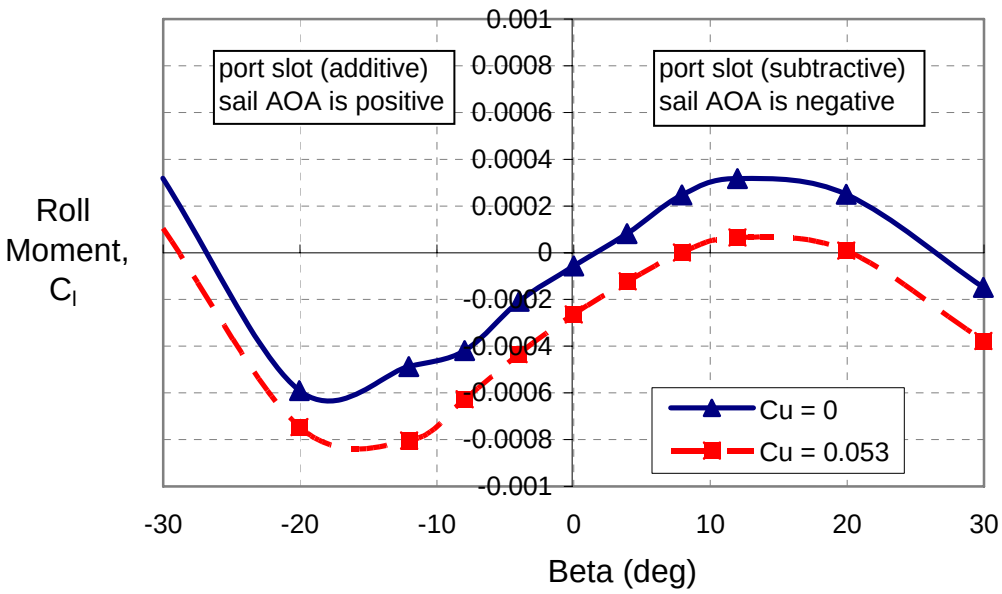

Figure A-57: Drift angle effects on roll moment. The labels “additive” and “subtractive” refer to turn-assistance and turn-reversal, respectively.

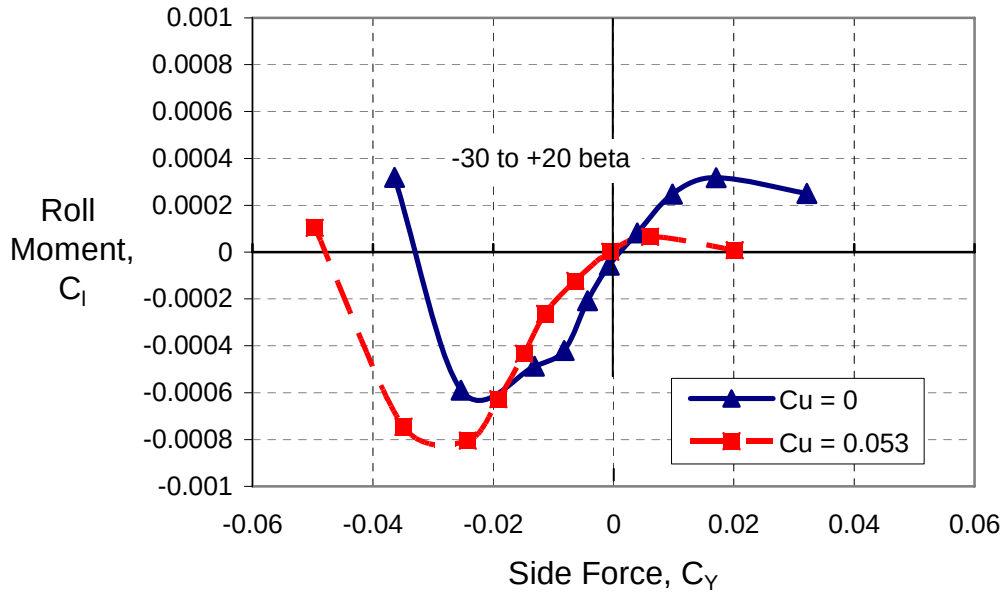

Figure A-58: Roll moment trends from perspective of developed side force.

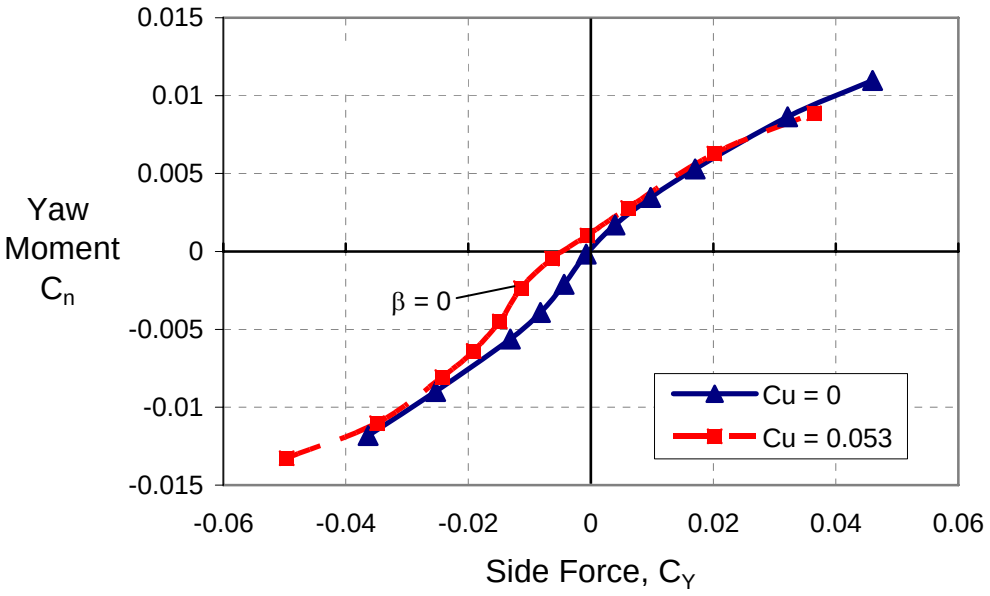

Figure A-59: Yaw moment trends as a function of side force. Beta angle coverage: -30 to +30 deg.

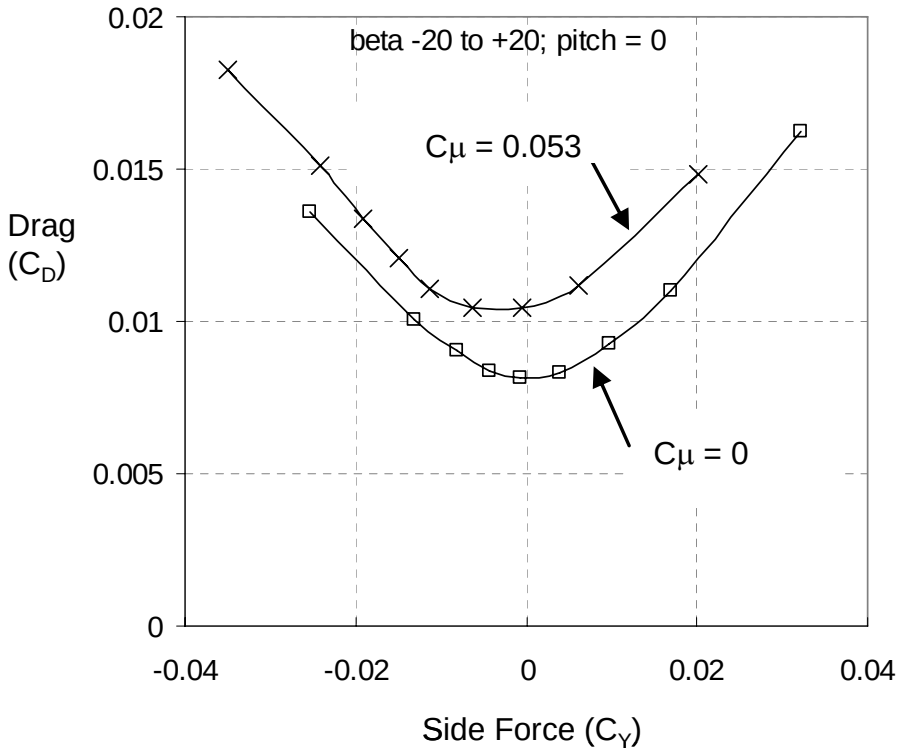

Figure A-60: Drag force trends as a function of side force, with and without augmented sail lift.

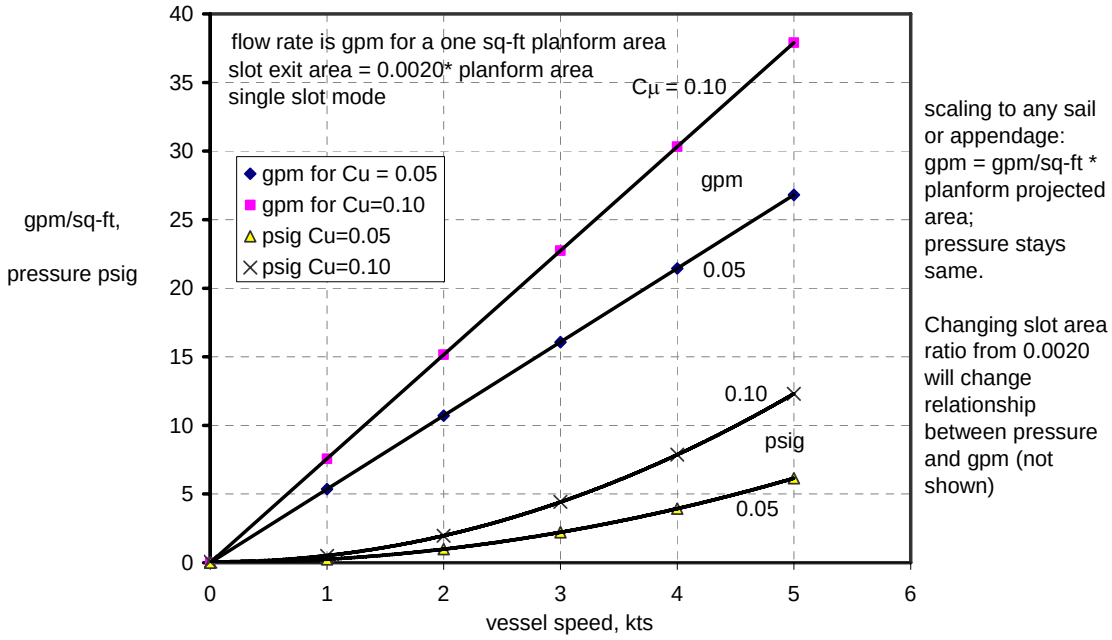

Figure A-61: Flow rates and duct pressure for CC hydrodynamic applications, for one mid-level and one higher value of slot momentum coefficient.

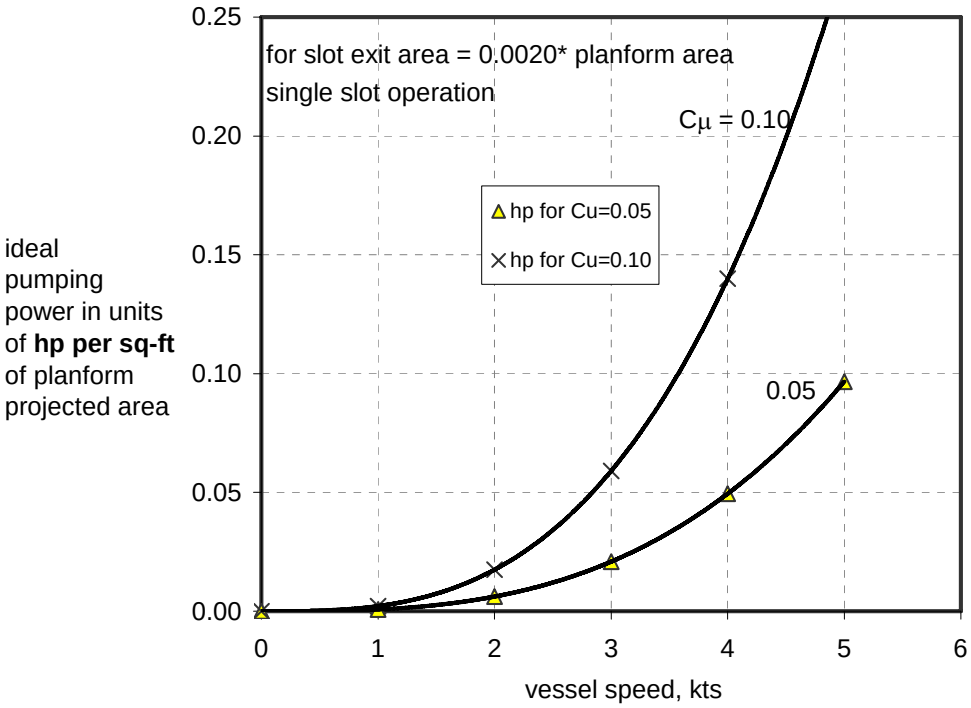

Figure A-62: Required pumping power per square foot of planform area.

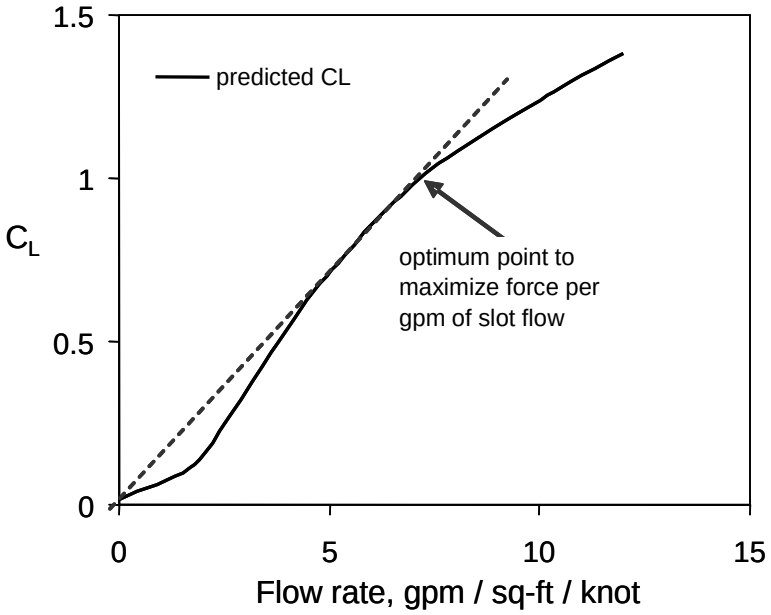

Figure A-63: Lift versus flow rate for an aspect ratio 1.0 CC wing. Flow volume is normalized by planform projected area and speed in knots.

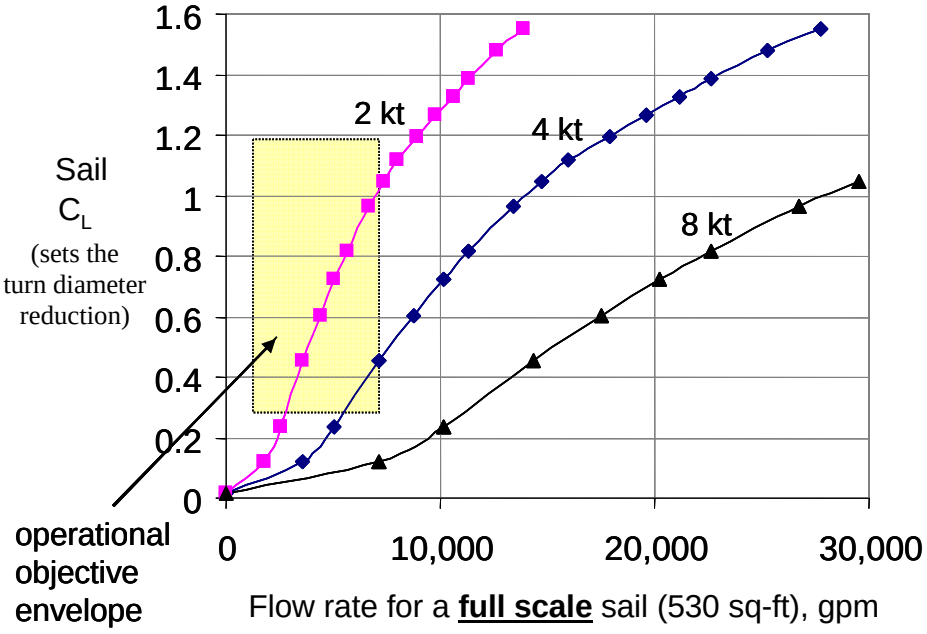

Figure A-64: Required flow rate on a full-scale sail as a function of lift coefficient and maneuver initiation speed.

APPENDIX B
DATA TABULATION

USER NOTES FOR THE TABULATED DATA:

1. Due to the general absence in the test procedure of using second-slot bleed flow to delay single-slot lift stall, all single slot data taken for P_{duct} pressures of greater than 0.9 psi ($C\mu$ > 0.09) are limited in relevance; the tabulated data for these conditions is flagged with an asterisk (*) next to the run number. There is one run where dual slots were used to prevent lift rolloff: Run 22.

2. Duct pressure, P_{duct}, is from a static probe in the model interior cavity, it is not the slot nozzle exit pressure from which to derive $C\mu$ or other slot flow parameters. See text section: "Slot Spanwise Pressure Distribution".

3. Balance data for negative beta when unappended (Runs 7-13) are considered erroneous.

4. See Figure A-21 for sign conventions, which conform to wind tunnel practice. The moment center location is x/l = 0.53.

5. Sometimes the balance data channels showed readings when the symmetry of the aerodynamic situation would preclude a legitimate load, that is, a data offset occurred that was not otherwise dealt with by the zeroing procedures of the recording system. For critical analysis of low-force data channels, any obvious offset should be removed before interpreting test results.

6. The dimensional values used for the coefficient data plots in appendix A are: area = 130 ft^2, length = 13.3 ft. The 130 ft^2 is the approximate wetted surface area of the NNemo-1 model.

Note: For all runs:
Sail is in the forward position, Bow planes are present and set to 0 deg.
All data collected on Friday, 9 December 2005. Slot air supply temperatures ranged from 44°F to 53°F.
Runs are listed in order taken, run numbers are not sequential.
* = data to be disregarded because single-slot lift stall reached and second-slot bleed was not used for improvement.

Table B-1: Run Number Key

Run Nos.	Tunnel q (psf)	Stern Planes (deg)	α Pitch (deg)	β Yaw (deg)	Port Duct (psi)	Starboard Duct (psi)	Comment/Goal
3.01 – 3.07	0	removed	0	0	0	0 – 2	Starboard slot flow, wind off, balance response check
3.08 – 3.14	0	removed	0	0	0 – 2	0	Port slot flow, wind off, balance response check
4.01 – 4.06	0	removed	0	0	0 – 1.4	0 – 1.4	Dual slot flow, wind off
5.01 – 5.06	6	removed	0	0	0 – 1.4	0 – 1.4	Dual slot flow, wind on
6.01 – 6.15	6	removed	0	0	0 – 2.2	0	Port slot flow, wind on
6.16 – 6.31	6	removed	0	0	0	0 – 2.2	Starboard slot flow, wind on
7.07 – 7.12	6	removed	0	-20 to 20	0	0	Beta sweep, no blowing
8.01 – 8.07	6	removed	0	-20 to 20	0.12	0	Beta sweep, port slot active
9.06 – 9.11	6	removed	0	-20 to 20	0.4	0	Beta sweep, port slot active
10.01 – 10.06	6	removed	0	-20 to 20	0.6	0	Beta sweep, port slot active
11.07 – 11.12	6	removed	0	-20 to 20	1.0	0	Beta sweep, port slot active
12.01 – 12.06	6	removed	0	-20 to 20	1.2	0	Beta sweep, port slot active
13.06 – 13.11	6	removed	0	-20 to 20	1.4	0	Beta sweep, port slot active
14.01 – 14.09	6	removed	+10	0	0 – 1.4	0	Pitch, port slot, sweep psi
14.10 – 14.18	6	removed	-10	0	0 – 1.4	0	Pitch, port slot, sweep psi
15.02 – 15.12	6	0	0	-30 to 30	0	0	Beta sweep, no blowing
16.01 – 16.11	6	0	0	-30 to 30	0.15	0	Beta sweep, port slot active
18.01 – 18.11	6	0	0	-30 to 30	0.65	0	Beta sweep, port slot active
20.01 – 20.11	6	0	0	-30 to 30	1.2	0	Beta sweep, port slot active
23.01 – 23.08	6	0	-10	0	0 – 1.2	0	Pitch, port slot, sweep psi
24.01 – 24.08	6	0	+10	0	0 – 1.2	0	Pitch, port slot, sweep psi
25.01 – 25.07	6	0	8	12	0 – 1.1	0	Pitch and beta combo with port psi
22.01 – 22.07	6	0	0	0 – 2.6	0 – 0.2	0	Dual blowing, second-slot assist

Table B-2: Experimental Data

Run No.	AOA (deg)	Beta (deg)	q (psf)	Axial (lb)	Normal (lb)	Side (lb)	Roll (in.-lb)	Pitch (in.-lb)	Yaw (in.-lb)	ΔP (psi)	Port Pduct (psi)	Starboard Pduct (psi)	Cμ Derived	V_{jet} Derived (ft/sec)
3.01	0.0	0	-0.04	-0.02	0.14	-0.20	-1.53	0.73	-0.01	-0.00161	0.000	0.000	-	0
3.02	0.0	0	-0.04	0.15	0.30	-0.22	-2.93	6.64	0.40	-0.00159	0.495	0.009	-	254
3.03	0.0	0	-0.04	0.35	0.42	-0.23	-4.02	15.31	1.00	-0.00153	0.983	0.021	-	354
3.04	0.0	0	-0.04	0.53	0.56	-0.26	-5.01	25.24	1.80	-0.00139	1.501	0.035	-	432
3.05	0.0	0	-0.04	0.65	0.55	-0.30	-6.18	32.21	1.70	-0.00140	1.830	0.044	-	474
3.06	0.0	0	-0.04	0.35	0.54	-0.24	-3.88	13.50	1.13	-0.00186	0.966	0.021	-	351
3.07	0.0	0	-0.04	0.11	0.20	-0.23	-2.54	5.25	0.50	-0.00222	0.374	0.006	-	222
3.08	0.0	0	-0.04	0.00	0.26	-0.18	-1.40	-2.40	0.04	-0.00238	0.002	0.000	-	17
3.09	0.0	0	-0.04	0.13	0.28	-0.19	-0.29	4.67	-0.49	-0.00269	0.009	0.467	-	35
3.10	0.0	0	-0.04	0.30	0.44	-0.12	1.25	14.92	-0.82	-0.00301	0.023	1.022	-	55
3.11	0.0	0	-0.04	0.44	0.56	-0.06	2.22	18.78	-0.81	-0.00329	0.032	1.384	-	66
3.12	0.0	0	-0.04	0.61	0.59	-0.07	3.73	30.84	-2.03	-0.00363	0.047	1.899	-	79
3.13	0.0	0	-0.05	0.28	0.42	-0.15	1.21	13.27	-0.89	-0.00314	0.021	0.951	-	53
3.14	0.0	0	-0.05	0.01	0.25	-0.20	-1.56	-2.35	0.10	-0.00271	0.001	0.002	-	11
4.01	0.0	0	-0.05	-0.01	0.19	-0.23	-1.60	-1.71	0.02	-0.00285	0.000	0.000	-	0
4.02	0.0	0	-0.04	-0.48	0.37	-0.16	-2.41	-12.21	-3.78	-0.00288	0.501	0.447	-	256
4.03	0.0	0	-0.04	-1.04	0.31	-0.31	-3.14	-20.90	-4.07	-0.00291	0.992	0.925	-	355
4.04	0.0	0	-0.04	-1.27	0.44	-0.22	-0.84	-27.42	-9.96	-0.00295	1.169	1.209	-	384
4.05	0.0	0	-0.04	-0.71	0.31	-0.25	-2.63	-15.44	-4.01	-0.00305	0.698	0.639	-	300
4.06	0.0	0	-0.04	0.00	0.20	-0.22	-1.55	-1.61	0.04	-0.00303	0.000	0.000	-	0
5.01	0.0	0	5.96	5.93	2.80	-0.25	-5.01	101.88	-7.96	-0.00246	0.000	0.000	-	0
5.02	0.0	0	6.01	5.48	3.77	-1.83	-11.14	135.58	-56.07	-0.00524	0.457	0.408	0.0484	244
5.03	0.0	0	6.00	4.96	3.99	-1.96	-6.16	27.78	-53.50	-0.00493	1.003	0.931	0.1049	357
5.04	0.0	0	5.99	4.71	4.57	-0.64	-0.92	4.00	-2.10	-0.00961	1.177	1.218	0.1228	385
5.05	0.0	0	5.99	5.20	3.79	-1.78	-7.33	62.58	-50.85	-0.00306	0.727	0.669	0.0767	306
5.06	0.0	0	5.96	5.96	3.23	-0.35	-4.73	128.88	-27.63	0.00027	0.000	0.000	-	0
6.01	0.0	0	5.96	5.95	3.06	-0.32	-4.22	115.71	-28.91	0.00000	0.000	-0.009	-	0
6.02	0.0	0	5.97	5.95	2.60	-1.64	-11.31	86.22	-58.94	-0.00275	0.050	0.002	0.0054	82
6.03	0.0	0	5.98	7.09	4.25	-5.90	-29.09	72.40	-178.51	-0.01056	0.259	0.011	0.0278	185

Table B-2: Experimental Data (Cont'd)

Run No.	AOA (deg)	Beta (deg)	q (psf)	Axial (lb)	Normal (lb)	Side (lb)	Roll (in.-lb)	Pitch (in.-lb)	Yaw (in.-lb)	ΔP (psi)	Port Pduct (psi)	Starboard Pduct (psi)	Cμ Derived	V_{jet} Derived (ft/sec)
6.04	0.0	0	5.97	8.09	4.54	-8.00	-37.96	99.04	-275.00	-0.01413	0.459	0.014	0.0490	245
6.05	0.0	0	5.97	9.33	5.22	-9.32	-45.46	105.76	-326.93	-0.01796	0.732	0.004	0.0777	307
*6.06	0.0	0	5.95	10.54	4.46	-7.19	-41.50	101.50	-314.34	-0.03936	0.929	-0.027	0.0983	344
*6.07	0.0	0	5.95	10.92	5.53	-6.82	-45.83	143.31	-326.60	-0.04094	1.193	-0.009	0.1251	388
*6.08	0.0	0	5.95	11.10	5.41	-6.66	-47.40	149.35	-347.19	-0.04108	1.397	0.004	0.1459	418
*6.09	0.0	0	5.97	11.37	6.00	-6.71	-51.43	159.64	-344.38	-0.04038	1.564	0.012	0.1622	441
*6.10	0.0	0	5.94	11.66	6.98	-6.33	-56.16	250.73	-368.35	-0.03803	1.879	0.028	0.1941	479
*6.11	0.0	0	5.93	11.05	5.23	-6.78	-47.10	133.10	-352.06	-0.04205	1.353	0.002	0.1420	412
*6.12	0.0	0	5.94	10.54	5.34	-6.85	-43.12	169.02	-316.18	-0.03732	0.922	-0.027	0.0976	343
6.13	0.0	0	5.92	7.80	4.01	-7.49	-35.20	93.78	-272.16	-0.01700	0.409	0.014	0.0440	231
6.14	0.0	0	5.92	5.94	3.25	-2.35	-14.72	129.04	-91.70	-0.00714	0.078	0.002	0.0084	102
6.15	0.0	0	5.93	5.89	2.53	-0.12	-3.66	88.69	-25.33	-0.00297	1.215	-0.009	-	0
6.16	0.0	0	5.93	5.86	3.04	-0.33	-4.53	134.51	-47.52	-0.00106	-0.008	-0.009	-	0
6.17	0.0	0	5.95	5.92	3.31	1.65	5.14	80.38	39.07	0.00605	0.001	0.060	0.0065	89
6.18	0.0	0	5.91	6.88	5.83	5.36	22.52	89.82	151.09	0.01024	0.010	0.240	0.0260	178
6.19	0.0	0	5.92	8.03	6.63	7.52	33.99	82.95	221.01	0.01330	0.016	0.455	0.0489	244
6.20	0.0	0	5.92	8.98	7.53	8.77	45.95	68.06	259.58	0.01755	0.013	0.663	0.0708	293
*6.21	0.0	0	5.92	10.77	8.01	7.31	43.75	131.41	272.85	0.03645	-0.027	0.950	0.1009	349
*6.22	0.0	0	5.91	10.94	8.29	7.41	44.82	123.31	296.59	0.03976	-0.010	1.137	0.1204	380
*6.23	0.0	0	5.92	11.26	8.30	7.46	50.01	102.61	312.36	0.04043	0.004	1.378	0.1448	416
*6.24	0.0	0	5.91	11.46	8.92	7.41	52.46	143.01	304.70	0.04020	0.016	1.551	0.1625	439
*6.25	0.0	0	5.92	11.85	9.75	7.58	57.11	181.34	330.19	0.03689	0.038	1.904	0.1973	483
*6.26	0.0	0	5.89	11.65	8.64	7.21	54.65	103.27	309.06	0.03845	0.026	1.721	0.1799	461
*6.27	0.0	0	5.96	11.17	8.31	7.52	48.22	129.67	306.07	0.04100	-0.001	1.305	0.1364	405
*6.28	0.0	0	5.94	10.79	8.64	7.41	41.35	152.53	251.61	0.03491	-0.033	0.908	0.0962	341
6.29	0.0	0	5.89	8.00	6.48	7.61	33.43	51.44	226.92	0.01379	0.015	0.464	0.0501	246
6.30	0.0	0	5.91	5.89	4.35	1.95	3.24	100.67	46.98	0.00272	0.002	0.071	0.0077	97
6.31	0.0	0	5.90	5.80	3.00	-0.47	-5.38	80.18	-30.78	-0.00125	-0.008	-0.007	-	0
7.07	0.0	0	5.96	5.82	3.58	0.23	-7.78	200.34	-11.95	0.00008	-0.008	-0.008	-	0
7.08	0.0	2	5.96	5.78	3.18	1.19	2.88	122.12	109.09	0.00160	-0.008	-0.008	-	0

Table B-2: Experimental Data (Cont'd)

Run No.	AOA (deg)	Beta (deg)	q (psf)	Axial (lb)	Normal (lb)	Side (lb)	Roll (in.-lb)	Pitch (in.-lb)	Yaw (in.-lb)	ΔP (psi)	Port Pduct (psi)	Starboard Pduct (psi)	Cμ Derived	V_{jet} Derived (ft/sec)
7.09	0.0	4	5.96	5.80	4.43	2.75	9.89	140.94	257.12	0.00344	-0.008	-0.007	-	0
7.10	0.0	8	5.98	5.85	4.04	6.06	28.37	54.67	519.58	0.00215	-0.010	-0.008	-	0
7.11	0.0	12	5.95	5.51	2.46	10.86	38.36	-77.98	807.47	0.00680	-0.011	-0.010	-	0
7.12	0.0	20	5.92	4.05	-0.58	20.38	36.03	-120.45	1329.43	0.01664	-0.015	-0.016	-	0
8.01	0.0	20	5.91	4.03	-1.64	20.23	23.83	-148.77	1329.02	0.02228	-0.015	-0.015	0.000	0
8.02	0.0	20	5.90	4.46	-0.31	16.07	7.62	-151.61	1209.65	0.01350	0.094	0.005	0.0102	112
8.03	0.0	12	5.94	5.69	3.83	6.88	21.73	-120.07	708.15	0.00376	0.101	0.003	0.0110	116
8.04	0.0	8	5.96	6.01	5.41	2.64	16.73	28.50	436.77	-0.00094	0.103	0.004	0.0111	117
8.05	0.0	4	5.95	6.05	5.36	-0.31	-2.98	95.88	171.03	-0.00279	0.105	0.006	0.0113	118
8.06	0.0	2	5.97	6.00	4.99	-1.75	-10.60	112.10	58.43	-0.00381	0.106	0.006	0.0114	119
8.07	0.0	0	5.96	6.00	4.51	-3.50	-21.73	199.46	-113.56	-0.00577	0.106	0.006	0.0114	119
9.06	0.0	0	5.93	7.20	4.12	-6.24	-34.10	123.45	-243.26	-0.01253	0.327	0.015	0.0352	208
9.07	0.0	2	5.93	7.21	4.90	-5.43	-28.47	124.65	-91.38	-0.01085	0.328	0.014	0.0354	208
9.08	0.0	4	5.92	7.16	6.15	-4.39	-16.92	92.02	44.21	-0.00933	0.329	0.014	0.0355	209
9.09	0.0	8	5.94	7.07	8.08	-0.82	-0.68	-14.57	332.46	-0.00686	0.329	0.012	0.0354	209
9.10	0.0	12	5.94	6.83	7.35	2.86	9.45	-63.05	571.87	-0.00432	0.328	0.010	0.0353	208
9.11	0.0	20	5.91	5.52	4.16	12.42	5.42	-201.90	1115.93	0.00270	0.325	0.003	0.0351	208
10.01	0.0	20	5.89	6.39	5.74	11.00	-5.97	-220.68	1069.61	-0.00184	0.510	-0.001	0.0551	259
10.02	0.0	12	5.94	7.54	7.84	1.86	-16.51	-150.31	535.53	-0.00715	0.514	0.011	0.0549	260
10.03	0.0	8	5.94	7.82	9.76	-2.25	-12.81	53.27	266.43	-0.01066	0.515	0.012	0.0551	260
10.04	0.0	4	5.91	7.98	7.22	-5.66	-33.80	53.50	9.82	-0.01277	0.515	0.014	0.0553	260
10.05	0.0	2	5.95	8.04	5.76	-7.42	-37.02	134.18	-120.67	-0.01428	0.514	0.015	0.0549	260
10.06	0.0	0	5.90	8.05	3.89	-9.09	-43.28	84.29	-279.61	-0.01623	0.512	0.016	0.0552	259
11.07	0.0	0	6.05	9.56	4.74	-7.85	-47.72	119.92	-342.88	-0.02100	0.795	-0.010	0.0831	321
11.08	0.0	2	6.02	9.56	5.21	-7.61	-49.43	138.15	-208.90	-0.01997	0.797	-0.016	0.0836	322
11.09	0.0	4	6.02	9.56	6.29	-6.43	-41.30	61.92	-25.66	-0.01953	0.800	-0.020	0.0839	322
11.10	0.0	8	5.99	9.28	8.71	-3.66	-28.96	0.06	212.35	-0.01554	0.801	-0.012	0.0843	322
11.11	0.0	12	6.00	9.26	8.78	0.92	-18.17	-111.80	490.14	-0.01955	0.800	-0.019	0.0842	322
11.12	0.0	20	5.98	8.50	6.08	9.68	-28.05	-263.69	1004.32	-0.00161	0.802	-0.017	0.0847	323

Table B-2: Experimental Data (Cont'd)

Run No.	AOA (deg)	Beta (deg)	q (psf)	Axial (lb)	Normal (lb)	Side (lb)	Roll (in.-lb)	Pitch (in.-lb)	Yaw (in.-lb)	ΔP (psi)	Port Pduct (psi)	Starboard Pduct (psi)	Cμ Derived	V_{jet} Derived (ft/sec)
*12.01	0.0	20	5.93	8.97	7.49	9.38	-18.24	-212.75	989.96	-0.00362	0.986	-0.010	0.1044	356
*12.02	0.0	12	6.00	10.15	9.15	1.18	-21.96	-88.33	475.46	-0.02629	0.987	-0.021	0.1032	356
*12.03	0.0	8	6.01	10.54	9.09	-2.56	-32.93	-36.01	215.58	-0.02973	0.987	-0.030	0.1031	356
*12.04	0.0	4	6.01	10.65	7.01	-6.10	-39.23	121.69	-54.89	-0.03561	0.988	-0.031	0.1033	357
*12.05	0.0	2	6.03	10.58	5.21	-7.41	-40.60	143.23	-175.76	-0.03724	0.990	-0.028	0.1032	357
*12.06	0.0	0	5.98	10.45	4.00	-8.10	-46.78	154.55	-313.82	-0.03894	0.991	-0.023	0.1040	358
*13.06	0.0	0	5.99	10.63	4.19	-6.05	-43.53	131.71	-313.89	-0.04131	1.134	-0.013	0.1185	381
*13.07	0.0	2	5.99	10.72	4.39	-6.06	-43.31	116.42	-189.74	-0.04014	1.133	-0.016	0.1183	381
*13.08	0.0	4	6.03	10.92	5.60	-5.69	-36.19	98.27	-79.61	-0.03892	1.130	-0.021	0.1172	381
*13.09	0.0	8	5.99	10.84	8.19	-2.80	-24.58	-5.12	210.45	-0.03383	1.129	-0.025	0.1179	380
*13.10	0.0	12	5.99	10.38	8.18	0.99	-26.61	-119.90	467.71	-0.02848	1.129	-0.015	0.1178	380
*13.11	0.0	20	5.95	9.15	7.47	9.36	-20.25	-213.00	982.80	-0.00429	1.130	-0.002	0.1188	381
14.01	10.0	0	5.99	5.49	32.13	0.03	-18.03	1580.91	-0.06	0.00033	0.000	-0.003	-	0
14.02	10.0	0	6.01	5.68	32.79	-6.51	-12.58	1569.27	-45.36	-0.00428	0.094	0.009	0.0101	113
14.03	10.0	0	6.04	6.84	34.44	-13.23	-18.10	1582.94	-119.22	-0.01171	0.312	0.019	0.0330	204
14.04	10.0	0	5.98	7.77	34.93	-16.30	-6.10	1590.07	-151.19	-0.01573	0.504	0.020	0.0536	258
14.05	10.0	0	6.02	8.82	35.14	-18.74	-21.87	1603.65	-210.55	-0.01952	0.726	0.013	0.0763	308
*14.06	10.0	0	6.02	10.28	35.93	-16.83	-3.73	1612.51	-181.37	-0.04095	0.988	-0.025	0.1031	357
*14.07	10.0	0	6.03	10.43	35.70	-15.62	-7.86	1590.77	-191.30	-0.04393	1.149	-0.011	0.1193	384
14.08	10.0	0	5.99	7.73	35.33	-16.55	-9.42	1588.95	-155.05	-0.01606	0.493	0.020	0.0524	255
14.09	10.0	0	6.01	5.40	31.76	-0.58	-19.17	1581.32	-7.59	0.00026	0.000	-0.003	-	0
14.10	-10.0	0	5.96	3.49	-26.66	-5.61	31.85	-1614.39	-20.81	0.00034	0.000	0.000	-	0
14.11	-10.0	0	5.97	3.68	-27.09	-7.26	7.59	-1627.45	-125.46	-0.00540	0.089	0.000	0.0096	110
14.12	-10.0	0	5.93	5.02	-25.46	-9.06	-38.22	-1578.46	-248.81	-0.01174	0.306	0.008	0.0330	202
14.13	-10.0	0	5.96	5.82	-26.17	-9.40	-55.16	-1587.93	-321.61	-0.01510	0.481	0.008	0.0513	253
14.14	-10.0	0	5.96	6.83	-24.86	-9.73	-84.25	-1570.45	-383.02	-0.01791	0.713	0.000	0.0756	306
*14.15	-10.0	0	5.96	7.90	-26.34	-9.72	-69.40	-1531.65	-321.63	-0.03516	0.988	-0.026	0.1040	358
*14.16	-10.0	0	5.98	8.21	-25.68	-9.44	-64.65	-1485.19	-324.49	-0.03718	1.123	-0.020	0.1175	380
14.17	-10.0	0	5.91	5.88	-26.51	-9.69	-60.27	-1596.83	-339.14	-0.01490	0.503	0.008	0.0542	258
14.18	-10.0	0	6.01	3.60	-26.32	-4.63	28.04	-1586.20	8.11	0.00010	0.000	0.000	-	0

Table B-2: Experimental Data (Cont'd)

Run No.	AOA (deg)	Beta (deg)	q (psf)	Axial (lb)	Normal (lb)	Side (lb)	Roll (in.-lb)	Pitch (in.-lb)	Yaw (in.-lb)	ΔP (psi)	Port Pduct (psi)	Starboard Pduct (psi)	Cμ Derived	V_{jet} Derived (ft/sec)
15.02	0.0	-30	6.01	5.84	8.34	-28.44	39.79	-66.24	-1474.50	-0.03705	-0.027	-0.029	-	0
15.03	0.0	-20	6.02	4.09	3.15	-19.83	-73.66	-34.79	-1121.93	-0.02009	-0.015	-0.016	-	0
15.04	0.0	-12	6.02	5.85	4.96	-10.27	-60.80	-27.96	-702.58	-0.00970	-0.010	-0.013	-	0
15.05	0.0	-8	5.99	6.21	5.67	-6.40	-52.10	50.65	-487.61	-0.00519	-0.008	-0.011	-	0
15.06	0.0	-4	6.02	6.34	4.89	-3.39	-25.95	71.70	-262.77	-0.00240	-0.007	-0.008	-	0
15.07	0.0	0	6.05	6.39	4.24	-0.58	-7.07	117.50	-19.82	0.00001	0.000	0.000	-	0
15.08	0.0	4	6.02	6.33	3.56	3.07	10.24	37.20	213.57	-0.00337	-0.008	-0.008	-	0
15.09	0.0	8	6.02	6.25	3.22	7.66	30.86	-10.65	432.95	-0.00191	-0.010	-0.008	-	0
15.10	0.0	12	6.00	5.96	1.82	13.31	39.58	-37.78	660.20	0.00248	-0.012	-0.011	-	0
15.11	0.0	20	5.96	4.35	-1.69	24.90	30.94	-138.20	1069.44	0.01243	-0.015	-0.016	-	0
15.12	0.0	30	5.96	4.71	2.05	35.63	-18.42	-583.17	1357.65	0.03282	-0.035	-0.031	-	0
16.01	0.0	30	5.94	6.87	2.01	30.45	-91.32	-406.84	1238.18	0.02327	0.083	-0.032	0.0090	106
16.02	0.0	20	5.99	4.76	-0.46	20.48	9.24	-189.56	939.63	0.00395	0.113	-0.005	0.0121	123
16.03	0.0	12	6.00	6.19	3.97	8.85	29.58	-48.66	533.97	-0.00503	0.119	0.002	0.0128	127
16.04	0.0	8	6.00	6.48	4.99	3.99	23.69	-6.90	336.59	-0.00875	0.121	0.004	0.0130	128
16.05	0.0	4	5.99	6.58	5.18	-0.92	0.22	36.43	112.34	-0.01081	0.123	0.006	0.0132	129
16.06	0.0	0	6.03	6.68	5.03	-4.42	-19.07	120.10	-139.16	-0.01431	0.124	0.007	0.0132	129
16.07	0.0	-4	5.99	6.55	4.59	-6.75	-36.35	34.22	-376.27	-0.01723	0.125	0.008	0.0134	130
16.08	0.0	-8	5.94	6.26	4.86	-9.30	-62.90	18.10	-599.92	-0.01983	0.129	0.007	0.0139	132
16.09	0.0	-12	6.00	5.84	5.23	-13.02	-83.18	32.36	-787.74	-0.02223	0.133	0.005	0.0143	134
16.10	0.0	-20	5.98	4.00	2.12	-21.44	-71.29	-50.99	-1175.97	-0.02903	0.136	-0.003	0.0146	136
16.11	0.0	-30	5.99	4.63	6.09	-32.89	65.25	118.88	-1480.15	-0.04621	0.146	-0.017	0.0156	140
18.01	0.0	-30	6.00	3.80	6.77	-38.78	13.10	171.89	-1653.12	-0.07630	0.477	0.004	0.0505	251
18.02	0.0	-20	6.01	5.24	1.58	-27.26	-93.01	-13.19	-1374.84	-0.04029	0.404	0.017	0.0429	232
18.03	0.0	-12	6.02	8.03	4.50	-18.96	-100.48	98.66	-1006.79	-0.03316	0.483	0.018	0.0511	253
18.04	0.0	-8	6.00	8.44	5.02	-14.93	-78.21	110.90	-796.30	-0.02885	0.493	0.017	0.0523	256
18.05	0.0	-4	6.01	8.64	6.02	-11.62	-54.06	99.57	-560.52	-0.02509	0.498	0.017	0.0528	257
18.06	0.0	0	6.01	8.63	6.24	-8.90	-32.92	129.98	-293.30	-0.02173	0.503	0.016	0.0532	258
18.07	0.0	4	5.99	8.50	7.23	-4.92	-15.29	62.52	-56.43	-0.01846	0.506	0.013	0.0537	259
18.08	0.0	8	5.99	8.27	7.43	-0.42	0.10	-50.18	127.65	-0.01630	0.506	0.011	0.0537	259

Table B-2: Experimental Data (Cont'd)

Run No.	AOA (deg)	Beta (deg)	q (psf)	Axial (lb)	Normal (lb)	Side (lb)	Roll (in.-lb)	Pitch (in.-lb)	Yaw (in.-lb)	ΔP (psi)	Port Pduct (psi)	Starboard Pduct (psi)	Cμ Derived	V_{jet} Derived (ft/sec)
18.09	0.0	12	5.98	7.90	7.40	4.73	8.10	-148.46	346.45	-0.01203	0.506	0.010	0.0539	259
18.10	0.0	20	5.96	6.59	4.04	15.66	1.05	-278.31	778.21	-0.00608	0.503	0.002	0.0535	258
18.11	0.0	30	5.97	8.48	6.80	28.32	-46.85	-437.84	1098.81	0.02072	0.482	-0.035	0.0514	253
*20.01	0.0	30	5.96	10.34	5.18	27.95	-78.98	-351.26	1085.01	0.02552	0.968	-0.024	0.1020	355
*20.02	0.0	20	5.95	9.05	8.26	14.72	8.39	-212.39	685.78	-0.00824	0.987	-0.009	0.1041	358
*20.03	0.0	12	5.99	10.46	8.49	4.20	-3.76	-142.26	292.32	-0.03089	0.987	-0.022	0.1036	358
*20.04	0.0	8	6.00	11.02	9.58	-1.04	-4.61	38.39	65.64	-0.03384	0.986	-0.032	0.1032	358
*20.05	0.0	4	6.03	11.21	8.22	-4.52	-20.60	105.92	-111.00	-0.03890	0.990	-0.031	0.1031	358
*20.06	0.0	0	5.99	11.02	6.99	-8.34	-40.61	178.48	-338.99	-0.04366	0.993	-0.022	0.1041	359
*20.07	0.0	-4	6.01	10.87	6.37	-11.22	-56.06	144.99	-565.96	-0.04526	0.992	-0.023	0.1038	359
*20.08	0.0	-8	6.01	10.66	5.64	-13.79	-68.63	123.83	-790.54	-0.04829	0.993	-0.029	0.1037	359
*20.09	0.0	-12	6.02	10.07	4.73	-17.03	-75.94	62.57	-998.53	-0.04934	0.996	-0.032	0.1040	359
*20.10	0.0	-20	6.02	7.69	4.30	-29.06	-83.52	9.69	-1454.84	-0.04994	0.962	-0.006	0.1005	353
*20.11	0.0	-30	5.98	5.02	7.34	-39.47	-11.36	8.19	-1812.05	-0.08743	1.048	0.019	0.1100	368
23.01	-10.0	0	5.98	3.72	-28.85	-1.05	24.21	-1526.49	-28.05	0.00000	0.000	0.000	0.0000	0
23.02	-10.0	0	5.95	4.05	-27.38	-2.65	-6.42	-1482.99	-132.31	-0.00588	0.097	0.000	0.0115	115
23.03	-10.0	0	5.96	5.03	-27.91	-3.38	-30.82	-1495.93	-278.14	-0.01144	0.275	0.008	0.0295	192
23.04	-10.0	0	5.97	6.18	-27.35	-3.47	-60.39	-1454.40	-371.54	-0.01625	0.524	0.008	0.0558	264
23.05	-10.0	0	5.98	6.63	-28.55	-1.65	-67.06	-1479.88	-441.91	-0.01810	0.664	0.004	0.0703	296
*23.06	-10.0	0	5.93	8.17	-27.39	-2.54	-65.99	-1358.01	-333.07	-0.03502	0.995	-0.026	0.1053	359
23.07	-10.0	0	5.96	5.99	-27.69	-2.94	-50.69	-1452.43	-363.99	-0.01482	0.476	0.008	0.0509	252
23.08	-10.0	0	5.97	3.84	-28.12	-0.82	35.82	-1489.15	-65.13	-0.00121	0.000	0.000	0.0000	0
24.01	10.0	0	5.96	5.54	36.90	-1.01	-18.77	1422.67	-14.89	0.00000	0.000	-0.002	0.0000	0
24.02	10.0	0	5.97	5.60	37.37	-6.11	-11.30	1404.55	-62.09	-0.00408	0.074	0.007	0.0080	100
24.03	10.0	0	5.98	6.95	38.83	-15.09	5.11	1407.31	-130.88	-0.01221	0.322	0.019	0.0344	208
24.04	10.0	0	5.95	7.88	39.97	-18.63	6.68	1427.45	-188.63	-0.01609	0.528	0.020	0.0564	264
24.05	10.0	0	5.98	9.02	39.97	-20.57	11.03	1447.00	-215.23	-0.01977	0.765	0.009	0.0809	317
*24.06	10.0	0	6.01	10.25	40.12	-18.23	18.45	1443.12	-206.08	-0.04030	0.973	-0.025	0.1016	355
24.07	10.0	0	6.02	7.63	39.65	-17.72	11.22	1429.88	-168.72	-0.01520	0.457	0.021	0.0483	246
24.08	10.0	0	6.03	5.55	36.29	-1.78	-27.62	1419.18	-34.87	-0.00818	0.000	-0.003	0.0000	0

Table B-2: Experimental Data (Cont'd)

Run No.	AOA (deg)	Beta (deg)	q (psf)	Axial (lb)	Normal (lb)	Side (lb)	Roll (in.-lb)	Pitch (in.-lb)	Yaw (in.-lb)	ΔP (psi)	Port Pduct (psi)	Starboard Pduct (psi)	Cμ Derived	V_{jet} Derived (ft/sec)
25.01	8.0	12	5.96	5.27	32.01	12.93	253.71	1061.58	620.83	0.00196	-0.008	-0.006	0.0000	0
25.02	8.0	12	5.97	5.66	32.91	7.18	248.54	948.72	553.40	-0.00444	0.102	0.006	0.0110	118
25.03	8.0	12	6.00	6.93	36.82	1.07	249.03	925.00	448.58	-0.01203	0.335	0.013	0.0357	212
25.04	8.0	12	5.98	9.13	39.20	-2.91	213.23	906.35	384.66	-0.01689	0.654	0.009	0.0694	293
*25.05	8.0	12	6.03	11.11	39.23	-2.14	216.16	984.43	370.26	-0.03284	0.946	-0.025	0.0987	351
25.06	8.0	12	6.00	8.09	38.47	-0.61	232.71	991.55	445.74	-0.01404	0.429	0.013	0.0456	239
25.07	8.0	12	6.02	5.80	30.36	12.49	236.79	1073.05	629.56	0.00165	-0.008	-0.006	-	0
22.01	0.0	0	5.98	6.27	2.89	-1.07	-11.63	131.27	-26.52	-0.00768	-0.007	-0.007	-	0
*22.02	0.0	0	5.99	11.10	6.45	-8.56	-44.02	175.90	-348.32	-0.03917	1.054	-0.018	0.1102	369
22.03	0.0	0	5.99	10.67	7.72	-10.84	-54.89	140.96	-403.90	-0.02139	1.158	0.080	0.1207	386
22.04	0.0	0	6.03	11.31	8.10	-10.73	-66.72	109.15	-445.80	-0.02328	1.476	0.100	0.1519	433
22.05	0.0	0	6.02	11.70	9.20	-11.20	-77.30	161.84	-461.23	-0.02443	1.789	0.125	0.1829	473
22.06	0.0	0	6.00	11.97	10.20	-11.90	-79.24	237.37	-489.05	-0.02577	1.973	0.142	0.2015	495
22.07	0.0	0	5.97	12.12	9.94	-10.81	-85.37	143.13	-501.72	-0.02560	2.135	0.156	0.2180	513
22.08	0.0	0	0.00	0.12	-0.92	-0.63	0.39	-13.47	-1.88	0.00000	0.001	0.000	1.0527	12

APPENDIX C
DATA PLOTS

USER NOTES FOR THE DATA PLOTS:

1. Due to the general absence in the test procedure of using second-slot bleed flow to delay single-slot lift stall, all data taken for P_{duct} pressures of greater than 0.9 psi are not to be used for performance assessment. There is one exception where dual slots were used to prevent lift rolloff: Run 22.

2. Duct pressure, P_{duct}, is from a static probe in the model interior cavity, it is not the slot nozzle exit pressure from which to derive C_μ or other slot flow parameters. See text section: "Slot Spanwise Pressure Distribution".

3. Balance data for negative beta when unappended (Runs 7-13) are considered erroneous and are not shown.

4. Double curves on the plots result from reversing the pressure sweeps.

5. See Figure A-21 for sign conventions. The moment center location is x/l = 0.53.

6. Sometimes the balance data channels showed readings when the symmetry of the aerodynamic situation would preclude a legitimate load, that is, a data offset occurred that was not otherwise dealt with by the zeroing procedures of the recording system. For critical analysis of low-force data channels, any obvious offset should be removed before interpreting test results.

7. The dimensional values used for the coefficient data plots in appendix A are: area = 130 ft^2, length = 13.3 ft. Dynamic pressure was 6 lb/ft^2.

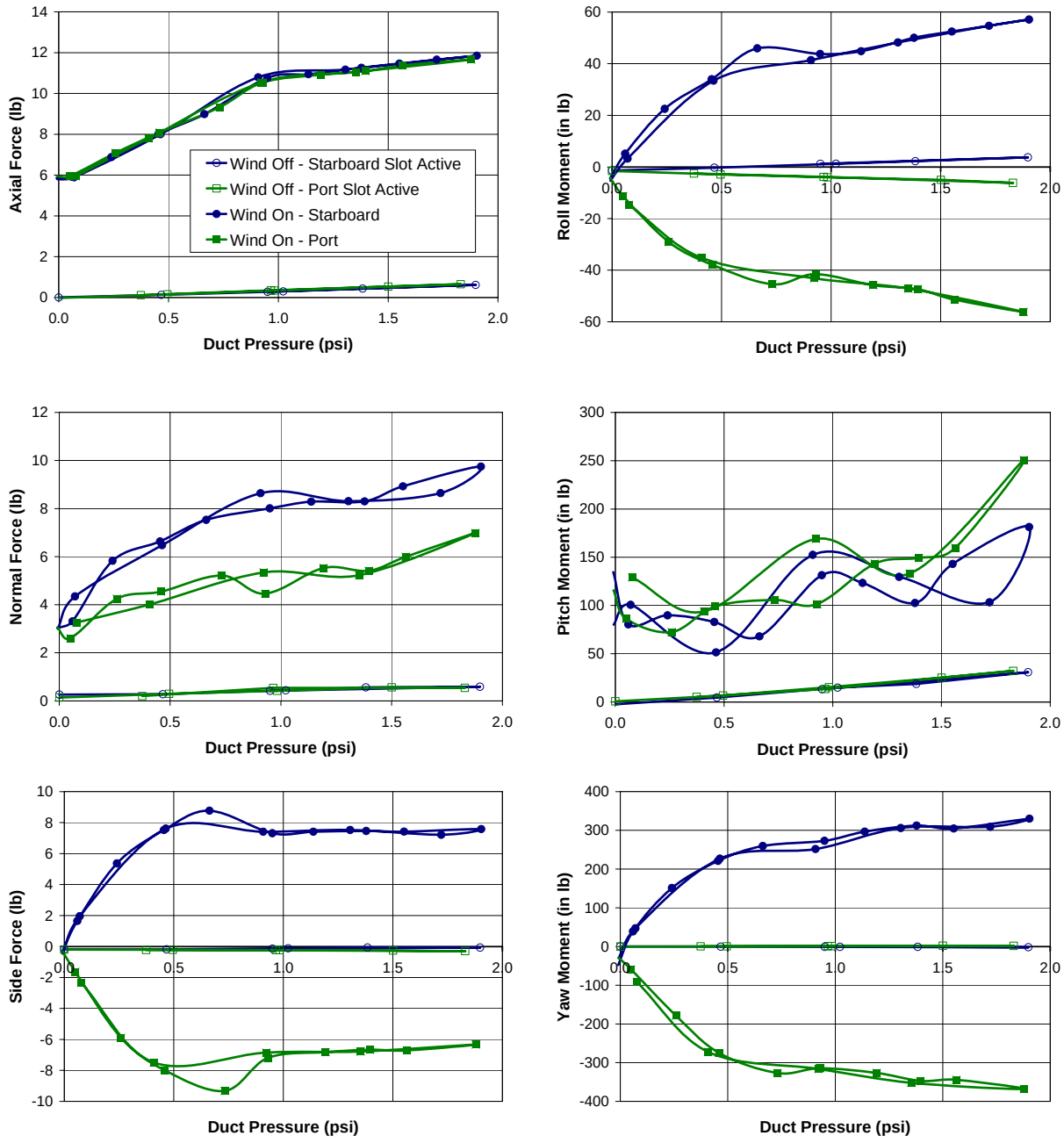

Figure C-1: Runs 3 and 6

Force and Moment Response to Duct Pressure
with and without Wind Tunnel Velocity
Stern Appendages Removed
Pitch = 0 deg, Yaw = 0 deg
All Force and Moment Response is due to the Active Flow Control

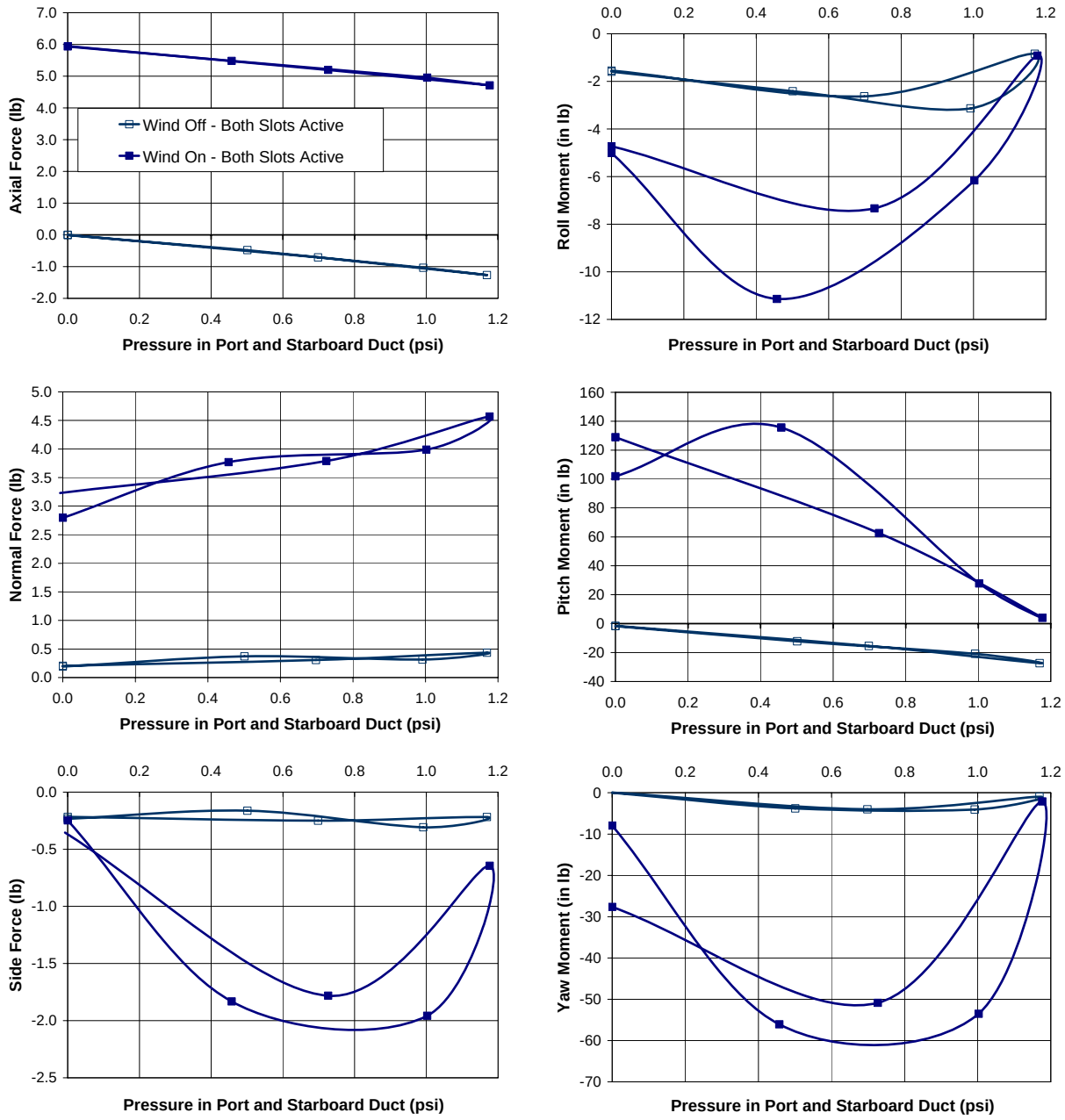

Figure C-2: Runs 4 and 5

Force and Moment Response to Equal Flow from Both CC Slots
with and without Wind Tunnel Velocity
Stern Appendages Removed
Pitch = 0 deg, Yaw = 0 deg
All Force and Moment Response is due to the Active Flow Control

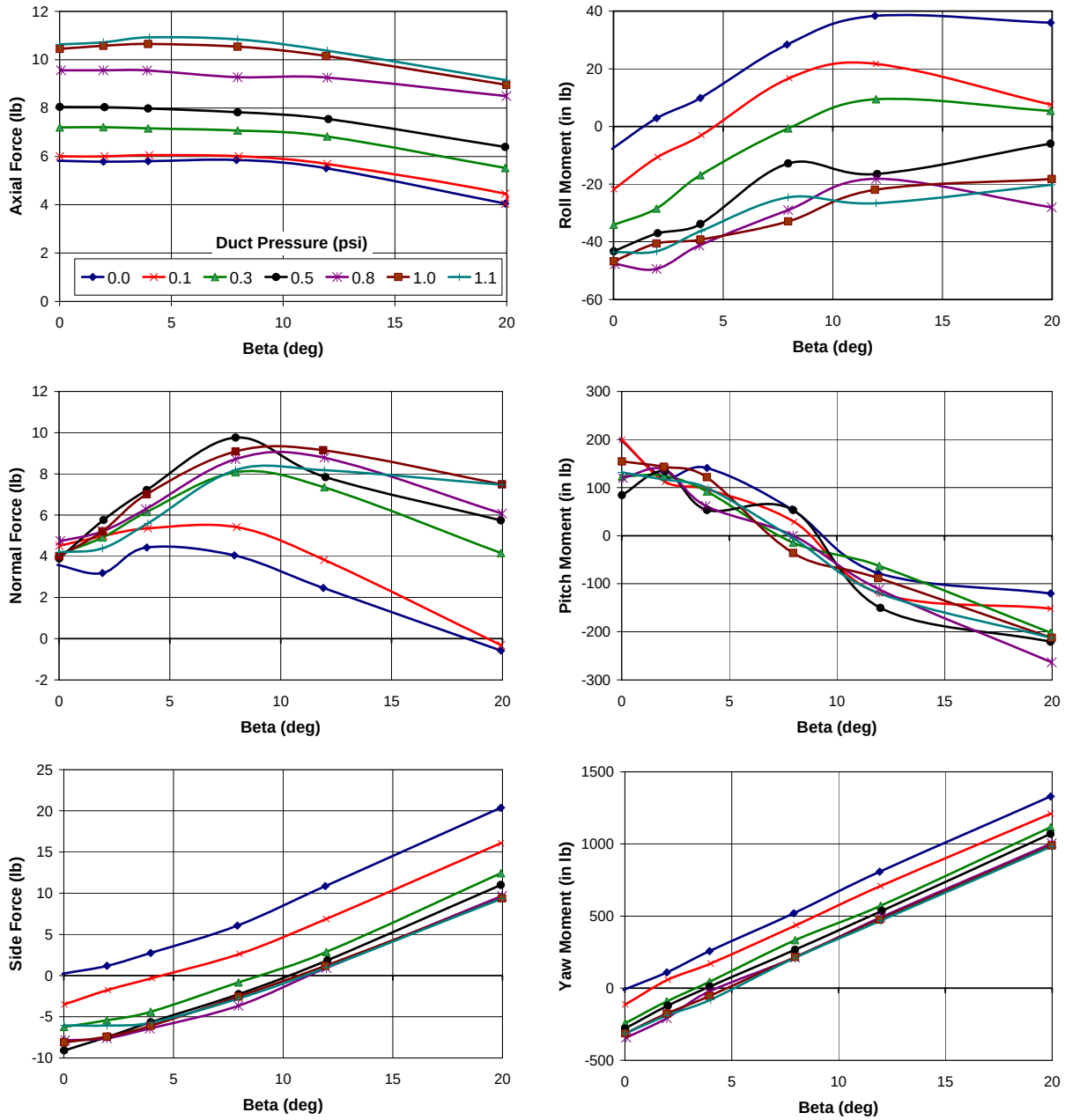

Figure C-3: Runs 7 - 13

Force and Moment Response to Drift Angle
Port Duct Active
Stern Appendages Removed
Pitch = 0 deg
q = 6 psf

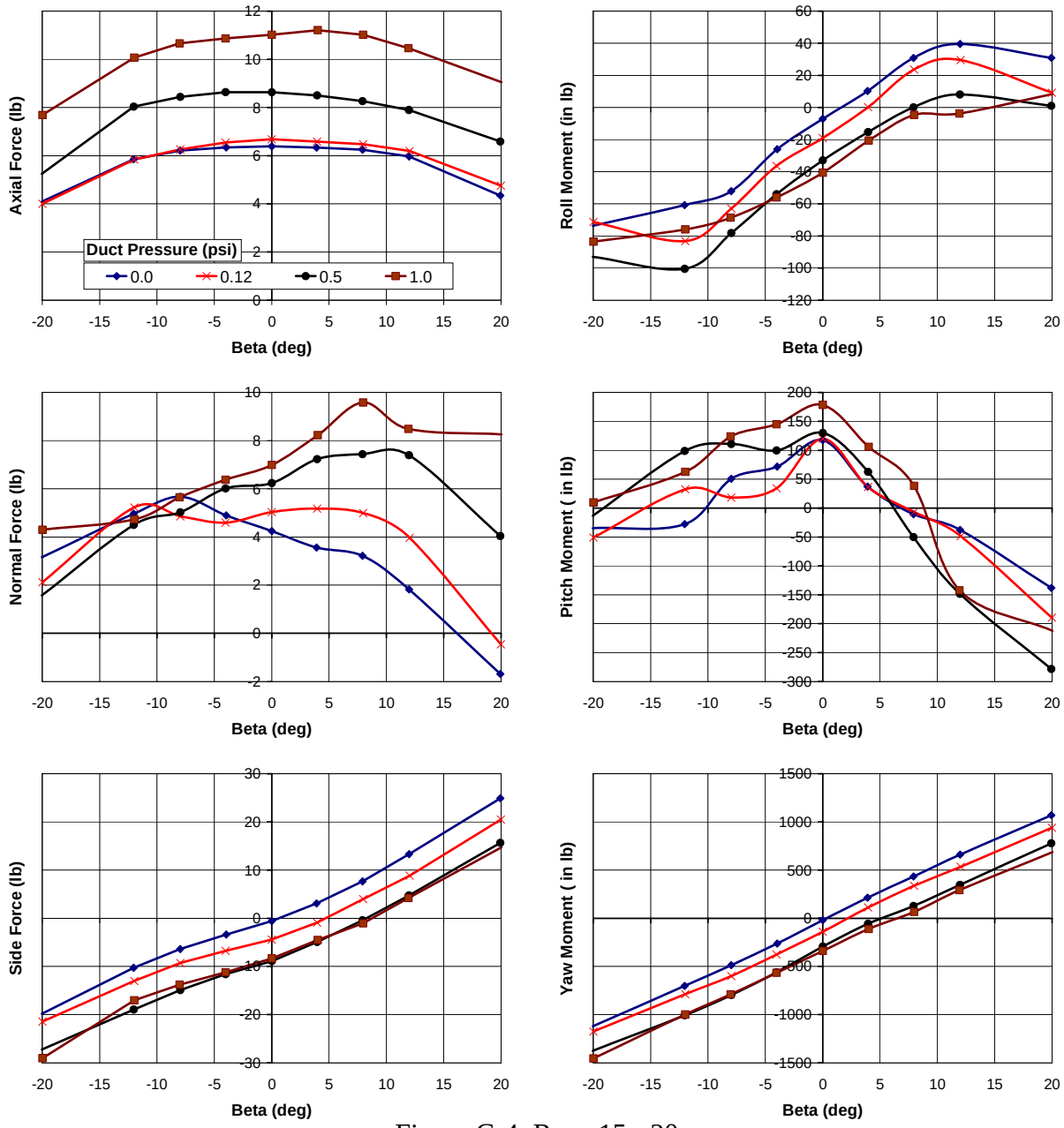

Figure C-4: Runs 15 - 20

Force and Moment Response to Drift Angle
Port Duct Active
Stern Appendages at 0 deg Setting
Pitch = 0 deg
q = 6 psf

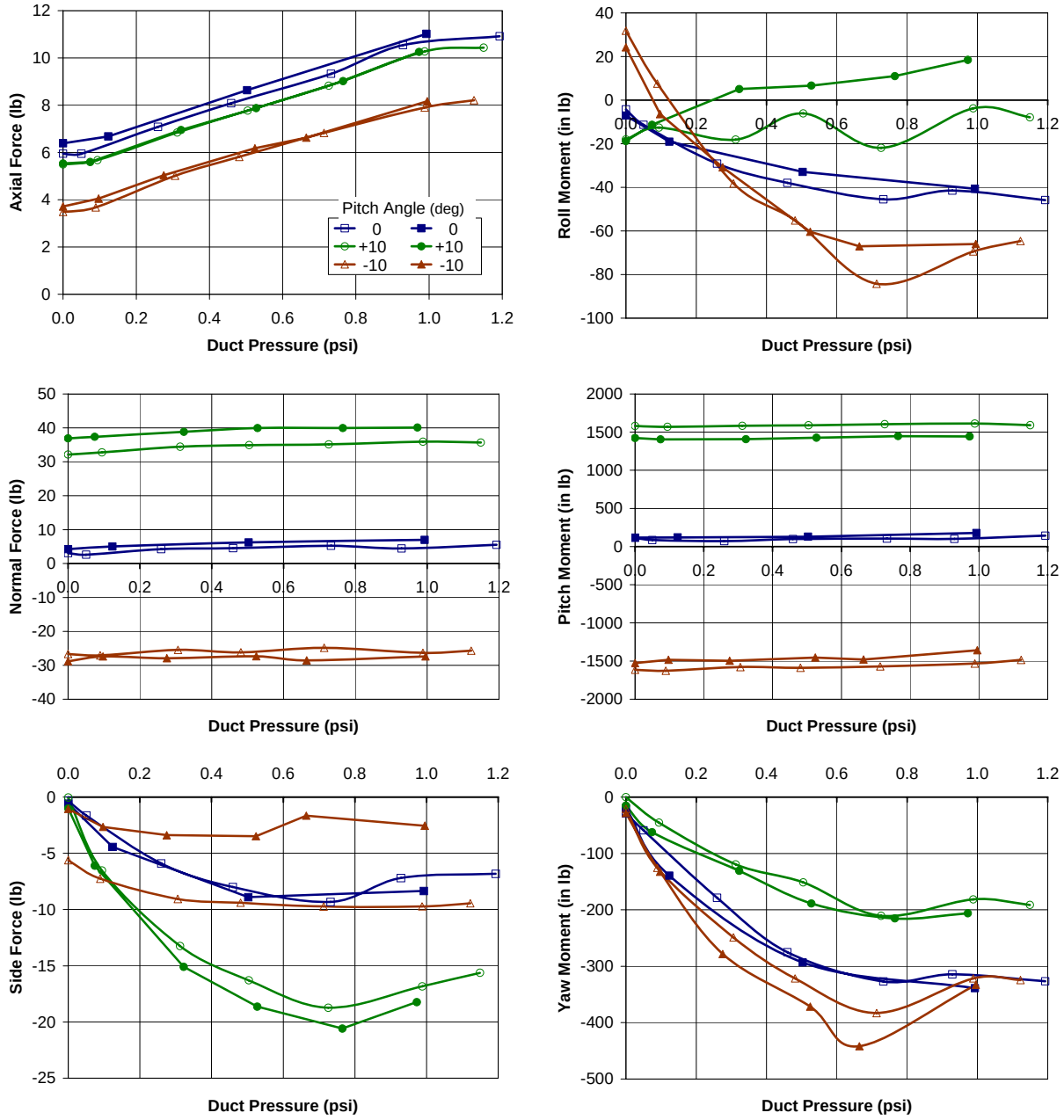

Figure C-5: Runs 14, 23, 24

Force and Moment Response to Pitch Angle
Port Duct Active
Stern Appendages as Noted
Open Symbols are without Stern Appendages
Closed Symbols are with Stern Appendages
Pitch Angle as Noted, Yaw Angle = 0 deg
q = 6 psf

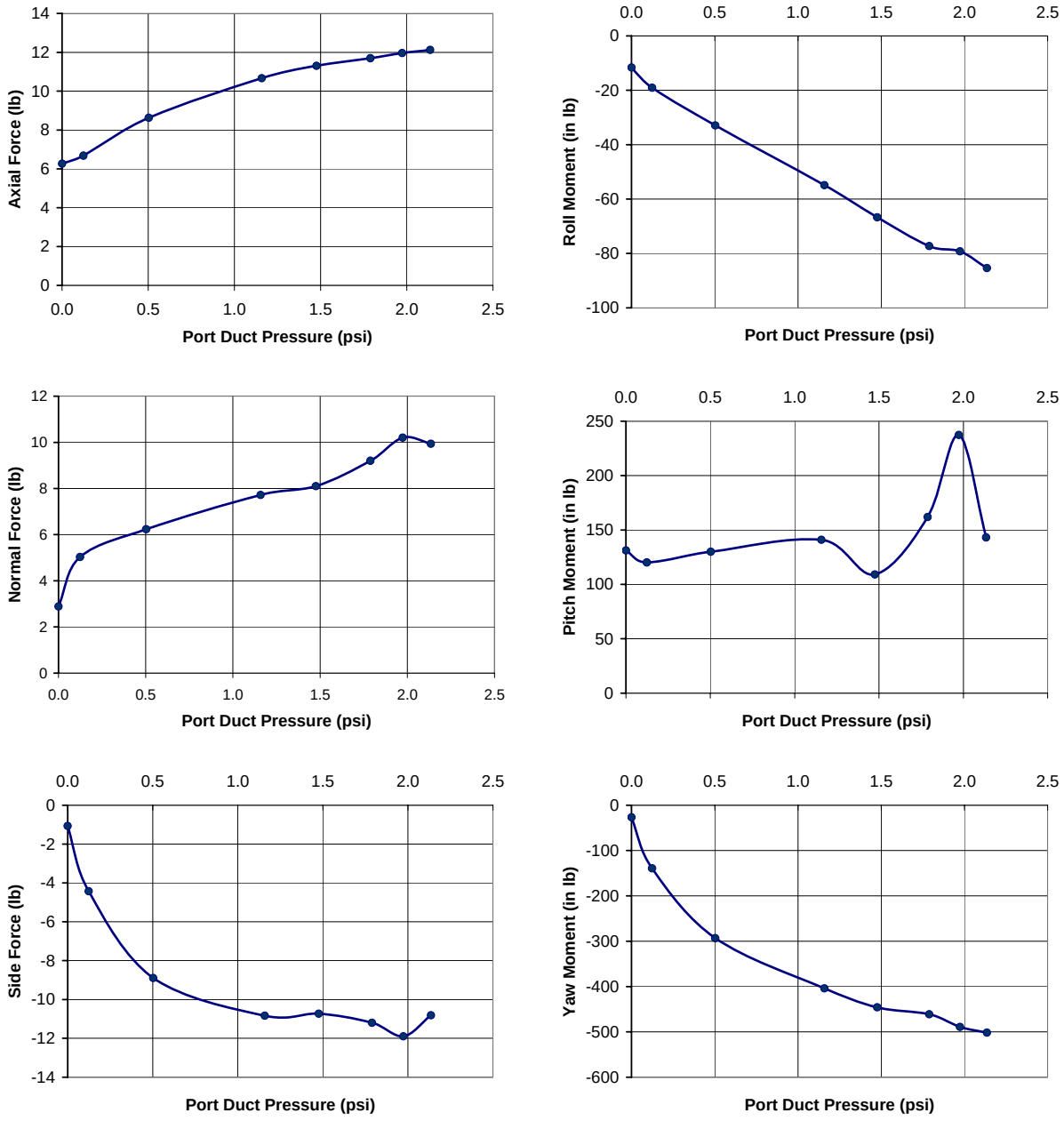

Figure C-6: Runs: 16, 18, 22

Force and Moment Response to Duct Pressure
Port Duct Primary, Starboard Slot 7% Assist after 1.0 psi Port
Stern Appendages Present at 0 deg
Pitch Angle = 0 deg, Yaw Angle = 0 deg
q = 6 psf

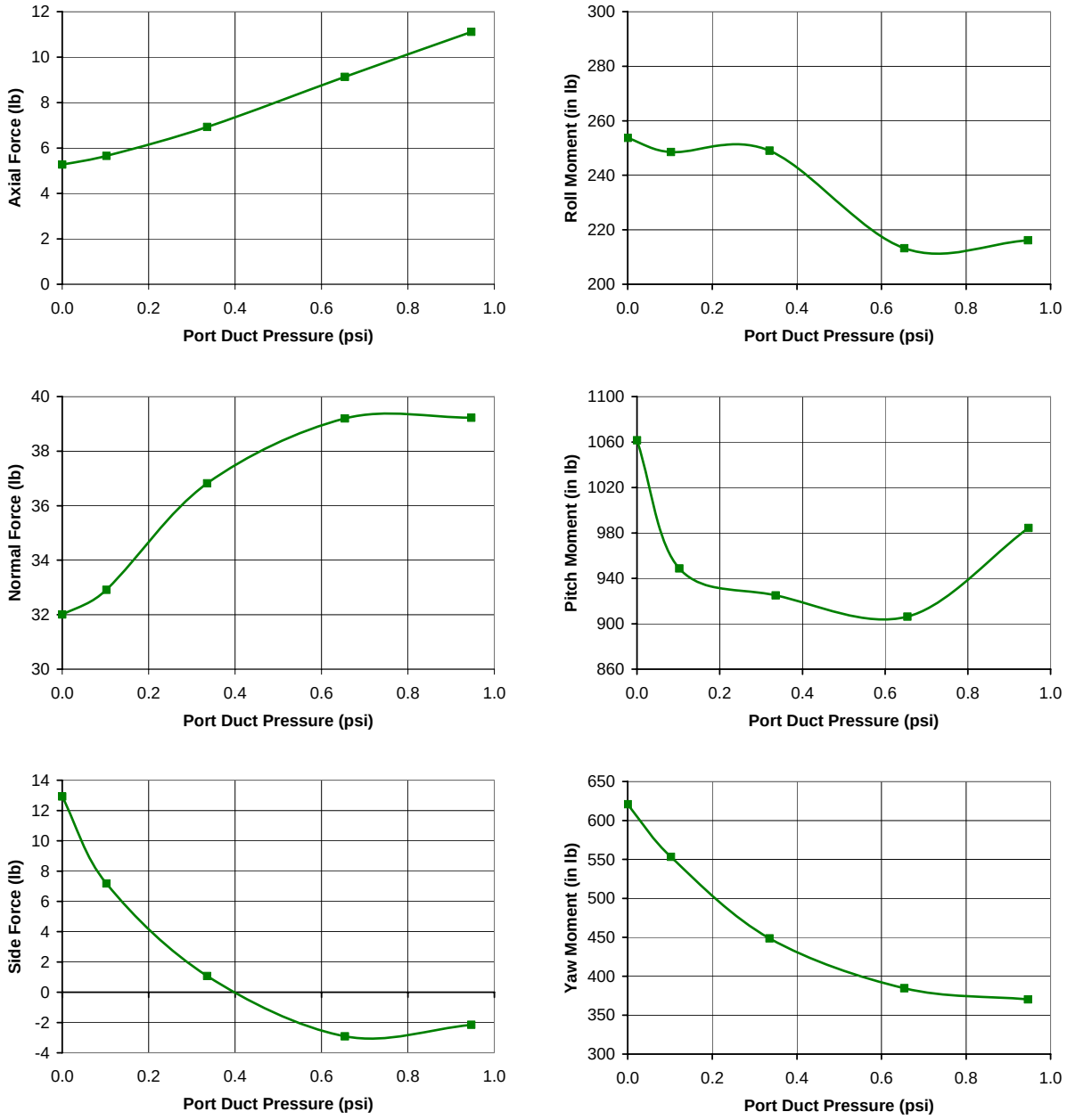

Figure C-7: Run: 25

Force and Moment Response to Duct Pressure
Stern Appendages Present at 0 deg
Pitch Angle = 8 deg, Yaw Angle = 12 deg
q = 6 psf

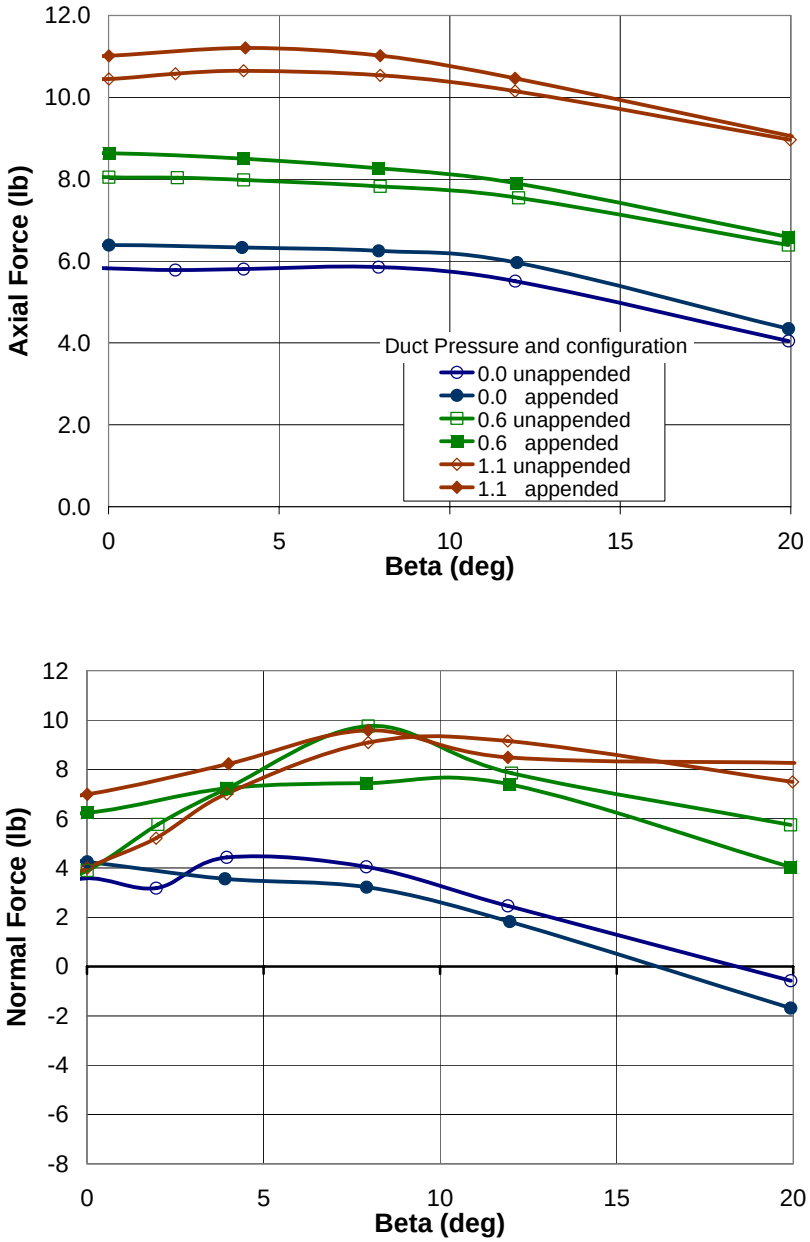

Figure C-8: Runs: 7, 10, 12, 15, 18, 20

Force and Moment Response to Drift Angle and Duct Pressure
Effect of Appendages
Stern Appendages as Noted
Pitch Angle = 0 deg
q = 6 psf

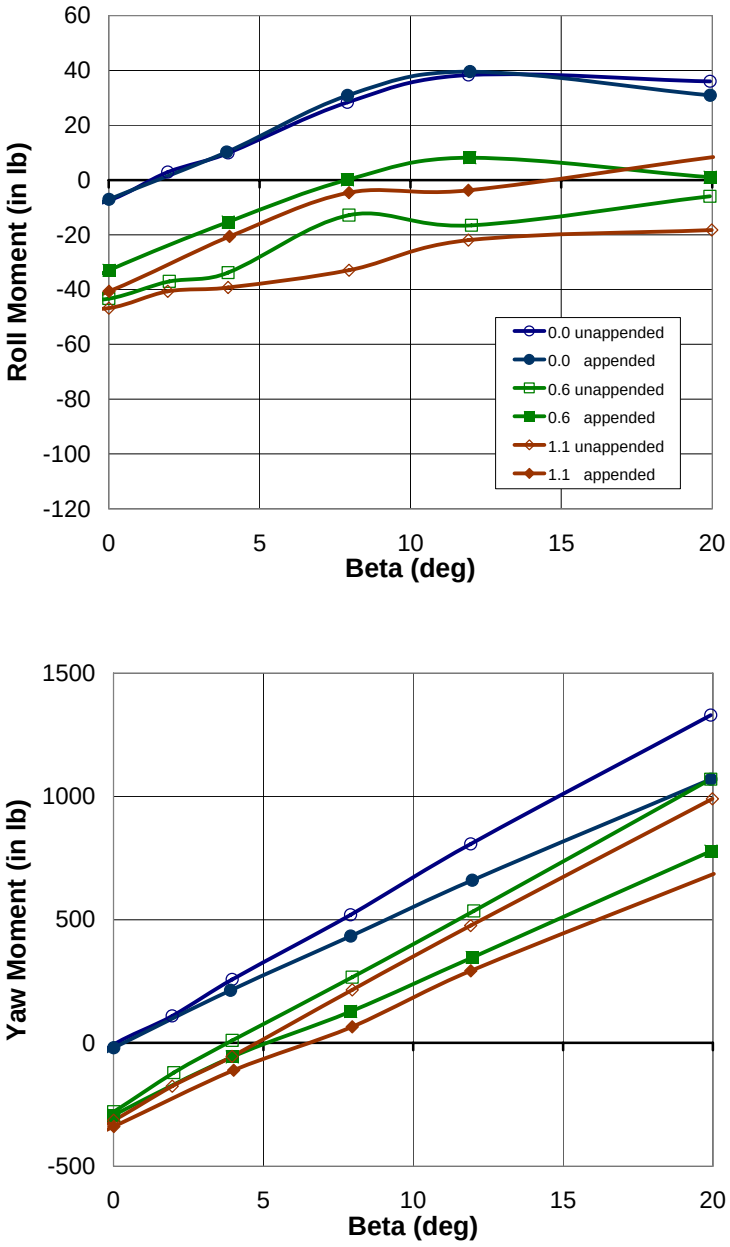

Figure C-8: Runs: 7, 10, 12, 15, 18, 20 (Cont'd)

Force and Moment Response to Drift Angle and Duct Pressure
Effect of Appendages
Stern Appendages as Noted
Pitch Angle = 0 deg
q = 6 psf

DISTRIBUTION:

Office of Naval Research, Dr. Ronald D. Joslin (3)
875 North Randolph Street, Suite 658, Arlington, VA 22203
NAVSURFWARCEN Carderock Division, Dr. Ed Ammeen, Code 5600 (2)
9500 MacArthur Boulevard, West Bethesda, MD 20817-5700
NAVSURFWARCEN Carderock Division, Dr. Peter Chang, Code 5400 (2)
9500 MacArthur Boulevard, West Bethesda, MD 20817-5700
NAVSURFWARCEN Carderock Division, Joe Slomski, Code 5400 (2)
9500 MacArthur Boulevard, West Bethesda, MD 20817-5700
NAVSURFWARCEN Carderock Division, Kurt Junghans, Code 5600 (1)
9500 MacArthur Boulevard, West Bethesda, MD 20817-5700
NAVSURFWARCEN Carderock Division, Tom Fu, Code 5600 (1)
9500 MacArthur Boulevard, West Bethesda, MD 20817-5700
NAVSURFWARCEN Carderock Division, Dr. Stuart Jessup, Code 5030 (2)
9500 MacArthur Boulevard, West Bethesda, MD 20817-5700
NAVSURFWARCEN Carderock Division, Library, Code 3442 (2)
9500 MacArthur Boulevard, West Bethesda, MD 20817-5700
Newport News Shipbuilding, Todd Sedler (2)
2401 West Ave., Newport News, VA 23607-4319
Old Dominion University, Office of Engineering, Dr. Drew Landman, (2)
4427 Hampton Blvd, Norfolk, VA 23529
NAVSEASYSCOM (PMS450), G. Larry Becker (2)
614 Sicard St., SE, Washington Navy Yard, Washington, DC 20376-7002
NAVSEASYSCOM (Sea 05U), Dr. Stuart H. Mennitt (2)
Washington Navy Yard, 05U6, 201-4E170, Washington, DC 20376-7002
NAVSEASYSCOM (Sea 05H), Dr. Matthew B. King (2)
Bldg 197, 2W-1000, 1333 Isaac Hull Ave., Washington, DC 20376-7002
General Dynamics Electric Boat, Ms. Jennifer Panosky (2)
75 Eastern Point Road, Groton, CT 06340-4989
General Dynamics Electric Boat, Dr. John Biederka (2)
75 Eastern Point Road, Groton, CT 06340-4989
Georgia Tech Research Institute, Robert Englar, Aerospace, Transportation and (2)
Advanced Systems Lab, Georgia Institute of Technology, Atlanta, GA 30332-0844
NASA Langley Research Center, Dr. Greg Jones, Flow Physics and Control Branch (2)
Bldg. 1247A, Room 209, M/S 170 1A East Reid Street, Hampton, VA 23681
Engineered Solutions & Products, LLC, David P. Hunt (2)
127 York Point Drive, Seaford, VA 23696
NAVAIRSYSCOM (AIR-5.1), Bldg. 304, Room 100 (1)
22541 Millstone Road, Patuxent River, MD 20670-1606
NAVAIRWARCENACDIV (4.3.2.1/David B. Findlay), Bldg. 2187, Unit 5, Suite 1323 (2)
48110 Shaw Road, Patuxent River, MD 20670-1906
NAVAIRWARCENACDIV (4.3.2.1/Robin D. Imber), Bldg. 2187, Unit 5, Suite 1320 (7)
48110 Shaw Road, Patuxent River, MD 20670-1906

NAVAIRWARCENACDIV (4.9.8.3), Bldg. 407, Room 116 (1)
22269 Cedar Point Road, Patuxent River, MD 20670-1120
NAVTESTWINGLANT (55TW01A), Bldg. 304, Room 200 (1)
22541 Millstone Road, Patuxent River, MD 20670-1606
DTIC (1)
8725 John J. Kingman Road, Suite 0944, Ft. Belvoir, VA 22060-6218